



UNIVERSITÀ DEGLI STUDI DI CAMERINO

DIPARTIMENTO DI FISICA

&

UNIVERSITEIT ANTWERPEN

DEPARTEMENT FYSICA

JOINT DOCTORAL COURSE IN

Theoretical and Experimental Physics

**Superfluidity in exciton bilayer systems:
Josephson effect and collective modes as
definitive identification-markers**

Author:
Filippo PASCUCCI

Supervisors:
Prof. Andrea PERALI
Prof. Jacques TEMPERE
Prof. David NEILSON

“Non fare mai nulla con precisione maggiore dello stretto necessario.”

“Never do anything with more precision than strictly necessary.”

Enrico Fermi

Abstract

Superfluidity in exciton bilayer systems: Josephson effect and collective modes as definitive identification-markers

This thesis investigates key fingerprints of superfluidity in exciton bilayer systems. Exciton bilayer superfluidity is a novel quantum phenomenon in semiconductor systems with two very thin conducting layers, one doped with electrons and the other with holes and separated by only a few nanometers. Recent theoretical predictions have outlined a very rich phase diagram for exciton bilayer systems, with superfluid, supersolid, exciton normal solid, and Wigner crystal phases.

With the expanding interest in the excitonic condensed phases together with the difficulties in practice of establishing their existence through transport measurements, it is crucial to identify clear markers that unambiguously signal superfluidity and coherent condensation in these systems. This thesis explores two phenomena that can identify such markers: the Josephson effect and the density collective modes.

For the Josephson effect, we propose an exciton bilayer Josephson junction in double monolayer Transition Metal Dichalcogenides. We propose an experimental measurement for the exciton Josephson current using the Shapiro method, and we propose a feasible experimental approach for fabricating the device with a tunable potential-barrier height. We investigate the system in the high and low potential-barrier regions, finding distinct behaviour in the gap energy and superfluid critical velocity. This can help delineate the boundary between the BEC and BCS-BEC crossover regimes. In the low potential-barrier region, the exciton superfluid can flow over the barrier. In the high potential-barrier region, however, the superfluid flow is driven purely by quantum tunnelling of the electron-hole pairs through the barrier. We find that the superfluid flow smoothly connects from the high to the low potential-barrier regions.

For the density collective modes, we explore their low-temperature behaviour to identify unambiguous fingerprints of the normal-superfluid transition as a function of density. At high density, the system is in the normal state and it responds to small external density perturbations with low energy optic and acoustic modes. Decreasing the density to enter the superfluid phase, the system-response changes dramatically. The propagation of the acoustic and optic modes is blocked by the presence of the superfluid gap in the single-particle dispersion relation. We expect that due to the finite-range nature of the Coulomb interaction, pair-breaking collective modes will appear at the onset of the exciton superfluidity considering the only density fluctuations. This is in contrast with the standard BCS theory where the contact interaction makes necessary the inclusion of the amplitude fluctuations of the superfluid order parameter to observe pair-breaking collective modes.

Our investigation is carried out using mean-field. The theoretical model, developed from a path-integral approach and the Hartree-Fock approximation, includes the effects of screening and intralayer correlations. The gap and number equations governing the superfluid phase behaviour are calculated, and we demonstrate that intralayer correlations enhance screening. The enhancement is particularly strong in the BCS-BEC crossover regime. The result is a reduction in the superfluid gap, a shift of the BEC to BCS-BEC crossover boundary to significantly lower densities, and the vanishing of a predicted minimum in the electron-hole pair size as a function of density.

This study advances the understanding of superfluidity in exciton bilayer systems and provides theoretical predictions and experimental proposals for future investigations. By identifying clear markers of superfluidity, the work contributes to the broader effort of realizing and characterizing excitonic condensed phases in realistic systems.

Samenvatting

Superfluiditeit in exciton-bilagsystemen: Josephson-effect en collectieve modi als definitieve identificatiemarkers

Deze thesis onderzoekt de belangrijkste kenmerken van superfluiditeit in excitoon dubbel-laag systemen. Excitoon bilayer superfluiditeit is een nieuw kwantumfenomeen in halfgeleidersystemen met twee zeer dunne geleidende lagen, waarvan één gedoteerd is met elektronen en de andere met gaten, gescheiden door slechts enkele nanometers. Recente theoretische resultaten voorspellen een zeer rijk fasesdiagram voor excitoon bilayersystemen, met superfluïde, supersolid, excitoon normale vaste stof en Wigner kristalfasen.

Met de groeiende interesse in de excitonische gecondenseerde fasen, samen met de moeilijkheden om hun bestaan vast te stellen door middel van transportmetingen, is het cruciaal om duidelijke markers te identificeren die ondubbelzinnig superfluiditeit en coherente condensatie in deze systemen signaleren. Deze thesis onderzoekt twee fenomenen die dergelijke markers kunnen identificeren: het Josephson-effect en de dichtheidscollectieve modi.

Voor het Josephson-effect stellen we een excitoon bilayer Josephson-junctie voor in dubbele monolayer overgangsmetaaldichalcogeniden. We stellen een experimentele meting voor van de excitoon Josephson-stroom met behulp van de Shapiro-methode, en we stellen een haalbare experimentele benadering voor om het apparaat te fabriceren met een regelbare potentiaalbarrièrehoogte. We onderzoeken het systeem in de hoge en lage potentiaalbarrière-regio's en vinden distinct gedrag in de gapenergie en de superfluïde kritische snelheid. Dit kan helpen om de grens tussen de BEC- en BCS-BEC crossover-regimes af te bakenen. In de lage potentiaalbarrière-regio kan het excitoon superfluidum over de barrière stromen. Echter, in de hoge potentiaalbarrière-regio, wordt de superfluïde stroom puur aangedreven door kwantumtunneling van de elektron-gatenparen door de barrière. We vinden dat de superfluïde stroom vloeiend overgaat van de hoge naar de lage potentiaalbarrière-regio's.

Voor de dichtheidscollectieve modi onderzoeken we hun gedrag bij lage temperatuur om ondubbelzinnige kenmerken van de normaal-superfluïde overgang als functie van de dichtheid te identificeren. Bij hoge dichtheid bevindt het systeem zich in de normale staat en reageert het op kleine externe dichtheidsstoornissen met lage energie optische en akoestische modi. Bij het verlagen van de dichtheid om de superfluïde fase binnen te gaan, verandert de systeemrespons drastisch. De propagatie van de akoestische en optische modi wordt geblokkeerd door de aanwezigheid van de superfluïde gap in de enkelvoudige deeltjesdispersierelatie. We verwachten dat, door de eindige afstands-bereik aard van de Coulomb-interactie, paarbreekende collectieve modi zullen verschijnen bij het begin van de exciton-superfluiditeit, waarbij alleen rekening wordt gehouden met de dichtheidsfluctuaties. Dit is in contrast met de standaard BCS-theorie, waar de contactinteractie het noodzakelijk maakt om de amplitude-fluctuaties van de superfluïde ordeparameter op te nemen om paarbreekende collectieve modi te kunnen waarnemen.

Ons onderzoek wordt uitgevoerd met behulp van mean-field. Het theoretische model, ontwikkeld vanuit een padintegraalmethode en de Hartree-Fock benadering, omvat de effecten van afscherming en intralaagcorrelaties. De gap- en nummervergelijkingen die het gedrag van de superfluïde fase bepalen, worden berekend, en we tonen aan dat intralaagcorrelaties de afscherming versterken. De versterking is bijzonder sterk in het BCS-BEC crossover-regime. Het resultaat is een vermindering van de superfluïde gap,

een verschuiving van de BEC naar BCS-BEC crossover-grens naar aanzienlijk lagere dichtheden, en het verdwijnen van een voorspeld minimum in de elektron-grootte van het gatenpaar als functie van dichtheid.

Deze studie bevordert het begrip van superfluiditeit in exciton bilayersystemen en biedt theoretische voorspellingen en experimentele voorstellen voor toekomstig onderzoek. Door duidelijke markers van superfluiditeit te identificeren, draagt dit werk bij aan de bredere inspanning om excitonische gecondenseerde fasen in realistische systemen te realiseren en te karakteriseren.

Sommario

Superfluidità nei sistemi a doppio strato di eccitoni: effetto Josephson e modi collettivi come marcatori di identificazione definitivi

Questa tesi indaga le principali impronte digitali della superfluidità nei sistemi a doppio strato di eccitoni. La superfluidità a doppio strato di eccitoni è un fenomeno quantistico innovativo nei sistemi con due strati semiconduttivi molto sottili, uno drogato con elettroni e l'altro con lacune, separati da soli pochi nanometri. Previsioni teoriche recenti hanno delineato un diagramma di fase molto ricco per i sistemi a doppio strato di eccitoni, con fasi superfluide, supersolide, di solido normale di eccitoni e di cristallo di Wigner.

Con l'interesse crescente per le fasi condensate eccitoniche insieme alle difficoltà pratiche di stabilire la loro esistenza attraverso misurazioni di trasporto, è cruciale identificare marcatori chiari che segnalino in modo inequivocabile la superfluidità e la condensazione coerente in questi sistemi. Questa tesi esplora due fenomeni che possono identificare tali marcatori: l'effetto Josephson e i modi collettivi di densità.

Per l'effetto Josephson, proponiamo una giunzione Josephson a doppio strato di eccitoni in diclogenuri di metalli di transizione a doppio monostrato. Proponiamo una misurazione sperimentale della corrente Josephson di eccitoni utilizzando il metodo di Shapiro, e proponiamo un approccio sperimentale fattibile per la fabbricazione del dispositivo con un'altezza della barriera potenziale regolabile. Esaminiamo il sistema nelle regioni di barriera potenziale alta e bassa, trovando comportamenti distinti nell'energia della gap e nella velocità critica superfluida. Questo può aiutare a delineare il confine tra i regimi di crossover BEC e BCS-BEC. Nella regione di barriera potenziale bassa, il superfluido di eccitoni può fluire sopra la barriera. Nella regione di barriera potenziale alta, tuttavia, il flusso superfluido è guidato puramente dal tunneling quantistico delle coppie elettrone-lacuna attraverso la barriera. Troviamo che il flusso superfluido si connette senza problemi dalle regioni di barriera potenziale alta a quelle basse.

Per le modalità collettive di densità, esploriamo il loro comportamento a bassa temperatura per identificare impronte digitali inequivocabili della transizione normale-superfluida in funzione della densità. Ad alta densità, il sistema è nello stato normale e risponde a piccole perturbazioni esterne di densità con modalità ottiche e acustiche a bassa energia. Diminuendo la densità per entrare nella fase superfluida, la risposta del sistema cambia drasticamente. La propagazione delle modalità acustiche e ottiche è bloccata dalla presenza del gap superfluido nella relazione di dispersione della particella singola. Ci aspettiamo che, a causa della natura a raggio finito dell'interazione di Coulomb, modalità collettive di rottura delle coppie appaiano all'inizio della superfluidità di eccitoni considerando le sole fluttuazioni di densità. Ciò è in contrasto con la teoria BCS standard dove l'interazione di contatto rende necessaria l'inclusione delle fluttuazioni dell'ampiezza del parametro d'ordine superfluido per osservare i modi collettivi di rottura di coppie.

La nostra indagine è condotta utilizzando il campo medio. Il modello teorico, sviluppato da un approccio di integrazione sui cammini e dall'approssimazione di Hartree-Fock, include gli effetti di screening e le correlazioni intra-strato. Le equazioni della gap e del numero di particelle che governano il comportamento della fase superfluida sono calcolate, e dimostriamo che le correlazioni intra-strato incrementano lo screening. L'incremento è particolarmente forte nel regime di crossover BCS-BEC. Il risultato è una

riduzione della gap superfluida, uno spostamento del confine di crossover da BEC a BCS-BEC a densità significativamente più basse e la scomparsa di un minimo previsto nella dimensione della coppia elettrone-lacuna in funzione della densità.

Questo studio avanza la comprensione della superfluidità nei sistemi a doppio strato di eccitoni e fornisce previsioni teoriche e proposte sperimentali per indagini future. Identificando marcatori chiari della superfluidità, il lavoro contribuisce allo sforzo più ampio di realizzare e caratterizzare le fasi condensate eccitoniche in sistemi realistici.

Acknowledgements

I would like to start this thesis by expressing my gratitude and giving credit to all those who have contributed to this work. First of all, I would like to thank my supervisors.

Thank you, Prof. Andrea Perali, for introducing me to the fantastic "super" world when I was still a Bachelor student.

Thank you, Prof. Jacques Tempere, for your support during my stay in Antwerp and for our valuable discussions.

Thank you, Prof. David Neilson. The energy and passion for physics that you have imparted to me are unparalleled. I have learned something new (not just about physics) with every discussion.

Thank you, Sara. You were my Belgian Virgilio, guiding me through my first fries and beer in Antwerp, and at the same time, making me feel at home, just like in Provincia di Macerata. Most of all, thank you for your patience and the constant and vital help you have provided in this work.

Thanks to my colleagues and all the people I have met at the conferences. Every discussion and input has somehow ended up in this thesis. Thanks to my family, friends in Italy, and friends in Belgium for always being there and for their constant support. Last but not least, thank you, Margherita.

Filippo Pascucci
Antwerp and Camerino, June 2024

Contents

Abstract	iii
Acknowledgements	ix
Introduction and State of Art	1
1 Electron-Hole superfluidity	3
1.1 Indirect excitons	3
1.2 BCS-BEC crossover in exciton bilayers	5
1.3 Experimental Techniques	7
Coulomb drag	7
Interlayer tunnelling	8
Counterflow measurements	8
Optical measurements	9
1.4 Materials	10
1.4.1 GaAs Double Quantum-Wells	10
From Double-Monolayer to Double-Bilayer Graphene	11
Double Monolayer Transition Metal Dichalcogenide	12
1.5 Motivation of the Thesis	13
Josephson Effect	15
Collective Modes	16
1.6 Organization of the thesis	18
1.7 Collaboration and publications	19
Research Activity and Publications	21
2 Model and method	23
2.1 Path Integral Approach for Electron-Hole superfluidity	23
2.2 Gap and number equation at zero temperature and equal electron-hole layers	35
2.3 Intralayer and Interlayer screened interaction	36
2.3.1 Random Phase Approximation for the Screening: Green's function equation of motion approach	37
2.4 Polarization functions with Green's function equation of motion in exciton superfluid phase	39
Normal Polarization in the superfluid state	40
Anomalous Polarization in the superfluid state	44
3 Josephson Effect in exciton bilayer systems	47
3.1 Experimental proposal	48
3.2 Model of exciton superfluid system in the presence of a potential barrier .	50
3.3 Josephson critical current	52
Low potential barrier region	52
High potential barrier region	54

3.4	Conclusions	57
4	Effects of intralayer correlations on electron-hole bilayer superfluidity	59
4.1	Hartree-Fock correlations in bilayer exciton system	60
4.2	Conclusions	66
5	Density Collective Modes	69
5.1	Exciton bilayer density response function	69
5.1.1	Density collective modes in BEC regime	71
5.1.2	Density collective modes in the Crossover regime	73
5.2	Differences and analogies with cold atoms	76
	On collective modes in ultracold gas atoms	76
	On collective modes in exciton bilayer systems	76
5.3	Conclusions	77
	Conclusions	79
6	Conclusion and Future perspectives	81
6.1	Conclusion	81
6.2	Future Prospectives	83
	1st Research Line: Superfluid order parameter collective modes	83
	2nd Research Line: Drag-Josephson measurement	83
	3rd Research Line: Pseudogap	84
	4th Research Line: Unified model phase diagram	84
A	Electron-Hole Feynman Diagrams in Self-Consistent Random Phase Approximation	87
B	Polarization function with Green's function equation of motion in normal state	91
C	Self-consistent solution of the Gap and Number Equations	97
D	Superfluid critical velocity	99
E	Chemical potential with intralayer correlations	101
F	Density collective modes in exciton bilayer normal state	103
G	Nozières Analytic Continuation procedure	109
G.1	Analytic Continuation of the Polarization function in the Normal State	110
	Bibliography	113
	Curriculum Vitae	125

List of Abbreviations

2D	2-Dimensional
3D	3-Dimensional
BCS	Bardeen-Cooper-Schiffer
BEC	Bose-Einstein Condensation
DQW	Double Quantum Well
DMG	Double Monolayer Graphene
DBG	Double Bilayer Graphene
TMD	Transition Metal Dichalcogenide
RPA	Random Phase Approximation
EBL	Electron Beam Litography
CVD	Chemical Vapor Deposition
QMC	Quantum Monte Carlo

Introduction and State of Art

Chapter 1

Electron-Hole superfluidity

Recent experimental observations of strongly correlated phases in dipolar bilayer exciton systems, even in the absence of magnetic fields, have sparked widespread interest among researchers [1–7]. This phenomenon holds great promise for the formation of a stable superfluid in equilibrium. In bilayers, electron-hole recombination can be suppressed by confining the electrons and holes in separate adjacent layers [8, 9]. Excitonic bilayer semiconductor systems have emerged as particularly intriguing platforms for exploring such phenomena. Strong Coulomb binding of the electron-hole pairs, and consequent expected high superfluid transition temperatures, make it an attractive platform for exploring novel quantum phenomena. The tunability of the system, achieved through variations in the layer separation and charge-carrier density, is predicted to lead to a rich phase diagram encompassing superfluid [10], supersolid [7], dipolar crystal [11], and independent Wigner crystal phases [12].

In this chapter, we describe the distinct properties and advantages of exciton bilayer superfluidity compared to conventional superfluidity. We will delve into the latest experimental techniques used to achieve and investigate exciton bilayer superfluidity. Additionally, we will discuss the current challenges and propose potential solutions.

1.1 Indirect excitons

The study of superconductivity and superfluidity has profoundly influenced the field of physics throughout the last century. Beginning with H. K. Onnes' discovery of charged superconductivity in 1911 [13] and the subsequent observation of neutral superfluidity in liquid helium-4 by P. Kapitsa [14] and J. F. Allen and A. D. Misener [15], these phenomena presented intriguing challenges and opportunities for physicists and the then newborn quantum mechanics.

By extending a calculation by S. N. Bose [16], A. Einstein found that below a critical temperature T_c , a gas of atoms obeying "Bose-Einstein statistics" should accumulate in a single quantum state [17]. In basic terms, all atoms start behaving identically below T_c , forming a macroscopic state of indistinguishable atoms.

The superfluidity of helium was first explained by L. Tisza and L. Landau [18, 19] with a macroscopic two-liquid model: superfluid helium as a surprising mixture of two fluids with independent velocity fields. F. London in 1938 [20] was the first to hypothesize the microscopic mechanism behind superfluidity of helium: a condensation of bosons described by Bose-Einstein condensation.

Since the mid-20th century there have been dramatic advances. For charged superconductors we have to wait until 1957 for the BCS theory by J. Bardeen, L. Cooper and R. Schrieffer [21] before we have a microscopic explanation of superconductivity. BCS proposed that the binding blocks of standard superconductivity are electron pairs, called

Cooper pairs. These pairs form due to an attractive interaction between electrons mediated by lattice vibrations (phonons) [22].

Below the critical temperature T_c , in both superfluidity and superconductivity, the phase coherence of the condensate wave function leads to long-range order, and this enables coherent motion of particles without dissipation.

Starting from the 1960s, several authors proposed that electron-hole pairs, called excitons, can exhibit properties characteristic of bosonic system [23, 24] and that they can undergo Bose-Einstein condensation and show superfluidity [25, 26].

To realize a system of electron-hole pairs, researchers initially thought to use semiconductors. In semiconductors, the energy gap between the valence and the conduction band is typically of the order of a few electron volts. This easily allows optical excitation of electrons from the valence to the conduction band leaving behind a hole in the valence. An attractive Coulomb interaction acts between the negatively charged electron and positively charged hole, leading to formation of an electron-hole bound state, the exciton. The exciton is a composite boson with integer spin 0 or 1 since it is formed by two fermions of spin 1/2.

Experimental realization of this stable excitonic system, however, proved to be very difficult. A small band gap is needed to guarantee a sufficiently strong attractive Coulomb interaction needed to form the electron-hole pair, but at the same time if the band gap is too small, electrons and holes tend to recombine with the emission of a photon. In addition, to be able to observe a stable exciton system, the exciton lifetime should be longer than the exciton cooling time [27, 28].

As a first attempt, semiconductors with an indirect band gap were proposed to address this issue [29, 30]: in the momentum space between the top of the valence band and the bottom of the conduction band, a mismatch W_0 , Fig. 1.1 reduces the electron-hole recombination probability. This ensures the presence of electron-hole pairs with lifetimes long enough to form excitons in equilibrium.

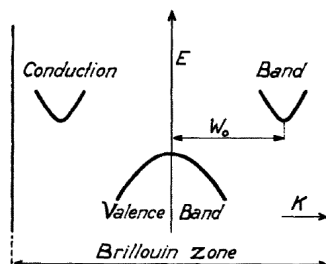


FIGURE 1.1: Indirect band structure of a semiconductor model, [29].

However, in Ref. [29, 30] it was shown that by introducing a mismatch between the valence and the conduction bands, the superfluidity disappears; the system loses its superfluid off-diagonal-long-range order and acquires a crystal diagonal-long-range-order. Thus, for exciton superfluidity a direct band gap, $W_0 = 0$, is necessary.

To meet the requirements of direct band gap together with sufficiently long lifetimes, a bound state formed from spatially separated electrons and holes was proposed for the first time in 1976 by Y. E. Lozovik and V. I. Yudson [9]. This exciton is called a *spatially indirect exciton*. The lifetime of indirect excitons in bilayer systems can be orders of magnitude longer than those of conventional excitons, even when choosing direct band gap semiconductor layers [31].

The device to host indirect excitons can be a double quantum well system [32] or a double layer system [33]. The latter consists of two bidimensional layers close to each other and separated by a distance d , Fig. 1.2. In one layer there are electrons and in the

other holes. The space between the layers is filled with an insulator to prevent recombination processes. This is also called a van der Waals heterostructure. A strong interlayer Coulomb interaction V_{eh} leads to the formation of electron-hole pairs. The advantage of a bilayer system with respect to a double quantum well system is the diminished dimensionality, which leads to a much stronger attraction between electrons and holes.

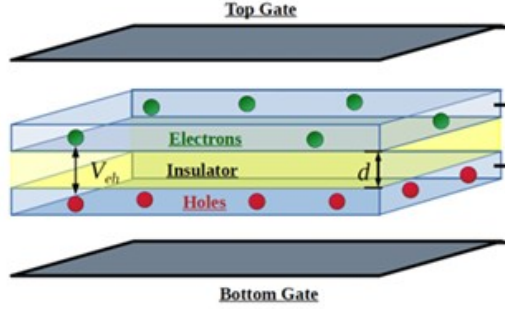


FIGURE 1.2: Schematization of a double layer system with electrons in the top layer and holes in the bottom layer. The d is the interlayer distance, and V_{eh} is the interlayer attractive Coulomb interaction.

Exciton bound states are hydrogen-like states of electron-hole pairs bound by the Coulomb interaction. The binding energy and the radius of an isolated exciton are determined by an effective Rydberg energy Ry^* and Bohr radius a_B^* ,

$$Ry^* = \frac{e^2}{4\pi\epsilon\epsilon_0} \frac{1}{2a_B} \quad (1.1)$$

$$a_B^* = \frac{\hbar^2 4\pi\epsilon\epsilon_0}{m_r e^2} \quad (1.2)$$

where $\epsilon\epsilon_0$ is the dielectric constant of the medium and $m_r = m_e^* m_h^* / (m_e^* + m_h^*)$ is the reduced effective mass. m_e^* and m_h^* are the effective electron and hole masses. The condition for superfluidity can be satisfied in general terms when the interlayer distance d is smaller than the effective Bohr radius a_B^* so that the binding energy ϵ_B of the exciton in the bilayer system is larger than the effective Rydberg Ry^* .

It is fundamental and challenging to identify optimal combinations of the bilayer materials, the insulator, and the interlayer distance to have the strongest, most stable exciton system.

1.2 BCS-BEC crossover in exciton bilayers

In 1985, P. Nozières and S. Schmitt-Rink [34] proposed that a system of electron pairs can be continuously tuned from a weakly interacting regime described by the BCS theory to a strongly interacting regime described by Bose-Einstein condensation (BEC). This phenomenon is called *BCS-BEC crossover*. In the BCS regime, the Cooper pair radius r_{pair} is larger than the average interparticle distance. The Cooper pairs greatly overlap and what prevails in the system is the fermionic behaviour of the single particles. In the BEC regime, the pair radius is smaller than the interparticle distance, the pairs are compact and do not overlap. Two compact bounded fermions can be treated as a composite boson so the pairs satisfy Bose-Einstein statistics.

It is possible to smoothly evolve the system from the BCS to the BEC regime, the two sides of the BCS-BEC crossover (Fig. 1.3). The system will pass through an intermediate *Crossover* regime.

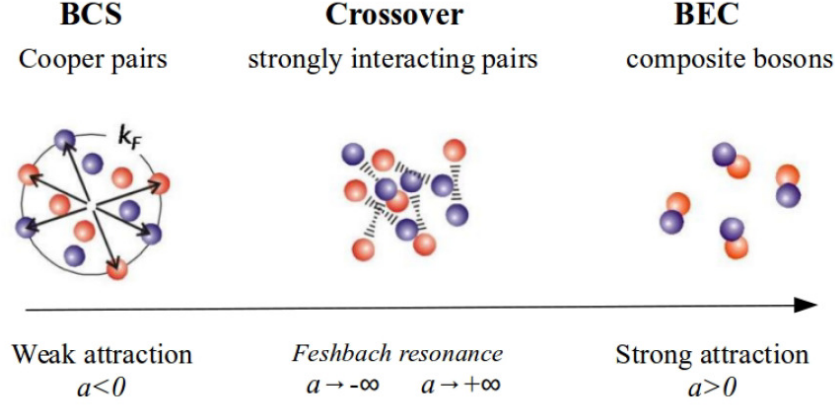


FIGURE 1.3: The weakly interacting BCS regime, the intermediate crossover regime and the strongly interacting BEC regime as a function of the s-wave scattering length a .

The BCS-BEC crossover regime has been extensively studied in three-dimensional ultracold gas atoms [35], especially using ^6Li and ^{40}K . In a system of attractive fermions, the interaction strength is described by the s-wave scattering length a . In the BCS regime with its weak attractive interactions, a is small and negative. In ultracold gas atoms, it is possible to change the value of a , and even its sign, through a mechanism called the Feshbach resonance [36], using an external magnetic field [37] or optical traps [38]. When a bound state appears and becomes resonant with the energy of the scattering state, the scattering length a diverges. This is called the unitarity regime. Crossing over to the other side of the resonance, the scattering a has now become positive and the bound state energy gets lower, leading to tightly bound molecules in the BEC regime [39]. The tuning of a can continuously drive the system from the BCS regime where $a < 0$, to the BEC regime where $a > 0$ [40]. Superfluidity in the BCS-BEC crossover has been unambiguously demonstrated by visualising the lattice of singly-quantized vortices that form when the system is rotated [41].

In 2D exciton bilayer systems, the parameter that characterizes the relative strength of the interaction is $r_s = \langle V_{ee} \rangle / \langle K \rangle$, where $\langle V_{ee} \rangle$ is the average potential energy and $\langle K \rangle$ the average kinetic energy. When $\langle V_{ee} \rangle > \langle K \rangle$, the correlations are important and the system is characterised by well-separated and strongly bound pairs, the BEC regime. When $\langle V_{ee} \rangle < \langle K \rangle$, correlations are negligible and the system is characterised by overlapping and weakly bound pairs, the BCS regime. This means that by tuning r_s in bilayer exciton systems, we can tune through the BCS-BEC crossover [12].

We can write r_s more explicitly:

$$r_s = \frac{\langle V_{ee} \rangle}{\langle K \rangle} = \frac{e^2}{4\pi\epsilon\epsilon_0 \langle r_0 \rangle} \frac{1}{E_F} = \frac{e^2 \sqrt{\pi n}}{4\pi\epsilon\epsilon_0} \frac{1}{E_F(n)} \quad (1.3)$$

where r_0 is the interparticle distance and E_F is the Fermi energy, given in 2D by $E_F(n) = \hbar^2 \pi n / m^*$. The r_s can be tuned by:

- Tuning the kinetic energy by modifying the electronic dispersion and the effective mass using an external magnetic field, gating, or applying strain.

- Tuning the interlayer interaction by modifying the interparticle distance r_0 , or by changing the dielectric ϵ of the system.

In the exciton bilayer system it is possible to tune the particle density n in the two conducting layers, and thus the interparticle distance r_0 , $n = 1/\pi r_0^2$, through external metal gates [42]. At very low density n (large interparticle distance r_0) the excitons barely interact with each other. The excitons are compact so the system is in the strongly coupled BEC regime. At high density n (small interparticle distance r_0) the pair size $r_{pair} > r_0$, so the excitons overlap. The system would be in the weakly interacting regime, the BCS regime [43, 44].

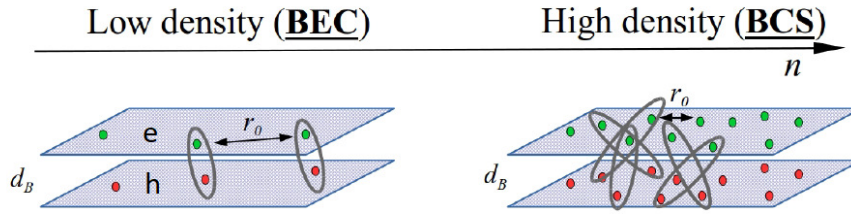


FIGURE 1.4: The BEC and BCS regimes of the BCS-BEC crossover in bilayer system.

Unlike BCS superconductivity, in the electron-hole system, the interlayer electron-hole attraction and the intralayer electron-electron repulsion are Coulombic and not short-ranged. Hence the screening of the interactions must be taken into account [45, 46]. At low density, where the excitons are compact and well-spaced, they behave as neutral pairs and the screening is negligible, but at high density where the excitons are overlapping, the screening becomes crucially important [46, 47]. The screening weakens the interlayer interactions and thus weakens the superfluid phase. Above a certain value of the density, called the *onset density*, the detrimental effect of the screening is too strong and the superfluidity disappears [48]. Screening makes it impossible for the system to enter the weakly interacting BCS regimes, thus the exciton superfluidity survives only in the BEC and crossover regimes of the BCS-BEC crossover.

1.3 Experimental Techniques

Different experimental techniques have been implemented to identify the presence of stable excitons and exciton superfluidity in bilayer systems. Some of these are based on transport measurements (Coulomb drag and counterflow measurement), some on the tunnelling conductance between the layers and others on optical observation of exciton luminescence.

Coulomb drag

Coulomb drag measures the friction between the spatially separated electrons and holes. An electric current is driven in one layer, the *drive current*, and this drags carrier in the other layer, generating a *drag current*. This happens because the attractive interlayer Coulomb interaction allows momentum transfer between layers.

The drag resistivity ρ_D is defined as the ratio between the induced potential in the drag layer and the drive current [49]. This measures how much the charges in one layer are dragged by the charges in the other layer. The ρ_D is sensitive to how the momentum

is exchanged between electrons and holes and thus to the phase of the exciton bilayer system.

Below the critical temperature, when exciton transport dominates over the free carrier transport, perfect Coulomb drag $I_{drive}/I_{drag} = 1$ is expected because a steady current of electrons driven through one layer must be accompanied by an equal current of holes in the other layer. The drag resistivity grows as the temperature decreases and it diverges at the limit of zero temperature [50].

In a bilayer electron-hole system with no condensate, only a small frictional drag is expected, $I_{drive}/I_{drag} < 1$. In the case of Fermi liquids, the phase space of electrons and holes available for Coulomb drag increases with temperature, the drag current ratio I_{drive}/I_{drag} scales quadratically with temperature and the drag resistance ρ_D is generally smaller than the isolated layer resistivity [51–55]. The transition from normal state to superfluid exciton state is predicted to be characterized by a jump in the behaviour of the drag resistance ρ_D .

The key requirement for this technique is to have independent electrical contacts between the electron and hole layer [56]. A recent very high-quality Coulomb drag experiment in double-layer Transition Metal Dichalcogenides system showed for the first time the perfect Coulomb drag [6]. However, there is no definite claim of superfluidity because of a lack of dissipationless transport due to the large contact resistance.

Interlayer tunnelling

In Sec. 1.1 we have discussed how the interlayer distance is a fundamental parameter for stable and long-lived excitons. Even in the presence of the insulator between the two spatially separated electron and hole layers, if the interlayer distance is too small the strongly interacting electron-hole pairs have a probability of quantum mechanically tunnelling through the insulator and recombining with the emission of a photon.

In interlayer tunnelling experiments a voltage bias is applied between the two layers and the interlayer conductance is measured [57].

Recently an enhancement of interlayer tunnelling has been observed in a double-bilayer graphene system [1] and in a double-layer Transition Metal Dichalcogenides system [58]. Such enhancement is explained by the presence of strongly correlated excitons in the system. This favours the recombination of a macroscopic number of excitons under a voltage bias which effectively electrically shorts the distance between the layers [59].

Counterflow measurements

A fundamental property of a superfluid is the zero-resistance coherent flow of particles under a critical temperature. The measurement of the flow of particles in a system is referred to as *counterflow measurement*.

In bilayer excitons, in the counterflow measurement, equal current is sent through both layers, flowing in the opposite direction, while measuring longitudinal resistance in each layer. Researchers have struggled to perform this measurement because of the difficulty (i) in controlling the density of the electrons and holes in the separated layers [42] and (ii) in maintaining a stable exciton flow [60].

A top and bottom metal gates are independently connected to the top and bottom layer of the system, as shown in Fig. 1.2. A bias voltage between the two layers can be induced: above a threshold value, the effective band gap between the conduction and valence band of the system is reduced to zero, so that electrons are induced in the conduction band of one layer, and holes in the valence band of the adjacent layer. Thus, by tuning the bias voltage, one controls the density of electrons and holes.

At the electrical contacts, a significant drop in the bias voltage has been detected. A large interlayer tunnelling current accompanies the injection of excitons, inducing non-negligible recombination between electrons and holes. Because of this, the electron/hole layer cannot be maintained at the same chemical potential as the contacts. The exciton density is thus determined by balancing the pumping rates and recombination rates of excitons. They are non-equilibrium exciton fluids, and the leakage current between the bilayers strongly influences the transport steady state [42].

This problem has been solved by using a new contact configuration (Fig. 1.5) [3]. The

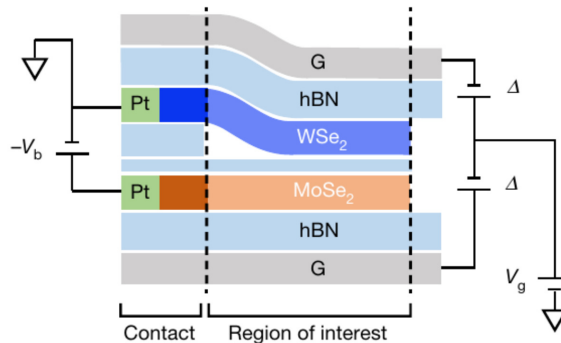


FIGURE 1.5: Dual-gated double-layer devices. The symmetric gating V_g shifts the electron and hole chemical potentials and tunes their density difference. V_b is the bias voltage, and Δ is the bottom gate voltage, top gate voltage difference divided by 2 [3].

new device manages to stop the recombination close to the contacts and equilibrium electron and hole density can be achieved.

As for the second problem, Ref. [60] shows how a steady-state dissipationless current cannot be induced simply by connecting the two layers in series to guarantee opposite currents in electron and hole layers. This method increases the interlayer tunnelling probability and electron-hole recombination. To prevent this the electron current should be injected into and removed from one layer, and another electron current, in the opposite direction, should be injected into and removed from the other layer.

In the presence of a superfluid exciton phase, the counterflow resistance should be zero. Up to now, clear measurements of a very low counterflow resistance have been reported only in the presence of an external magnetic field in the quantum Hall regime [61, 62].

Optical measurements

Several techniques have been proposed to optically identify macroscopic spatial coherence in exciton systems using various traps. These include electrostatic traps [63], strain-induced traps [64], laser-induced interdiffusion traps [65], magnetic traps [66], and laser-induced traps [67, 68]. Optical identification methods involve:

- Observing bright localized spots with enhanced luminescence at fixed points on the sample in photoluminescence measurements [69].
- Detecting a sharp inter-well exciton line abruptly appearing in the photoluminescence spectra [70].
- Noting an abrupt increase in the amplitude of interference fringes using shift-interferometry measurements, indicating enhanced exciton coherence length [71].

However, pre-2007 optical measurements were inconclusive because they overlooked the role of dark excitons in Bose-Einstein condensates [72, 73]. Dark excitons, which are optically inactive due to the same spin of their electron and hole, have lower energy than bright excitons and are not affected by repulsive interband Coulomb processes like photon emission. The internal spin structure of the exciton condensate, influenced by exchanges between excitons, allows bright excitons to enter the condensate at high densities. Thus, at high density, the exciton condensate radiates weak photoluminescence, which can be used as a signature of macroscopic spatial coherence [74].

1.4 Materials

In this section, we give an overview of the materials proposed for observing electron-hole superfluidity and the main experimental results.

1.4.1 GaAs Double Quantum-Wells

One of the first systems proposed to study electron-hole superfluidity was a Gallium Arsenide (GaAs) Double Quantum-Well (DQW) structure [75]. This setup consists of two GaAs quantum wells where electrons and holes are confined in separate wells by a static electric field. The quantum wells are separated by a thin insulating barrier of $\text{Al}_x\text{Ga}_{1-x}\text{As}$, which prevents recombination (Fig. 1.6). The strength of electron-hole pairing is controlled by the barrier thickness d_B and the widths of the quantum wells d_W [76]. Experimental configurations for these structures are challenging due to scattering

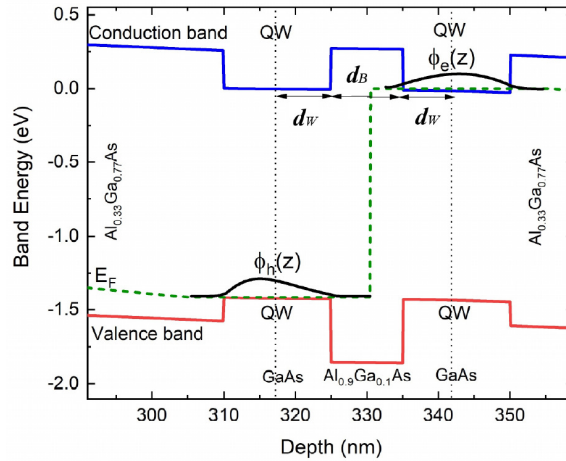


FIGURE 1.6: Conduction and valence bands for a GaAs DQW with quantum well widths $d_W = 15\text{nm}$ and $\text{Al}_{0.9}\text{Ga}_{0.1}\text{As}$ barrier thickness $d_B = 10\text{nm}$ [76]. The dashed green line is the Fermi level ε_F . The vertical back dotted lines mark the centres of the wells. $\phi_e(z)$ and $\phi_h(z)$ are the resulting electron and hole single-particle wavefunctions confined in the wells.

issues that lower mobilities if the wells are too narrow. In a stable exciton sample with $d_B = 15\text{nm}$ quantum wells and $d_W = 10\text{nm}$ barriers, the average distance between electron and holes is $d = 12\text{nm}$. Because of the large separations the electron-hole interaction is weak and the superfluidity is predicted only at low densities ($n < 10^{10}\text{cm}^{-2}$) and low temperature $T < 1\text{K}$, which are difficult to achieve experimentally.

In Ref. [32, 77] an initial increase in Coulomb drag resistivity at temperatures around 0.5K was observed in GaAs Double Quantum-Wells. These results are not definitive enough to claim superfluidity since they cannot keep lowering the temperature due to excessive noise in the Coulomb drag measurement but they strongly probe the presence of a stable exciton system.

While definitive observations of superfluidity in GaAs DQWs are still lacking, this system remains promising due to the significant difference in electron and hole effective masses, potentially leading to a rich phase diagram of exotic superfluid phases [78]. These include the Fulde–Ferrell–Larkin–Ovchinnikov phase [79], the Sarma phase [80] and a superlattice quantum solid [81]. Similar phases have been explored in ultracold atomic gases, but at much lower temperatures, $T_c \simeq 50\text{nK}$ [82].

From Double-Monolayer to Double-Bilayer Graphene

After the discovery of graphene [83], a bidimensional atomic layer of carbon atoms, and hexagonal Boron Nitride (hBN) [84, 85], an effective insulating layer, a van der Waals configuration (Fig. 1.2) consisting of a top layer of graphene doped with electrons and a bottom layer of graphene doped with holes, separated by few layers of hBN, was proposed as a candidate for high-temperature exciton superfluidity [33, 77]. The main advantages of Double-Monolayer-Graphene (DMG) respect GaAs double quantum-wells are:

- Carrier confined in a single thin layer. It overcomes the problem of the large well widths d_B in DQW.
- Insulating barrier consisting in trilayers of hBN, corresponding to $d_B \simeq 1\text{nm}$. It is one order of magnitude smaller than the barrier width d_B in DQW.

Because of this minimum distance between electrons and holes, it is reasonable to expect a very strong attractive interlayer Coulomb interaction in double-monolayer graphene.

Unfortunately however, since the energy bands follow a linear dispersion, the kinetic energy decreases linearly with the interparticle spacing r_0 , making r_s independent of density and always $r_s < 1$. This means that the strongly interacting regime is not accessible even at small densities and temperatures. For this reason, no exciton superfluidity is expected in DMG [45]. This result has been confirmed in a Coulomb drag experiment in DMG [86, 87].

Double-bilayer graphene (DBG) was proposed to access the strongly interacting regime and realize exciton bilayer superfluidity [46, 88]. In this configuration the van der Waals heterostructure is composed of two top graphene layers vertically stacked doped with electrons and two bottom graphene layers vertically stacked doped with holes, separated by a few layers of hBN (Fig. 1.7). Unlike monolayer graphene, the single-particle dispersion in bilayer graphene is parabolic (Fig. 1.7), as conventional semiconductors, with an effective mass $m_e^* = m_h^* = 0.05m_e$.

Two research groups independently fabricated and characterized double graphene bilayer devices [89, 90]. Both measured the Coulomb drag resistivity, ρ_D , as a function of carrier density, controlled via voltages applied between the bilayers and metallic gates [91]. Unlike double monolayer graphene, for equal carrier densities in both bilayers, the drag resistance was nearly as high as the bilayer graphene resistance itself, pointing toward the presence of a stable exciton system. A second surprising observation is negative drag. This behaviour was linked to multi-band effects in bilayer graphene [92, 93]. Recently, tunnelling current measurements confirmed the presence of a stable exciton system in DBG systems, with enhanced interlayer tunnelling around 1.5K [1].

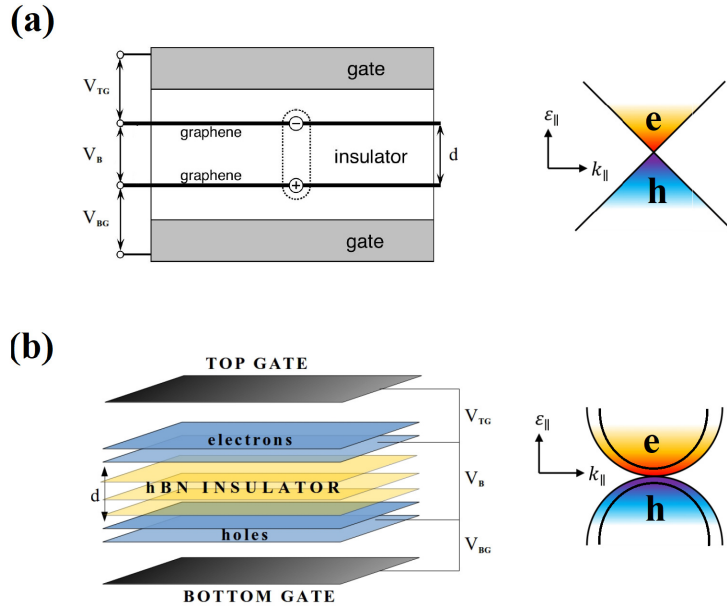


FIGURE 1.7: (a) Schematization of double-monolayer-graphene (Ref. [33]). On the right is the linear dispersion relation of single-layer graphene. (b) Schematization of double-bilayer graphene. On the right is the parabolic dispersion relation of the double-bilayer graphene.

Double Monolayer Transition Metal Dichalcogenide

In recent years, 2D semiconductors from the group-VI Transition Metal Dichalcogenides (TMDs) have garnered attention due to their large effective masses and high exciton binding energies. These TMD monolayers, with the formula MX_2 (where M is a transition metal like Molybdenum or Tungsten, and X is a chalcogen like Sulfur or Selenium), feature a hexagonal structure. High-quality TMD hetero-bilayers consist of two different TMD monolayers, one electron-doped and the other hole-doped, directly coupled and separated by a few layers of hBN [94]. The main advantages of this device are:

- Electron and hole effective mass $m_e^* = m_h^* \simeq 0.5m_e$, one order of magnitude larger than in bilayer graphene, which guarantees a high exciton binding energy of $\epsilon_B = 1\text{eV}$ [95, 96].
- Band gap $E_g > 1.5\text{eV}$ between the electron and the hole band. This is enough to prevent the electron-hole recombination [97].
- Combining two different TMDs in the top and bottom layers results in a *type-II* band alignment [98]. In this setup, the conduction band minimum and valence band maximum are in different layers but at the same k -point in reciprocal space (Fig. 1.8). This configuration strengthens exciton formation and weakens recombination.

For these reasons, double monolayer TMDs are interesting platforms to host strong interlayer excitons [99, 100]. Furthermore, high transition temperature, $T_c \simeq 150\text{K}$ in double monolayer TMDs have been predicted [101, 102].

A possible signature of exciton superfluidity was reported using interlayer tunnelling and electroluminescence measurements [2]. Enhancement of electroluminescence is observed up to 100K. However, the claim has been disproved by showing that the system was in the non-equilibrium excitons regime.

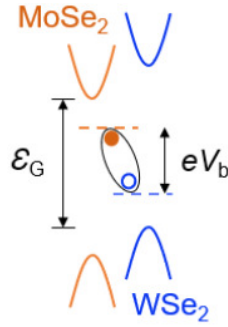


FIGURE 1.8: Type-II band alignment in the double monolayer transition metal dichalcogenide system made of a MoSe₂ layer doped with electrons and a WSe₂ layer doped with holes used in Ref. [6].

A recent very high-quality Coulomb drag experiment in MoSe₂-hBN-WSe₂ showed for the first time the perfect Coulomb drag, $I_{drive}/I_{drag} \simeq 1$ up to 20K [6]. However, Ref. [6] could make no definite claim of superfluidity because of a lack of dissipationless transport due to the large contact resistance.

1.5 Motivation of the Thesis

The richness of the excitonic physics and the experimental progress achieved in two-dimensional materials in the last few years [59, 103], make the exciton bilayer systems particularly attractive.

In this first chapter, we have mainly examined the predictions of the exciton superfluid phase when the interlayer distance is small enough and the density is low enough. However, over different ranges of density and interlayer distance, exciton bilayer systems can host an extremely rich diagram of phases [7].

Tuning the interlayer d and average interparticle r_0 distance, it is possible to explore different regimes of the intralayer repulsive and interlayer attractive interactions. When the interlayer distance is much larger than the average separation between the carriers, $d \gg r_0$, the repulsive Coulomb interaction dominates over the attractive interlayer Coulomb interaction, leading to a ground state of decoupled Fermi liquids. However, when $r_0 > d$ so that the attractive interlayer interaction dominates, the electrons and holes will form bound excitonic states. For $r_0 > d$ at low densities, r_0 large, when the interlayer distance d is small, the superfluid phase is predicted to be the ground state [43, 46, 104]. Still with $r_0 > d$, but for large d , the ground state is predicted to be a normal state crystal phase [11, 12, 105, 106]. Finally, in the region of the phase diagram at low densities and intermediate distances, a variational approach has predicted a supersolid phase with one exciton per site, in which, remarkably, superfluid spatial off-diagonal long-range order coexists with the periodic order of the solid [7], Fig. 1.9.

From a theoretical point of view, a unified model capable of fully disentangling all the phases is still missing. The mean-field theory model used to describe exciton bilayer at zero temperature [45–48, 78] neglects the correlations within the layers, and incorrectly predicts that the superfluid phase extends into the $d > r_0$ region at large interlayer distances, Fig. 1.9. Approaching the $r_0 - d$ diagonal from below, the intralayer repulsion becomes more and more important and the intralayer correlations cannot be neglected.

From an experimental viewpoint, there exists no technique which provides an unambiguous signature of exciton superfluidity. Coulomb drag, interlayer tunnelling, and electron luminescence measurements have established the presence of a stable exciton

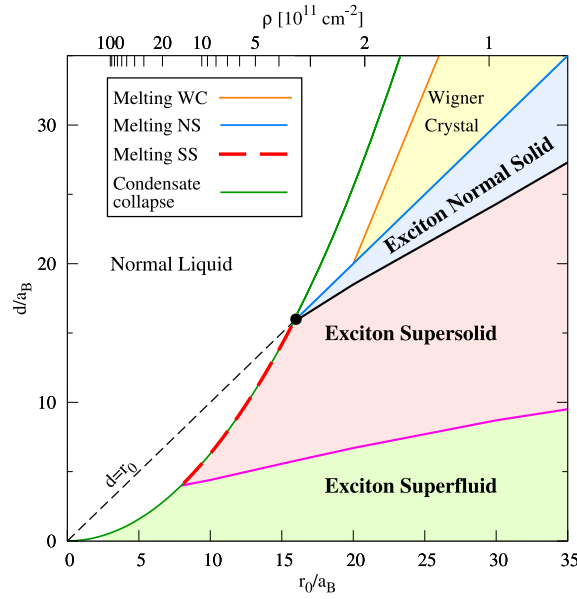


FIGURE 1.9: Phase diagram at zero temperature of a bilayer exciton system as a function of the interlayer distance d and the interparticle distance r_0 [7]. The black dashed line is the diagonal $d = r_0$. The green solid line "Condensate collapse" is obtained in the mean-field approximation without the inclusion of the intralayer correlations.

phase. The counterflow measurements could reveal a dissipationless current in the system. However, the presence of stable excitons or non-dissipative currents is not sufficient by themselves to claim superfluidity. Measurement of very low resistances is always accompanied by uncertainties associated with the experimental equipment, for example electrical contacts [107]. The conventional criterion used to identify superconductivity, a combination of dissipationless conduction with the Meissner effect (perfect diamagnetism under an external magnetic field) cannot of course be employed here because the excitons are neutral [60].

In view of the recent explosion of interest in the exciton condensed phases, the inability of transport measurements to directly establish the existence of these phases makes it important, timely, and extremely interesting to search for and identify fingerprints that can unambiguously identify superfluidity and coherent condensation in exciton systems.

This thesis accordingly aims to investigate and identify such fingerprints, to unambiguously identify exciton superfluidity and to characterize it. We aim to answer several important open questions:

- Which phenomena can be experimentally explored in exciton bilayer systems to work around the current experimental problems in probing the existence of exciton superfluidity?
- Which are the major ingredients needed in a unified theoretical model to describe the different phases of the exciton phase diagram?

We seek fingerprints of exciton superfluidity within the observables of the Josephson effect and collective modes. We have developed a sophisticated theoretical model for exciton superfluidity, one in which the effects of both screening and the intralayer correlations are fully accounted for.

Josephson Effect

In 1962, B. D. Josephson predicted that a static tunnelling supercurrent I_J could exist between two superconductors separated by a thin insulating barrier [108]. Observation of a dissipationless supercurrent I_J through the barrier in the absence of a driving potential is regarded as an optimal direct experimental technique to confirm the existence of a quantum condensed state [109, 110]. The magnitude of this supercurrent is :

$$I_J = I_c \sin(\Delta\phi) , \quad (1.4)$$

where $\Delta\phi$ is the difference in the phases of the two superconductor order parameters, $\Delta\phi = \phi_L - \phi_R$ (Fig. 1.10), and the maximum current I_c is called Josephson critical current. Josephson further predicted that if a voltage difference V were maintained across the junction, the phase difference evolves in time according to:

$$\frac{d(\Delta\phi)}{dt} = \frac{2eV}{\hbar} , \quad (1.5)$$

so the supercurrent is an alternating current of amplitude I_c and frequency $\nu = 2eV/\hbar$. The energy $\hbar\nu$ is the tunnelling energy of a Cooper pair across the junction [111].

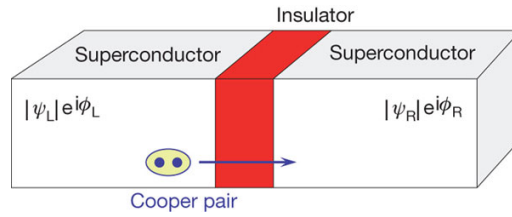


FIGURE 1.10: Schematic representation of the Josephson junction consisting of a left and a right superconductor (white) separated by an insulating barrier (red). A current of Cooper pairs without external driving potential flows between the superconductors.

Josephson's prediction was based on a theoretical study of the tunnelling of electrons through an insulating barrier, but it is now known that the Josephson effect is much more general. The effect is seen whenever two superconductors are connected by a "weak link". The weak link can be the insulating barrier as originally proposed by Josephson, a normal metal barrier that becomes weakly superconductive through the so-called proximity effect, or a constriction barrier linking two superconductors [112].

Existence of a dissipationless current through a Josephson barrier without any driving potential confirms the existence of the single amplitude and phase of the macroscopic wave function characterizing a quantum condensed state. In conventional superconductors, the Josephson effect is widely used to establish the presence of superconductivity.

Investigations have been extended to superfluid ultracold gas atoms [113–115] throughout the BCS-BEC crossover [116, 117]. The critical Josephson current and its evolution in time depend on where the system is located in the BCS-BEC crossover [109, 110]. In the BEC regime, the critical Josephson current is driven by the sound velocity of the bosonic excitation of the entire Cooper pair, described by the Bogoliubov-Anderson dispersion relation [118, 119]. In the BCS regime, the critical Josephson current is driven by the pair-breaking velocity of the fermionic excitations of the single particles, described by the BCS pair-breaking dispersion relation [110, 116].

Advances in Josephson-junction technology have made possible the development of a variety of sensors for detecting ultralow magnetic fields and weak electromagnetic radiation [120]. For example, Superconducting Quantum Interference Devices (SQUID) are very sensitive magnetometers based on superconducting loops containing Josephson junctions [121], and are widely used in hospitals and biology laboratories to improve the precision of magnetic resonance imaging (MRI) [122]. This heightened sensitivity improves the quality of imaging, aiding in better diagnosis and monitoring of medical conditions.

A first theoretical and qualitative attempt at studying the Josephson effect in an exciton bilayer system was made in Ref. [123]. The direct and alternating Josephson current was studied in an exciton Josephson junction made up of two DMG systems separated by a generic "tunnelling barrier". The exciton current was created in the junction by a density and phase imbalance between the left and right bilayer exciton systems. By connecting the two layers in series, the same current flows in one layer in one direction, and in the opposite direction in the other layer. The phenomenon was theoretically described by a mean-field approach neglecting screening.

In this Thesis, we report a theoretical study of the Josephson effect in exciton bilayer systems, taking screening into account. Unlike Ref. [123], this study is based on a realistic experimental setup.

Collective Modes

Collective modes describe the cooperative response to an external perturbation acting on a many-body system. We will exploit the fact that the dispersion and lifetime of the collective modes of the exciton bilayer system vary dramatically depending on which phase the system is in.

Collective modes have been widely studied theoretically in superconductors, ultracold gases and neutron stars [124–128]. Recently, interest in collective excitations in superfluids and superconductors has been reinforced by experiments to study their response properties [129, 130].

The response functions of macroscopic observables, the density, or in the case of a coherent condensed system, the order parameter can be measured by externally perturbing the system at a given wavenumber q and drive frequency ω . In the theoretical case, the collective mode is undamped, so an infinitely narrow resonance (a Dirac peak) in the response function is expected when the perturbation energy coincides with the collective mode energy. The peak corresponds to a real pole in the response function, lying outside the continuum.

However, in reality, collective modes are damped and coupled with each other. The system response is then less abrupt, a broadened resonance. The resonance peak corresponds to an imaginary pole of the response function in the continuum region at the complex frequency $\Omega(q) = \omega(q) - i\Gamma(q)$ [131]. $\Gamma(q)$ is the damping parameter, reflecting the lifetime of the collective mode and the $(-)$ sign is for the stability of the collective modes.

The response function in the continuum is a non-analytical function. Nozières used analytic continuation to move the non-analytic points from the real Ω axis to the imaginary semi-plane [132, 133].

Superfluid Fermi gases can be described using the Random-Phase Approximation (RPA) by investigating the fluctuations of three collective fields: the total density n of particles and the phase and modulus of the superfluid order parameter.

- **Collective modes associated with density fluctuations.** These plasma modes appear in the normal state [131]. In the long-wavelength limit, the plasma modes are q -independent in a 3D system, while in a 2D system they are proportional to \sqrt{q} [134].
- **Collective modes associated with phase fluctuations of the order parameter.** In neutral superfluid systems, these are gapless soundlike modes [133, 135–137], the Anderson–Bogoliubov modes. In the long-wavelength limit, they are linear in q . In charged systems, the gapless modes are affected by the Coulomb interaction and they are pushed up to the plasma mode [138, 139].
- **Collective modes associated with amplitude fluctuations of the order parameter.** These modes are gapped. They are the so-called pair-breaking modes. They lie in the continuum. Their dispersion relation is characterized by a damping parameter.

In the general case, the fluctuations of the fields are coupled, so the collective modes have components in all three fields.

The collective modes can be used to identify the boundary between the normal and superfluid phases and to map the BCS-BEC crossover. The collective modes at zero temperature are as follows:

- **BCS regime.** Amplitude collective modes appear in the amplitude response function. Phase collective modes appear in the phase and in the density response function and as a Dirac peak at zero temperature [140].
- **BCS-BEC crossover regime.** In the crossover regime, neither the plasma, nor the Anderson–Bogoliubov, nor the pair-breaking mode can be attributed exactly to amplitude or phase responses, because there is amplitude-phase mixing.
- **BEC regime** Phase collective modes appear in the phase response function. The amplitude modes are observable in the amplitude response channel and also in the density response channel.

Throughout the BCS-BEC crossover, the density fluctuations are sensitive to the fluctuations of the order parameter, so that both amplitude and phase collective modes are visible in the density response, but the opposite is not true. The amplitude and phase fluctuations of the order parameter are not sensitive to density fluctuations.

For neutral atomic Fermi superfluid systems, the spectra of both Anderson–Bogoliubov and pair-breaking modes have been studied experimentally using two-photon Bragg spectroscopy [130]. For charge superconductors, pair-breaking has only recently been identified experimentally [129] by performing terahertz pulse excitation on the system. The density can be excited by a Bragg pulse [130] or by shaking the confinement walls [141].

A systematic investigation of the collective modes in exciton systems is needed and can help to disentangle all the predicted exciton phases.

Collective modes in a superfluid exciton bilayer system have recently been investigated by De Palo *et al.* [142]. The authors focus on density collective modes in a bilayer exciton system adopting a "quasi-localized particle approximation" [143] in which electrons and holes are assumed to be highly localized. They demonstrate the presence of acoustic and optic collective modes as in the normal exciton phase [144], and they show that the modes are gapped in the superfluid phase. Physically, the quasi-localized particle model is a good approximation for low densities and large interlayer distances where the particles interact only weakly with each other. The picture is consistent with results in

Ref. [145] for a dilute exciton solid, in which the excitons organize into a crystal structure, making the electrons and holes highly localized.

In this Thesis, we present a theoretical investigation of the collective modes in an exciton bilayer system, basing it on a model that realistically describes the exciton superfluid phase.

1.6 Organization of the thesis

The thesis is organized as follows.

In the **second chapter** we introduce a theoretical model for electron-hole superfluidity in bilayer systems that includes intralayer correlations via the Hartree-Fock approximation, and Coulomb screening effects in both the interlayer and intralayer interactions using a self-consistent Random Phase Approximation (RPA). We use a path-integral approach to derive the gap and number equations for superfluidity across the BCS-BEC crossover. Existing models neglect the intralayer correlations. The chapter sets the foundation for further exploration of these correlations in the BCS-BEC crossover, with the aim of a unified electron-hole theory.

In the **third chapter**, we explore the static Josephson effect in an electron-hole superfluid bilayer Transition Metal Dichalcogenides (TMD) heterostructure. We propose a design for a bilayer Josephson junction in which it is possible to control the potential energy barrier, and we discuss experimental techniques for fabricating it. We analyze the superfluid characteristics and crossover physics for a rectangular Josephson junction. We determine the superfluid properties and the critical current across Josephson junctions with varying potential barrier heights. For low potential barriers, we investigate the BCS-BEC crossover physics of the Josephson current. For high potential barriers, we calculate the exciton pair tunnelling in order to study the Josephson current. By exploring the physics of the junction, we are able to identify for the first time in a semiconductor system, an experimental method to locate the boundary between the BEC and BCS-BEC crossover regimes in the BCS-BEC crossover phenomenon.

In the **fourth chapter**, we investigate the intralayer correlations acting within the layers in the superfluid phase of electron-hole spatially separated layers. We establish that the Hartree-Fock approximation is everywhere valid for treating the intralayer repulsive interaction in electron-hole bilayer superfluids. We investigate the effect of the intralayer correlations on the superfluid properties as a function of the density. We benchmark the results with quantum Monte Carlo numerical simulations in the case of double-bilayer graphene. We explore the effect of intralayer correlation in the BCS-BEC crossover, by tuning the interlayer distance for fixed density. Finally, we study the effect of intralayer correlations on the exciton pair size as a function of the density. We find in the BCS-BEC crossover regime that the superfluid gap is significantly weakened by the intralayer correlations, but that in the BEC regime, superfluid properties are insensitive to the intralayer correlations.

In the **fifth chapter**, we explore the collective modes in the exciton bilayer system. Our aim is to identify a fingerprint for the presence of the superfluid exciton phase. We focus on collective modes associated with density fluctuations within the Random Phase approximation. We compare results in the normal and superfluid states. We discuss the major differences between the collective modes originating from the long-range Coulomb interactions in an exciton bilayer compared with the collective modes originating from the contact interaction in cold atom gases. Finally, we discuss qualitatively, the collective modes associated with fluctuations in the amplitude and phase of the superfluid order parameter.

In the **sixth chapter** we summarize our new results. The thesis ends with an overview of some potential extensions in future work.

1.7 Collaboration and publications

The research presented in this thesis is the result of the joint PhD project born from the collaboration between the University of Camerino (Italy) and the University of Antwerp (Belgium). The thesis is inspired by many discussions, research notes and joint publications. The research was supervised by Prof. Andrea Perali from the University of Camerino, and by Prof. Jacques Tempere and Prof. David Neilson from the University of Antwerp. The research presented in this thesis was performed in collaboration with FWO Postdoctoral Fellow Sara Conti at the University of Antwerp. During the work on the thesis, there have been the following publications and other collaborations :

- Chapter 2: The theoretical approach was further refined thanks to discussions with Gaetano Senatore and Stefania De Palo (University of Trieste).
- Chapter 3: A manuscript was published in Physical Review B [146].
- Chapter 4: A manuscript was published in Physical Review B [44].
- Chapter 5: The discussion and interpretation of the results were further refined thanks to discussions with Hadrien Kurkjian and Sergei Klimin. A manuscript is in preparation.

The future outcomes presented in Chapters 3 and 5 are included in the Project that was successfully chosen by the Research Foundation - Flanders "Fonds Wetenschappelijk Onderzoek" (FWO).

Research Activity and Publications

Chapter 2

Model and method

In this chapter we introduce the theoretical approach used to describe electron-hole superfluidity in bilayer systems, including intralayer correlations. The effect of the Coulomb screening in the attractive interlayer and repulsive intralayer interaction are considered through the Random Phase approximation. For the first time, the complete and extensive calculation of the Random Phase approximation in exciton bilayer systems based on the evaluation of the Green's functions equation of motion has been reported. With a path-integral approach, we calculate the fundamental equations to describe the superfluidity throughout the BCS-BEC crossover.

The mean-field model with the inclusion of only the RPA-screened interlayer interaction wrongly predicts that the superfluid phase also survives in the $r_0 > d$ region [7, 46, 147], for large d , as reported in the $r_0 - d$ phase diagram Fig. 1.9. Approaching the $r_0 - d$ diagonal from below the intralayer repulsion becomes more and more important and the intralayer correlation can not be neglected.

In this chapter, we aim to build a theoretical model able to describe exciton superfluidity with the inclusion of the intralayer correlation. We explicitly calculate the mean-field gap and number equations of a bilayer electron-hole system as a function of the exciton density and interlayer distance through a path-integral approach [148–152]. In particular, we extend the existing theoretical mean-field approach [46, 153] by including the screened repulsive interaction between electrons (holes) within the same layer using the Hartree-Fock approximation.

We will further investigate the effect of the intralayer correlations throughout the BCS-BEC crossover in Chapter 4. We will show that their inclusion is a first and fundamental step toward an electron-hole unified theory.

2.1 Path Integral Approach for Electron-Hole superfluidity

To study the phenomena of spatially separated electrons and holes binding together in bilayer systems in the superfluid phase the particle-hole transformation is adopted. For the p -doped layer characterized by empty electron states in the valence band, the valence band is mapped to a conduction band populated by positive charges up to the hole Fermi level.

The system is described by the total grand-canonical Hamiltonian for electron-hole gas in second quantization:

$$\begin{aligned} \hat{H} = \sum_{\lambda} \int d\mathbf{x} \Psi_{\lambda}^{\dagger}(\mathbf{x}) T_{\lambda}(\mathbf{x}) \Psi_{\lambda}(\mathbf{x}) + \frac{1}{2} \sum_{\lambda} \int d\mathbf{x} \int d\mathbf{x}' V_{\lambda\lambda}(\mathbf{x}, \mathbf{x}') \Psi_{\lambda}^{\dagger}(\mathbf{x}) \Psi_{\lambda}^{\dagger}(\mathbf{x}') \Psi_{\lambda}(\mathbf{x}') \Psi_{\lambda}(\mathbf{x}) \\ + \frac{1}{2} \sum_{\lambda \neq \lambda'} \int d\mathbf{x} \int d\mathbf{y} V_{\lambda\lambda'}(\mathbf{x}, \mathbf{y}) \Psi_{\lambda}^{\dagger}(\mathbf{x}) \Psi_{\lambda'}^{\dagger}(\mathbf{y}) \Psi_{\lambda'}(\mathbf{y}) \Psi_{\lambda}(\mathbf{x}) \end{aligned} \quad (2.1)$$

where Ψ and Ψ^{\dagger} are the annihilation and creation field operators for an electron ($\lambda = e$) or an hole ($\lambda = h$). In Eq. (2.1), T_{λ} is the electron and hole kinetic energy, $V_{\lambda\lambda}$ is the intralayer repulsive interaction between same charges and $V_{\lambda\lambda'}$ is the attractive interlayer interaction between electrons and holes. The spatial coordinate \mathbf{x} refers to the electron layer while \mathbf{y} refers to the hole layer.

Noticing that:

$$V_{eh}(\mathbf{x}, \mathbf{y}) \Psi_e^{\dagger}(\mathbf{x}) \Psi_h^{\dagger}(\mathbf{y}) \Psi_h(\mathbf{y}) \Psi_e(\mathbf{x}) = V_{he}(\mathbf{y}, \mathbf{x}) \Psi_h^{\dagger}(\mathbf{y}) \Psi_e^{\dagger}(\mathbf{x}) \Psi_e(\mathbf{x}) \Psi_h(\mathbf{y}), \quad (2.2)$$

the Hamiltonian states:

$$\begin{aligned} \hat{H} = \sum_{\lambda} \int \Psi_{\lambda}^{\dagger}(\mathbf{x}) T_{\lambda}(\mathbf{x}) \Psi_{\lambda}(\mathbf{x}) d\mathbf{x} + \frac{1}{2} \sum_{\lambda} \int V_{\lambda\lambda}(\mathbf{x}, \mathbf{x}') \Psi_{\lambda}^{\dagger}(\mathbf{x}) \Psi_{\lambda}^{\dagger}(\mathbf{x}') \Psi_{\lambda}(\mathbf{x}') \Psi_{\lambda}(\mathbf{x}) d\mathbf{x} d\mathbf{x}' \\ + \int V_{eh}(\mathbf{x}, \mathbf{y}) \Psi_e^{\dagger}(\mathbf{x}) \Psi_h^{\dagger}(\mathbf{y}) \Psi_h(\mathbf{y}) \Psi_e(\mathbf{x}) d\mathbf{x} d\mathbf{y}. \end{aligned} \quad (2.3)$$

Because the carriers are strongly confined to 2D layers, the field operator $\Psi_e(\mathbf{x})$ ($\Psi_h(\mathbf{y})$) is separable in the in-plane x (y) and out-plane x_{\perp} (y_{\perp}) spatial coordinate.

$$\Psi_e(x, x_{\perp}) = \psi_e(x) \phi_e(x_{\perp}), \quad (2.4)$$

$$\Psi_h(y, y_{\perp}) = \psi_h(y) \phi_h(y_{\perp}). \quad (2.5)$$

The kinetic energy T_{λ} can be separated in the in-plane and out-plane spatial components:

$$T_e(\mathbf{x}) = T_e(x) + T_e(x_{\perp}) - \mu_e \quad (2.6)$$

$$T_e(\mathbf{y}) = T_h(y) + T_h(y_{\perp}) - \mu_h \quad (2.7)$$

where μ_e (μ_h) is the electron (hole) single-particle chemical potential.

Here will we assume that each layer is in the quasi-2D regime, meaning that only a single mode $\phi_{\lambda}(x_{\perp})$ in the perpendicular direction is occupied, for the electron layer as well as the hole layer. Since $\int dx_{\perp} \phi_{\lambda}^*(x_{\perp}) \phi_{\lambda}(x_{\perp}) = 1$, we obtain for the kinetic energy

$$\begin{aligned} \hat{K} = \sum_{\lambda} \int d\mathbf{x} \Psi_{\lambda}^{\dagger}(\mathbf{x}) T_{\lambda}(\mathbf{x}) \Psi_{\lambda}(\mathbf{x}) \\ = K_{\perp} + \sum_{\lambda} \int dx \psi_{\lambda}^{\dagger}(x) (T_{\lambda}(x) - \mu_{\lambda}) \psi_{\lambda}(x), \end{aligned} \quad (2.8)$$

where

$$K_{\perp} = \sum_{\lambda} \int dx_{\perp} \phi_{\lambda}^*(x_{\perp}) T_{\lambda}(x_{\perp}) \phi_{\lambda}(x_{\perp}) \quad (2.9)$$

is a constant energy shift, due to the confinement in the perpendicular direction. As it is merely a constant shift, we will drop this term.

Taking the expectation value of the interlayer interaction, $V_{eh}(\mathbf{x} - \mathbf{y})$ over the perpendicular wave functions yields an effective interaction depending on the interlayer separation and the in-plane distance $|x - y|$:

$$\int dx_{\perp} \int dy_{\perp} \phi_e^*(x_{\perp}) \phi_h^*(y_{\perp}) V_{eh}(\mathbf{x} - \mathbf{y}) \phi_e(x_{\perp}) \phi_h(y_{\perp}) \approx V_{eh} \left(\sqrt{d^2 + (x - y)^2} \right). \quad (2.10)$$

Here, and for the rest of the thesis, we will assume that the confinement in the electron layer and in the hole layer is strong enough such that the above expression holds. This implies that the interlayer distance d should be larger than the confinement lengths

$$\ell_{\lambda,\perp} = \int dx_{\perp} \phi_{\lambda}^*(x_{\perp}) (x_{\perp} - \langle x_{\perp} \rangle)^2 \phi_{\lambda}(x_{\perp}), \quad (2.11)$$

In a typical experimental setup, for example, double-bilayer-graphene, $d \simeq 1 - 2$ nm and the confinement length in the perpendicular direction is $\ell_{\lambda,\perp} \simeq 0.5$ nm, so this assumption is satisfied. Using this assumption, the contribution of the interlayer interaction to the Hamiltonian becomes

$$V_{inter} = \int dx \int dy V_{eh} \left(\sqrt{d^2 + (x - y)^2} \right) \psi_e^{\dagger}(x) \psi_h^{\dagger}(y) \psi_e(y) \psi_e(x). \quad (2.12)$$

The quasi-2D approximation can also be made for the *intralayer* interaction. Here, the underlying assumption is that the distance between the electrons (or holes) is larger than the effective 2D confinement length. If this condition is violated, one can no longer assume that only a single perpendicular mode is occupied. This restricts the results to $r_s > \ell_{\lambda,\perp}$ (and we already required $d > \ell_{\lambda,\perp}$). Both conditions are well met in the experimental realizations. The contribution of intralayer interactions to the Hamiltonian then becomes

$$V_{intra} = \frac{1}{2} \sum_{\lambda} \int dx \int dx' V_{\lambda\lambda}(x - x') \psi_{\lambda}^{\dagger}(x) \psi_{\lambda}^{\dagger}(x') \psi_{\lambda}(x') \psi_{\lambda}(x). \quad (2.13)$$

In 1948, after the *matrix formulation of quantum mechanics* by Werner Heisenberg, Max Born and Pascual Jordan [154] and the *wave function formulation of quantum mechanics* by Erwin Schrödinger [155], a third interpretation of quantum mechanics was introduced by Richard Feynman [148], building on the work previously done by Paul Dirac [156]. The new development is called *path integral formulation of quantum mechanics*. The interpretation of quantum mechanics by Feynman can be summarized as follows. The quantum mechanical amplitude $K(B, t | A, 0)$ to find a particle at time t in a final state B , given that it was in an initial state A at time $t = 0$, is given by a weighted sum over all possible paths going from A to B in state space, in a time t , where the weight a path is given by to $e^{iS/\hbar}$, with S the classical action computed along the path. This amplitude also called the path integral propagator, is linked to the density matrix in thermal equilibrium at temperature $T = 1/(k_B\beta)$. One finds that the density matrix $\rho_{\beta}(B, A) = \langle B | \hat{\rho}_{\beta} | A \rangle$ is equal to the imaginary time propagator $K(B, -i\hbar\beta | A, 0)$ which can be found by analytic continuation of the dynamical propagator. Although it might be easier to use other methods to study quantum systems, Feynman's path integral approach has benefits in evaluating thermodynamic properties and in providing physical insights by looking at the structure of the action S . A detailed description of the path integral method can be found in refs. [148–152].

The path integral approach for quantum statistical field theory relies on the calculation of the partition function of the system:

$$\mathcal{Z} = \int \mathcal{D}[\psi_\lambda^\dagger, \psi_\lambda] \exp \left\{ -S[\psi_\lambda^\dagger, \psi_\lambda] / \hbar \right\}. \quad (2.14)$$

The sum (integral) now runs over all possible field configurations rather than all paths of individual particles. The transition to imaginary time $\tau = it$ provides each field configuration with a weight $e^{-S/\hbar}$ where S is the euclidean action [148]. In the case of bilayer electron-hole system the action S is given by:

$$\begin{aligned} S[\psi_\lambda^\dagger, \psi_\lambda] = & \int_0^\beta d\tau \left[\sum_\lambda \left(\int dx \psi_{\lambda,\tau}^\dagger(x) (\partial_\tau + T_\lambda - \mu_\lambda) \psi_{\lambda,\tau}(x) \right. \right. \\ & + \frac{1}{2} \int dx \int dx' V_{\lambda\lambda}(x, x') \psi_{\lambda,\tau}^\dagger(x) \psi_{\lambda,\tau}^\dagger(x') \psi_{\lambda,\tau}(x') \psi_{\lambda,\tau}(x) \Big) \\ & \left. + \int dx \int dy V_{eh}(x, y) \psi_{e,\tau}^\dagger(x) \psi_{h,\tau}^\dagger(y) \psi_{h,\tau}(y) \psi_{e,\tau}(x) \right], \end{aligned} \quad (2.15)$$

in the partial derivative over the imaginary time, τ is needed to turn the Hamiltonian into a Lagrangian and the integral over τ of the Lagrangian yields the Euclidean action. As before, $\beta = 1/k_B T$ is the inverse temperature with k_B Boltzmann constant.

The interaction terms, both interlayer and intralayer, are quartic in the fermionic field, making analytical integration over the fermionic field ψ impossible. To tackle this issue, the Hubbard-Stratonovich transformation is widely used [157–159]. This transformation effectively decouples the four fermionic terms into two fermionic terms coupled to an auxiliary bosonic field, enabling Gaussian functional integration. This leaves the choice of which pairs of fermionic operators to select open. For the intralayer term, possible combinations of fermionic operators include: $\psi_e^\dagger(x) \psi_e(x)$, termed the Hartree or direct channel; $\psi_e^\dagger(x) \psi_e(x')$, termed the Fock or exchange channel; and $\psi_e^\dagger(x) \psi_e^\dagger(x')$, termed the Bogoliubov pair channel.

Importantly, regardless of the chosen channel, the action remains exact, no approximations are applied with the Hubbard-Stratonovich transformation. However, performing the path integral over the auxiliary Hubbard-Stratonovich field in any channel is challenging, often requiring additional approximations. In our system, we adopt the mean-field approximation [159], leading to three potential outcomes:

- (a) Applying mean-field to the direct channel results in the loss of Fock exchange energy, leaving only the direct Hartree correlation term. Considering a uniform neutralizing background in each layer cancels out the Hartree term. This gives a zero contribution.
- (b) Applying mean-field to the pairing channel eliminates both the Fock and Hartree terms, leaving only the Bogoliubov pairing term. Given the unlikelihood of intralayer electron-electron or hole-hole pairing in this system, the pairing channel is excluded. This gives a zero contribution.
- (c) Applying mean-field to the exchange channel retains only the Fock exchange energy correlation term [160]. This gives a non-zero contribution and represents the only viable choice for the intralayer interaction.

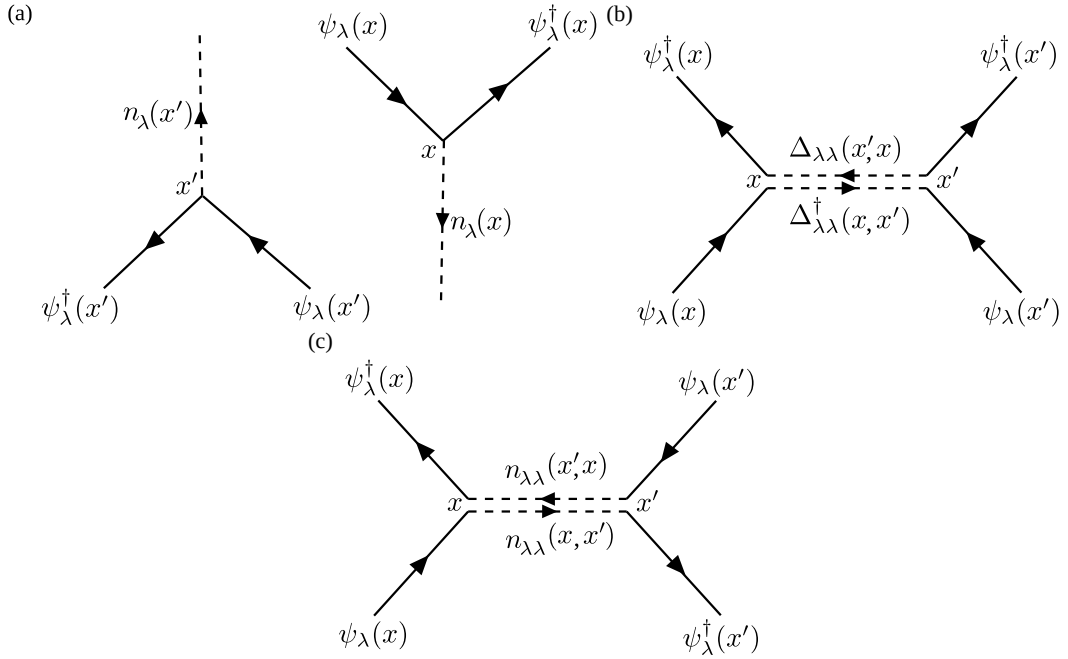


FIGURE 2.1: The Feynman diagrammatic representation of the mean-field Hartree channel (a), pairing channel (b) and Fock channel (c) to decouple the intralayer interaction term through the Hubbard-Stratonovich transformation.

The Hubbard-Stratonovich transformation of the intralayer term in the exchange channel reads:

$$\begin{aligned}
 & \exp \left[-\frac{1}{2} \sum_{\lambda} \int d\tau \int dx \int dx' V_{\lambda\lambda}(x, x') \psi_{\lambda,\tau}^{\dagger}(x) \psi_{\lambda,\tau}^{\dagger}(x') \psi_{\lambda,\tau}(x') \psi_{\lambda,\tau}(x) \right] \\
 & = \int \mathcal{D}[\Gamma_{\lambda,\tau}] \exp \left[-\frac{1}{2} \sum_{\lambda} \int d\tau \int dx \int dx' \left(\Gamma_{\lambda,\tau}(x, x') \psi_{\lambda,\tau}^{\dagger}(x) \psi_{\lambda,\tau}(x') \right. \right. \\
 & \quad \left. \left. + \Gamma_{\lambda,\tau}(x', x) \psi_{\lambda,\tau}^{\dagger}(x') \psi_{\lambda,\tau}(x) - \frac{\Gamma_{\lambda,\tau}(x, x') \Gamma_{\lambda,\tau}(x', x)}{V_{\lambda\lambda}(x, x')} \right) \right], \quad (2.16)
 \end{aligned}$$

where $\Gamma_{\lambda,\tau}(x, x') = V_{\lambda\lambda}(x, x') \psi_{\lambda,\tau}^{\dagger}(x') \psi_{\lambda,\tau}(x)$ is the bosonic auxiliary field introduced by the Hubbard-Stratonovich transformation to decouple the intralayer term. The mean-field approximation can be performed by taking the mean expectation value of the bosonic field,

$$\Gamma_{\lambda}^{MF}(x, x') = \langle V_{\lambda\lambda}(x, x') \psi_{\lambda,\tau}^{\dagger}(x') \psi_{\lambda,\tau}(x) \rangle = V_{\lambda\lambda}(x, x') n_{\lambda}(x, x'), \quad (2.17)$$

where $n_{\lambda,\tau}(x, x')$ is the density matrix. Eq. (2.16) becomes:

$$\begin{aligned}
 & \int \mathcal{D}[n_{\lambda}] \exp \left[-\frac{1}{2} \sum_{\lambda} \int d\tau \int dx \int dx' \left(V_{\lambda\lambda}(x, x') n_{\lambda}(x, x') \psi_{\lambda,\tau}^{\dagger}(x) \psi_{\lambda,\tau}(x') \right. \right. \\
 & \quad \left. \left. + V_{\lambda\lambda}(x', x) n_{\lambda}(x', x) \psi_{\lambda,\tau}^{\dagger}(x') \psi_{\lambda,\tau}(x) - n_{\lambda}(x, x') n_{\lambda}(x', x) V_{\lambda\lambda}(x, x') \right) \right]. \quad (2.18)
 \end{aligned}$$

Since $V_{\lambda\lambda}(x, x') = V_{\lambda\lambda}(x', x)$ the intralayer term simplifies to:

$$\int \mathcal{D}[n_\lambda] \exp \left[-\frac{1}{2} \sum_\lambda \int d\tau \int dx \int dx' \left(2V_{\lambda\lambda}(x, x') n_\lambda(x, x') \psi_{\lambda,\tau}^\dagger(x) \psi_{\lambda,\tau}(x') - n_\lambda(x, x') n_\lambda(x', x) V_{\lambda\lambda}(x, x') \right) \right]. \quad (2.19)$$

For the interlayer term instead the transformation is performed in the pairing channel $\Psi_e(x)\Psi_h(y)$ [158, 159], and the mean-field approximation results in the introduction of the bosonic pair field $\Delta_\tau(x, y)$, which represents the order parameter of exciton superfluid phase. The Hubbard-Stratonovic transformation of the interlayer term results:

$$\exp \left[-\int_0^\beta d\tau \int dx \int dy V_{eh}(x, y) \psi_{e,\tau}^\dagger(x) \psi_{h,\tau}^\dagger(y) \psi_{h,\tau}(y) \psi_{e,\tau}(x) \right] = \int \mathcal{D}[\Delta, \Delta^\dagger] \exp \left[-\int_0^\beta d\tau \int dx \int dy \left(\frac{|\Delta_\tau(x, y)|^2}{V_{eh}(x, y)} + \Delta_\tau^\dagger(x, y) \psi_{e,\tau}(x) \psi_{h,\tau}(y) + \Delta_\tau(x, y) \psi_{e,\tau}^\dagger(x) \psi_{h,\tau}^\dagger(y) \right) \right]. \quad (2.20)$$

Replacing Eq. (2.20) in the partition function one obtains:

$$\begin{aligned} \mathcal{Z} &= \int \mathcal{D}[\psi^\dagger, \psi, \Delta^\dagger, \Delta, n] \exp [-S(\psi^\dagger, \psi, \Delta^\dagger, \Delta, n) / \hbar] \\ &= \int \mathcal{D}[\psi^\dagger, \psi, \Delta^\dagger, \Delta, n] \exp \left\{ -\sum_\lambda \int_0^\beta d\tau \int dx \left[\psi_{\lambda,\tau}^\dagger(x) (\partial_\tau + T_\lambda - \mu_\lambda) \psi_{\lambda,\tau}(x) \right. \right. \\ &\quad + \frac{1}{2} \int dx' V_{\lambda\lambda}(x, x') n_\lambda(x, x') \left(2\psi_{\lambda,\tau}^\dagger(x) \psi_{\lambda,\tau}(x') - n_\lambda(x', x) \right) \\ &\quad \left. \left. + \int dy \left(\frac{|\Delta_\tau(x, y)|^2}{V_{eh}(x, y)} + \Delta_\tau^\dagger(x, y) \psi_{e,\tau}(x) \psi_{h,\tau}(y) + \Delta_\tau(x, y) \psi_{e,\tau}^\dagger(x) \psi_{h,\tau}^\dagger(y) \right) \right] \right\}. \quad (2.21) \end{aligned}$$

The partition function is now quadratic in the fermionic field ψ . Before proceeding with the Gaussian integration it is useful to change the momentum space representation, by introducing the Fourier transformation of the fermionic and bosonic fields:

$$\psi_{\lambda,\tau}(x) = \frac{1}{\sqrt{\beta\mathcal{S}}} \sum_{k,n} e^{-i\omega_n\tau + ikx} \psi_{\lambda,n}(k), \quad (2.22)$$

$$n_e(x, x') = \frac{1}{\sqrt{\beta\mathcal{S}}} \sum_{p,m} e^{ip(x-x')} n_e(p), \quad (2.23)$$

$$\Delta_\tau(x, y) = \frac{1}{\sqrt{\beta\mathcal{S}}} \sum_{q,l} e^{-i\tilde{\omega}_m\tau + iq(x-y)} \Delta_m(q), \quad (2.24)$$

$$V_{ee}(z) = \frac{1}{\mathcal{S}} \sum_q e^{iqz} V_{ee}(q), \quad (2.25)$$

$$V_{eh}(z) = \frac{1}{\mathcal{S}} \sum_q e^{iqz} V_{eh}(q), \quad (2.26)$$

where $\omega_n = 2\pi(n+1)/\beta$ and $\tilde{\omega}_m = 2\pi m/\beta$ are the fermionic and bosonic Matsubara frequencies, respectively. For simplicity, we use the same prefactor $1/\sqrt{\beta\mathcal{S}}$ for Ψ , n and

2.1. Path Integral Approach for Electron-Hole superfluidity

Δ . After the Fourier transformation, we will fix the dimensionality of each quantity. The (Dirac and Kronecker) deltas are given by:

$$\frac{1}{\beta S} \int_0^\beta d\tau \int dx e^{-i(\omega_n - \omega_{n'})\tau + i(k' - k)x} = \delta(k - k') \delta_{nn'}. \quad (2.27)$$

The Fourier transformation of the kinetic term is given by:

$$\begin{aligned} \hat{K} &= \sum_\lambda \int_0^\beta d\tau \int dx \frac{1}{\sqrt{\beta S}} \sum_{k,n} e^{i\omega_n \tau - ikx} \psi_{\lambda,n}^\dagger(k) \left(\partial_\tau - \frac{\hbar^2 \nabla^2}{2m} - \mu_\lambda \right) \frac{1}{\sqrt{\beta S}} \sum_{k',n'} e^{-i\omega_{n'} \tau + ik'x} \psi_{\lambda,n'}(k') \\ &= \sum_\lambda \frac{1}{\beta S} \sum_{\substack{n,k \\ n',k'}} \int_0^\beta d\tau e^{-i\tau(\omega_n - \omega_{n'})} \int dx e^{-i(k-k')x} \psi_{\lambda,n}^\dagger(k) \left(-i\omega_{n'} + \frac{\hbar^2 k'^2}{2m} - \mu_\lambda \right) \psi_{\lambda,n'}(k') \\ &= \sum_\lambda \sum_{\substack{n,k \\ n',k'}} \delta_{n,n'} \delta(k - k') \psi_{\lambda,n}^\dagger(k) \left(-i\omega_{n'} + \frac{\hbar^2 k'^2}{2m} - \mu_\lambda \right) \psi_{\lambda,n'}(k') \\ &= \sum_\lambda \sum_{k,n} \psi_{\lambda,n}^\dagger(k) \left(-i\omega_n + \frac{\hbar^2 k^2}{2m} - \mu_\lambda \right) \psi_{\lambda,n}(k). \end{aligned} \quad (2.28)$$

For the intralayer interaction term, the Fourier transform is divided into the two terms of Eq.(2.19). The first term reads:

$$\begin{aligned} &\frac{1}{2} \sum_\lambda \int_0^\beta d\tau \int dx \int dx' 2V_{\lambda\lambda}(x, x') n_\lambda(x, x') \psi_\lambda^\dagger(x) \psi_\lambda(x') \\ &= \frac{1}{2(\beta S)^{\frac{3}{2}}} \sum_\lambda \sum_{\substack{n_1, k_1 \\ n_2, k_2}} \sum_{m,p} \int_0^\beta d\tau \int dx \int dx' e^{i\omega_1 \tau - ik_1 x} \psi_{\lambda, n_1}^\dagger(k_1) \\ &\quad \times 2V_{\lambda\lambda}(x - x') e^{-ip(x-x')} n_\lambda(p) e^{-i\omega_2 \tau + ik_2 x'} \psi_{\lambda, n_2}(k_2), \end{aligned} \quad (2.29)$$

where $z = x - x'$, so replacing $x' = x - z$ this expression reduces to:

$$\begin{aligned} &\frac{1}{2(\beta S)^{\frac{3}{2}}} \sum_\lambda \sum_{\substack{n_1, k_1 \\ n_2, k_2}} \sum_p \int_0^\beta d\tau e^{-i\tau(\omega_2 - \omega_1)} \int dx e^{ix(k_2 - k_1)} \int dz 2V_{\lambda\lambda}(z) e^{iz(p - k_2)} \\ &\quad \times \psi_{\lambda, n_1}^\dagger(k_1) n_\lambda(p) \psi_{\lambda, n_2}(k_2), \end{aligned} \quad (2.30)$$

The first two integrals are the definition of Dirac delta Eq. (2.27), and the third one is the Fourier transform of the intralayer Coulomb repulsion. Thus:

$$\begin{aligned} &\frac{1}{2\sqrt{\beta S}} \sum_\lambda \sum_{\substack{n_1, k_1 \\ n_2, k_2}} \sum_p \delta_{\omega_2 - \omega_1} \delta(k_2 - k_1) 2V_{\lambda\lambda}(p - k_2) \psi_{e, n_1(k_1)}^\dagger n_m(p) \psi_{e, n_2}(k_2) = \\ &= \frac{1}{\sqrt{\beta S}} \sum_\lambda \sum_{n,k} \psi_{\lambda, n}^\dagger(k) \left(\sum_p V_{\lambda\lambda}(p - k) n_\lambda(p) \right) \psi_{\lambda, n}(k). \end{aligned} \quad (2.31)$$

The Fourier transform of the second term of the Eq. (2.19) is:

$$\begin{aligned}
 & \frac{1}{2} \sum_{\lambda} \int_0^{\beta} d\tau \int dx \int dx' n_{\lambda}(x, x') n_{\lambda}(x', x) V_{\lambda\lambda}(x, x') \\
 &= \frac{1}{2S} \sum_{\lambda} \sum_{\substack{p_1 \\ p_2}} \int dx \int dx' V_{\lambda\lambda}(x - x') e^{ip_1(x-x')} n_{\lambda}(p_1) e^{ip_2(x'-x)} n_{\lambda}(p_2) \\
 &= \frac{1}{2S} \sum_{\lambda} \sum_{p_1, p_2} \int dx \int dz V_{\lambda\lambda}(z) e^{iz(p_2-p_1)} n_{\lambda}(p_1) n_{\lambda}(p_2) \\
 &= \frac{1}{2} \sum_{\lambda} \sum_{p_2, p_1} V_{\lambda\lambda}(p_2 - p_1) n_{\lambda}(p_1) n_{\lambda}(p_2) .
 \end{aligned} \tag{2.32}$$

The intralayer interaction term in momentum space reads:

$$\begin{aligned}
 V_{intra} &= \sum_{\lambda} \frac{1}{\sqrt{\beta S}} \sum_{n, k} \psi_{\lambda, n}^{\dagger}(k) \left(\sum_p V_{\lambda\lambda}(p - k) n_{\lambda}(p) \right) \psi_{\lambda, n}(k) \\
 &\quad - \frac{1}{2} \sum_{p_2, p_1} V_{\lambda\lambda}(p_2 - p_1) n_{\lambda}(p_1) n_{\lambda}(p_2) .
 \end{aligned} \tag{2.33}$$

For the interlayer interaction term, the Fourier transform of Eq. (2.12) is:

$$\begin{aligned}
 V_{inter} &= \int d\tau \int dx \int dy V_{eh}(x, y) \psi_e^{\dagger}(x) \psi_h^{\dagger}(y) \psi_h(y) \psi_e(x) = \\
 &= \frac{1}{(\beta S)^2} \sum_{\substack{n_1, k_1 \\ n_2, k_2}} \sum_{\substack{n_3, k_3 \\ n_4, k_4}} \int d\tau \int dx \int dy V_{eh}(x - y) e^{i\omega_1\tau - ik_1x} \psi_{ek_1n_1}^{\dagger} e^{i\omega_2\tau - ik_2y} \psi_{hk_2n_2}^{\dagger} \\
 &\quad \times e^{-i\omega_3\tau + ik_3y} \psi_{hk_3n_3} e^{-i\omega_4\tau + ik_4x} \psi_{ek_4n_4} ,
 \end{aligned} \tag{2.34}$$

replacing $x = z + y$ one obtains:

$$\begin{aligned}
 V_{inter} &= \frac{1}{(\beta S)^2} \sum_{\substack{n_1, k_1 \\ n_2, k_2}} \sum_{\substack{n_3, k_3 \\ n_4, k_4}} \int d\tau e^{i\tau(\omega_2 + \omega_1 - \omega_3 - \omega_4)} \int dy e^{-iy(k_2 - k_3 - k_4 + k_1)} \\
 &\quad \times \int dz V_{eh}(z) e^{-iz(k_1 - k_4)} \psi_{e, n_1}^{\dagger}(k_1) \psi_{h, n_2}^{\dagger}(k_2) \psi_{h, n_3}(k_3) \psi_{e, n_4}(k_4) .
 \end{aligned} \tag{2.35}$$

The first two integrals give the delta Dirac functions while the third one is the Fourier transform of the attractive interlayer Coulomb interaction. Thus:

$$\begin{aligned}
 V_{inter} &= \frac{1}{\beta S} \sum_{\substack{n_1, k_1 \\ n_2, k_2}} \sum_{\substack{n_3, k_3 \\ n_4, k_4}} \delta(\omega_2 + \omega_1 - \omega_3 - \omega_4) \delta(k_2 - k_3 - k_4 + k_1) V_{eh}(k_1 - k_4) \\
 &\quad \times \psi_{e, n_1}^{\dagger}(k_1) \psi_{h, n_2}^{\dagger}(k_2) \psi_{h, n_3}(k_3) \psi_{e, n_4}(k_4) .
 \end{aligned} \tag{2.36}$$

The dependence on four different momenta is simplified by imposing that electron-hole pairs have zero centre of mass, as in BCS theory [111]. This means that the interacting electrons and holes must have opposite momenta, as shown in Fig. 2.2.

2.1. Path Integral Approach for Electron-Hole superfluidity

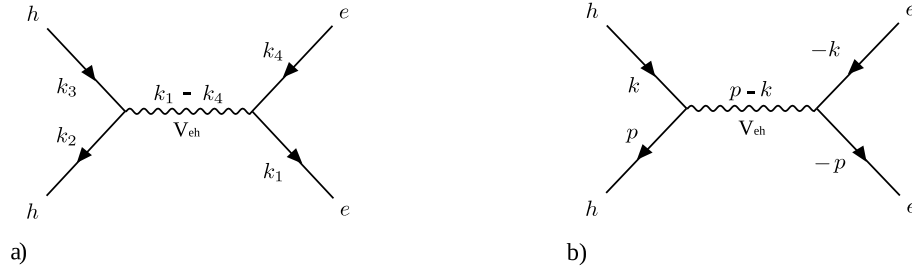


FIGURE 2.2: a) Generic electron-hole scattering through an attractive Coulomb interaction V_{eh} . b) Electron-hole scattering imposing zero centre of mass electron-hole pair condition.

With the notation $k_3 = k$, $k_4 = -k$, $k_2 = p$, $k_1 = -p$, and the same notation for the Matsubara indices, the interlayer term states:

$$V_{inter} = \frac{1}{\beta S} \sum_{\substack{n,k \\ l,p}} V_{eh}(k-p) \psi_{e,-n}^\dagger(-p) \psi_{h,n}^\dagger(p) \psi_{h,-l}(k) \psi_{e,l}(-k). \quad (2.37)$$

With this condition, the Fourier transform on the intralayer term after the Hubbard-Stratonovic transformation, Eq.(2.20) is:

$$\begin{aligned} V_{inter} &= \frac{|\Delta_\tau(x,y)|^2}{V_{eh}(x,y)} + \Delta_\tau^\dagger(x,y) \psi_{e,\tau}(x) \psi_{h,\tau}(y) + \Delta_\tau(x,y) \psi_{e,\tau}^\dagger(x) \psi_{h,\tau}^\dagger(y) \\ &= \sum_{n,k,p} \sqrt{\frac{S}{\beta}} \left(\Delta^\dagger(k) \psi_{h,-n}(k) \psi_{e,n}(-k) + \Delta(p) \psi_{e,-n}^\dagger(p) \psi_{h,n}^\dagger(-p) + S^2 \frac{\Delta^\dagger(k) \Delta(p)}{V_{eh}(k-p)} \right). \end{aligned} \quad (2.38)$$

The partition function after the Fourier transform becomes:

$$\begin{aligned} \mathcal{Z} &= \int \mathcal{D}[\psi, n, \Delta] \exp \left[\right. \\ &\quad - \sum_\lambda \sum_{kn} \psi_{\lambda,n}^\dagger(k) \left[\left(-i\omega_n + \frac{\hbar^2 k^2}{2m} - \mu_\lambda \right) - \frac{1}{\sqrt{\beta S}} \sum_p V_{\lambda\lambda}(p-k) n_\lambda(p) \right] \psi_{\lambda,n}(k) \\ &\quad - \sum_\lambda \sum_{p_2 p_1} \frac{V_{\lambda\lambda}(p_2 + p_1) n_\lambda(p_1) n_\lambda(p_2)}{2} \\ &\quad \left. + \sum_{n,k,p} \sqrt{\frac{S}{\beta}} \left(\Delta^\dagger(k) \psi_{h,-n}(k) \psi_{e,n}(-k) + \Delta(p) \psi_{e,-n}^\dagger(p) \psi_{h,n}^\dagger(-p) \right) + S^2 \frac{\Delta^\dagger(k) \Delta(p)}{V_{eh}(k-p)} \right], \end{aligned} \quad (2.39)$$

We fix the dimensionality Ψ , n and Δ as follows: $\Delta(q) \rightarrow \Delta(q) \sqrt{\beta/S}$ and $n(q) \rightarrow n(q) \sqrt{\beta/S}$.

The action in the momentum space is quadratic in the fermionic field, allowing the Gaussian field integration. To do so, we rewrite the action in a matrix form using the

Nambu spinors [161]:

$$\eta_n(k) = \begin{pmatrix} \psi_{e,-n}(-k) \\ \psi_{h,n}^\dagger(k) \end{pmatrix} \quad \bar{\eta}_n(k) = (\psi_{e,-n}^\dagger(-k) \quad \psi_{h,n}(k)) \quad (2.40)$$

Eq. (2.39) in Nambu formalism reads:

$$\begin{aligned} \mathcal{Z} = \int \mathcal{D}[\eta, n, \Delta] \exp \left[- \sum_{k,n} \bar{\eta}_n(k) (-\mathbf{G}^{-1}) \eta_n(k) - \frac{\beta}{S} \sum_{\lambda} \sum_{p_2, p_1} \frac{V_{\lambda\lambda}(p_2 - p_1) n_{\lambda}(p_1) n_{\lambda}(p_2)}{2} \right. \\ \left. + \beta S \sum_{k,p} \frac{\Delta^\dagger(k) \Delta(p)}{V_{eh}(k-p)} \right]. \end{aligned} \quad (2.41)$$

where $-\mathbf{G}^{-1}$ is the Gor'kov single-particle propagator:

$$-\mathbf{G}^{-1} = \begin{pmatrix} -i\omega_n + \xi_e(k) & -\Delta(k) \\ -\Delta^\dagger(k) & -i\omega_n - \xi_h(k) \end{pmatrix}, \quad (2.42)$$

Eq. (2.42) is formally identical to the single-particle propagator in BCS theory [159]. The intralayer correlation in the Hartree-Fock approximation acts like a deformation of the single-particle parabolic dispersion relation. Here, $\xi_\lambda(k) = \epsilon_\lambda(k) - \mu_\lambda - \frac{1}{S} \sum_p V_{\lambda\lambda}(p-k) n_\lambda(p)$. In Chap. 4 we will explore the effect of the $V_{\lambda\lambda}$ term in $\xi_\lambda(k)$ on the superfluid properties.

The Gaussian integral over the spinor $\eta_n(k)$ results in:

$$\begin{aligned} \mathcal{Z} &= \int \mathcal{D}[n, \Delta] \exp[-S_{eff}[\Delta, \Delta^\dagger, n]/\hbar] = \\ &= \int \mathcal{D}[n, \Delta] \exp \left[\sum_{k,n} \ln \left[-\det(\mathbf{G}^{-1})_{k,n} \right] - \frac{\beta}{S} \sum_{\lambda} \sum_{p_2, p_1} \frac{V_{\lambda\lambda}(p_2 - p_1) n_{\lambda}(p_1) n_{\lambda}(p_2)}{2} \right. \\ &\quad \left. + \beta S \sum_{k,p} \frac{\Delta^\dagger(k) \Delta(p)}{V_{eh}(k-p)} \right], \end{aligned} \quad (2.43)$$

where S_{eff} is the effective action: the action of the system after the Hubbard-Stratonovic transformation and the integration of the fermionic fields.

The result still contains a path integral over the bosonic pair fields Δ and n . This integral cannot yet be done analytically, however, with the action in this form, we have access to additional information about the bosonic fields.

Why go through all the trouble of introducing these bosonic fields, if in the end the result is another path integral that cannot be done exactly? The advantage of having the action written with the bosonic fields is that we can use our interpretation of these collective fields to introduce saddle-point approximations. For example, if we assume that the pairs form a Bose-Einstein condensate, then the mode in which they condense is macroscopically occupied, and this 'classical' field configuration will provide the dominant contribution to the path integral. A judicious choice of saddle point configurations allows to add gaussian fluctuations and perform the approximated integral analytically.

In general, the saddle point values of the fields are obtained by minimizing the effective action. For the pair field, this leads to the following gap equation for the saddle point $\Delta(q)$:

$$\begin{aligned}
 & \frac{\partial \mathcal{S}_{eff}}{\partial \Delta^\dagger(q)} = 0 \\
 & \sum_{k,n} \frac{1}{\det(-\mathbf{G}^{-1})_{k,n}} \frac{\partial(\det(-\mathbf{G}^{-1}))_{k,n}}{\partial \Delta^\dagger(q)} + \beta \mathcal{S} \sum_{k,p} \frac{1}{V_{eh}(k-p)} \frac{\partial \Delta^\dagger(k) \Delta(p)}{\partial \Delta^\dagger(q)} = 0 \\
 & \sum_n \frac{-\Delta(q)}{(-i\omega_n + \xi_e(q))(-i\omega_n - \xi_h(q)) - |\Delta(q)|^2} + \beta \mathcal{S} \sum_p \frac{\Delta(p)}{V_{eh}(q-p)} = 0 \\
 & \sum_n \frac{-\Delta(q)}{-\omega_n^2 - i\omega_n(\xi_e - \xi_h) - \xi_e \xi_h - |\Delta(q)|^2} + \beta \mathcal{S} \sum_p \frac{\Delta(p)}{V_{eh}(q-p)} = 0 \\
 & \sum_p \frac{\Delta(p)}{V_{eh}(q-p)} = \frac{1}{\beta \mathcal{S}} \sum_n \frac{\Delta(q)}{-\omega_n^2 - 2i\omega_n \Delta \xi(q) - \bar{\xi}^2(q) + \Delta \bar{\xi}^2(q) - |\Delta(q)|^2}. \quad (2.44)
 \end{aligned}$$

In the most general case of unequal electron and hole effective masses $m_e \neq m_h$ and single-particle chemical potential $\mu_e \neq \mu_h$ it is convenient to introduce the following notation:

$$\bar{\xi}(k) = \frac{\bar{\epsilon}(k) - \bar{\mu} - \bar{U}(k)}{2} \quad \text{and} \quad \Delta \bar{\xi}(k) = \frac{\Delta \epsilon(k) - \Delta \mu - \Delta U(k)}{2} \quad (2.45)$$

with:

$$\bar{\epsilon}(k) = \epsilon_h(k) + \epsilon_e(k) \quad \text{and} \quad \Delta \epsilon(k) = \epsilon_e(k) - \epsilon_h(k), \quad (2.46)$$

$$\bar{\mu} = \mu_h + \mu_e \quad \text{and} \quad \Delta \mu = \mu_e - \mu_h, \quad (2.47)$$

$$\bar{U}(k) = V_{e,e}(k)n_e(k) + V_{h,h}(k)n_h(k) \quad \text{and} \quad \Delta U(k) = V_{e,e}(k)n_e(k) - V_{h,h}(k)n_h(k). \quad (2.48)$$

Eq. (2.44) can then be rewritten as [159, 162]:

$$\Delta(k) = \frac{1}{\beta \mathcal{S}} \sum_{q,n} V_{eh}(q-k) \frac{\Delta(q)}{(-\omega_n^2 - 2i\omega_n \Delta \bar{\xi}(q) - \bar{\xi}^2(q) + \Delta \bar{\xi}^2(q) - |\Delta(q)|^2)}. \quad (2.49)$$

After summing over the fermionic Matsubara frequency ω_n :

$$\Delta(k) = -\frac{1}{\mathcal{S}} \sum_q V_{eh}(q-k) \frac{\Delta(q)}{2\bar{E}(q)} (1 - f_-(q, T) - f_+(q, T)), \quad (2.50)$$

where $\bar{E}(q) = \sqrt{\bar{\xi}^2(q) + |\Delta(q)|^2}$ and $f_+(q, T) = n_F(\bar{E}(q) + \Delta \bar{\xi}(q), T)$, $f_-(q, T) = n_F(\bar{E}(q) - \Delta \bar{\xi}(q), T)$ are the Fermi distribution functions at temperature T . At zero temperature $T = 0$:

$$f_-(q, 0) = \begin{cases} 1 & \text{for } \bar{E}(q) < \Delta \bar{\xi}(q) \\ 0 & \text{for } \bar{E}(q) > \Delta \bar{\xi}(q), \end{cases} \quad (2.51)$$

$$f_+(q, 0) = \begin{cases} 1 & \text{for } \bar{E}(q) < -\Delta \bar{\xi}(q) \\ 0 & \text{for } \bar{E}(q) > -\Delta \bar{\xi}(q). \end{cases} \quad (2.52)$$

Combining Eq.(2.51) and Eq.(2.52) one obtains:

$$1 - f_-(q) - f_+(q) = \begin{cases} 1 & \text{for } \bar{E}(q) > |\Delta\zeta(q)| \\ 0 & \text{for } \bar{E}(q) < |\Delta\zeta(q)|. \end{cases} \quad (2.53)$$

If $|\zeta_h - \zeta_e|$ is too large it is not possible to form pairs. This value depends on the density, effective mass and chemical potential differences between the particles in the two layers. A similar effect appears in conventional BCS theory: if the Fermi energies of the two pairing partners differ by more than the gap, pairing is suppressed. This is called the Clogston limit [163], and has been generalized to the BEC-BCS crossover where it has been observed [164].

When $|\zeta_h - \zeta_e| < \bar{E}(q)$, the gap equation Eq. (2.50) at zero temperature reduces to:

$$\Delta(k) = -\frac{1}{S} \sum_q V_{eh}(q-k) \frac{\Delta(q)}{2\bar{E}(q)} \quad (2.54)$$

This relation is equivalent to the one obtained through the Bogoliubov amplitudes [75].

By imposing $\Delta(k) = \Delta_0(k)$ in the partition function, we can remove the functional integral over Δ field, and Eq.(2.43) reads:

$$\begin{aligned} \mathcal{Z} = \int \mathcal{D}[n] \exp[-S_{eff}[n]/\hbar] = \int \mathcal{D}[n] \exp \left[\sum_{k,n} \ln \left[-\det(-\mathbf{G}^{-1}(n))_{k,n} \right] \right. \\ \left. + \beta S \sum_{k,p} \frac{\Delta_0^\dagger(k)\Delta_0(p)}{V_{eh}(k-p)} - \frac{\beta}{S} \sum_\lambda \sum_{p_2,p_1} \frac{V_{\lambda\lambda}(p_2+p_1)n_\lambda(p_1)n_\lambda(p_2)}{2} \right]. \end{aligned} \quad (2.55)$$

The same procedure is adopted for the density n field. In the generic case of $n_e \neq n_h$ the action must be minimised for both densities.

For the density field $n_e(q)$:

$$\begin{aligned} \frac{\partial S_{eff}}{\partial n_e(q)} = 0 \\ \sum_{k,n} \frac{1}{\det(-\mathbf{G}^{-1})_{k,n}} \frac{\partial(\det(-\mathbf{G}^{-1}))_{k,n}}{\partial n_e(q)} - \frac{\beta}{S} \sum_\lambda \sum_{p_1,p_2} \frac{V_{\lambda\lambda}(p_2-p_1)}{2} \frac{\partial n_\lambda(p_1)n_\lambda(p_2)}{\partial n_e(q)} = 0 \\ \sum_{k,n} \frac{(-i\omega_n - \zeta_h(k))}{(-i\omega_n + \zeta_e(k))(-i\omega_n - \zeta_h(k)) - |\Delta(q)|^2} \frac{\partial \zeta_e(k)}{n_e(q)} - \frac{\beta}{S} \sum_p V_{ee}(p-q)n_e(p) = 0 \\ \sum_{k,n} \frac{(i\omega_n + \zeta_h(q))}{(-i\omega_n + \zeta_e(q))(-i\omega_n - \zeta_h(q)) - |\Delta(q)|^2} \frac{1}{S} V_{ee}(k-q) - \frac{\beta}{S} \sum_p V_{ee}(p-q)n_e(p) = 0 \\ \sum_{k,n} \frac{1}{\beta} \frac{(i\omega_n + \zeta_h(q))}{(-i\omega_n + \zeta_e(q))(-i\omega_n - \zeta_h(q)) - |\Delta(q)|^2} V_{ee}(k-q) = \sum_k V_{ee}(k-q)n_e(k) \\ \sum_n \frac{1}{\beta} \frac{(i\omega_n + \zeta_h(q))}{(-i\omega_n + \zeta_e(q))(-i\omega_n - \zeta_h(q)) - |\Delta(q)|^2} = n_e(k). \end{aligned} \quad (2.56)$$

Introducing $\bar{\zeta}$ and $\Delta\zeta$, the equation for the electron density of states reads:

$$n_e(k) = \sum_n \frac{1}{\beta} \frac{(i\omega_n + \bar{\zeta}(q) - \Delta\zeta(q))}{-\omega_n^2 - 2i\omega_n\Delta\zeta(q) - \bar{\zeta}^2(q) + \Delta\zeta^2(q) - |\Delta(q)|^2}. \quad (2.57)$$

2.2. Gap and number equation at zero temperature and equal electron-hole layers

After summing over the fermionic Matsubara frequencies, one obtains:

$$n_e(k) = \frac{1}{2} \left[\left(1 + \frac{\bar{\zeta}(k)}{\bar{E}(k)} \right) f_+(k) + \left(1 - \frac{\bar{\zeta}(k)}{\bar{E}(k)} \right) (1 - f_-(k)) \right]. \quad (2.58)$$

By minimizing instead respect to $n_h(k)$ the result is:

$$n_h(k) = \frac{1}{2} \left[\left(1 + \frac{\bar{\zeta}(k)}{\bar{E}(k)} \right) f_+(k) + \left(1 - \frac{\bar{\zeta}(k)}{\bar{E}(k)} \right) (1 - f_+(k)) \right]. \quad (2.59)$$

Replacing $n_e(k)$ and $n_h(k)$ in the partition function one obtains the saddle-point partition function of the system:

$$\begin{aligned} \mathcal{Z}_{sp} = \exp & \left[\sum_{kn} \ln \left[\det(-\mathbf{G}^{-1}(n))_{k,n} \right] + \beta S \sum_{k,p} \frac{\Delta_0^+(k)\Delta(p)}{V_{eh}(k-p)} \right. \\ & \left. - \frac{\beta}{2S} \sum_{\lambda} \sum_{p_2, p_1} V_{\lambda\lambda}(p_2 + p_1) n_{\lambda}(p_1) n_{\lambda}(p_2) \right]. \end{aligned} \quad (2.60)$$

The set of equations that regulate the saddle-point partition function of a generic electron-hole superfluid system at finite temperature are the following:

$$\Delta(k) = -\frac{1}{S} \sum_q V_{eh}(q-k) \frac{\Delta(q)}{2\bar{E}(q)} (1 - f_-(q) - f_+(q)) \quad (2.61)$$

$$n_e = \frac{1}{2} \sum_k \left[\left(1 + \frac{\bar{\zeta}(k)}{\bar{E}(k)} \right) f_+(k) + \left(1 - \frac{\bar{\zeta}(k)}{\bar{E}(k)} \right) (1 - f_-(k)) \right] \quad (2.62)$$

$$n_h = \frac{1}{2} \sum_k \left[\left(1 + \frac{\bar{\zeta}(k)}{\bar{E}(k)} \right) f_-(k) + \left(1 - \frac{\bar{\zeta}(k)}{\bar{E}(k)} \right) (1 - f_+(k)) \right] \quad (2.63)$$

$$\bar{E}(q) = \sqrt{\bar{\zeta}^2(q) + |\Delta(q)|^2} \quad (2.64)$$

$$\bar{\zeta}(k) = \frac{1}{2} \left[\epsilon_e(k) - \mu_e + \epsilon_h(k) - \mu_h - \frac{1}{S} \sum_p [V_{ee}(p-k)n_e(p) + V_{hh}(p-k)n_h(p)] \right] \quad (2.65)$$

Equation (2.61) is the so-called gap equation and Eq. (2.62)-(2.63) are the electron and hole number equations respectively. Solving this coupled set of equations one gets the behaviour of the gap energy, the chemical potential and the carrier densities for the system in the mean-field superfluid ground state at finite temperature.

2.2 Gap and number equation at zero temperature and equal electron-hole layers

For this thesis, we will restrict the calculation to the case of zero temperature, equal effective masses, and equal densities between the electron and hole layer. With $m_e = m_h = m$, and thus $\mu_e = \mu_h = \mu_s$, $V_{ee} = V_{hh} = V_S$, $V_{he} = V_{eh} = V_D$ and $T = 0$ the gap and number

equations read:

$$\Delta(k) = -\frac{1}{S} \sum_q V_D(|q-k|) \frac{\Delta(q)}{2E(q)}, \quad (2.66)$$

$$n = \frac{g_s g_v}{S} \sum_p n(p). \quad (2.67)$$

Where:

$$E(q) = \sqrt{\xi^2(q) + |\Delta(q)|^2}, \quad (2.68)$$

$$\xi(q) = \frac{\hbar^2 q^2}{2m} - \mu_s - \frac{1}{S} \sum_p V_S(|p-q|) n(p), \quad (2.69)$$

$$n(p) = \frac{1}{2} \left(1 - \frac{\xi(p)}{E(p)} \right), \quad (2.70)$$

where g_s and g_v are the spin and valley degeneracy.

The interlayer, V_D , and intralayer, V_S , interactions in the exciton gap and number equations are Coulomb long-range interactions, thus screening is an important ingredient to consider. In the next section, we calculate the effective screened intralayer and interlayer interaction for the gap and number equations in the Random Phase approximation.

2.3 Intralayer and Interlayer screened interaction

The formation of excitons in bilayer systems is due to the attractive finite-range Coulomb interaction between the opposite charged electrons and holes. Thus, unlike standard superconductors, the interaction originating superfluidity cannot be approximated with a contact-like interaction.

Due to the long-range nature of the interactions, the presence of other particles in the system strongly affects the interactions through screening processes. Increasing the particle density reduces the interparticle distance r_0 . Screening becomes important when r_0 becomes smaller than the interlayer distance d . A particle in one layer induces a charge density response, both in the same layer and in the opposite layer, thus both intralayer and the interlayer Coulomb interactions are strongly affected by screening.

Accounting for screening in the interlayer interaction is fundamental for a realistic description of bilayer exciton systems throughout the BCS-BEC crossover [48, 165]. The coupled BCS mean-field equations for the superfluid gap Δ_k and density n , remain a good approximation in the BCS-BEC crossover and BEC regimes at zero temperature also in 2D [166, 167]. However, the effect of the intralayer interaction with screening has not yet been studied.

Here we report for the first time a detailed and complete Random Phase approximation (RPA) calculation of both the screened interlayer and intralayer interactions, for a bilayer electron-hole system in the superfluid state. The calculation is based on the equation of motion of the Green's function.

2.3.1 Random Phase Approximation for the Screening: Green's function equation of motion approach

The screened interactions can be described by a Dyson equation [168]: a self-consistent equation which provides a relation between the bare interaction $V(q)$ and the dressed screened $W(q, \omega)$ interaction in a many-body system. It states:

$$W(q, \omega) = V(q) + V(q)\Pi^*(q, \omega)W(q, \omega), \quad (2.71)$$

where $\Pi^*(q, \omega)$ is the complete proper polarization consisting of an infinite series of all the orders, of all the interactions involved in the system. $\Pi^*(q, \omega)$ is generally simplified adopting approximations, depending on the type of system and interactions.

In the bilayer exciton system a comparison of the good agreement of zero-temperature superfluid properties calculated using the Random Phase approximation approach [169], with corresponding results calculated using diffusion quantum Monte Carlo [43], indicated that the Random Phase approximation approach should be a quantitatively good approximation for the effective screened interactions. In the Random Phase approximation, electrons respond as mutually non-interacting particles to a sum of the external potentials plus the mean-field Hartree potentials from the charge densities induced by the electrons [131].

The Dyson equation in the Random Phase approximation is:

$$W^{RPA}(q, \omega) = V(q) + V(q)\Pi_0(q, \omega)W^{RPA}(q, \omega), \quad (2.72)$$

where $\Pi_0(q, \omega)$ is the zero-order non interacting polarization function. The dressed RPA interaction $W^{RPA}(q, \omega)$ reads:

$$W^{RPA}(q, \omega) = \frac{V(q)}{1 - V(q)\Pi_0(q, \omega)}. \quad (2.73)$$

In equal mass and equal density electron-hole bilayer systems:

$$W^{RPA}(q, \omega) = \begin{pmatrix} V_S^{sc}(q, \omega) & V_D^{sc}(q, \omega) \\ V_D^{sc}(q, \omega) & V_S^{sc}(q, \omega) \end{pmatrix}, \quad (2.74)$$

where $V_{ee}^{sc}(q) = V_{hh}^{sc}(q) = V_S^{sc}(q)$ is the screened intralayer interaction and $V_{eh}^{sc}(q) = V_{he}^{sc}(q) = V_D^{sc}(q)$ is the screened interlayer interaction. The bare interaction matrix is

$$V(q) = \begin{pmatrix} V_S(q) & V_D(q) \\ V_D(q) & V_S(q) \end{pmatrix}, \quad (2.75)$$

where the bare intralayer $V_{ee}(q) = V_{hh}(q) = V_S(q)$ and interlayer $V_{eh}(q) = V_{he}(q) = V_D(q)$ interactions [170] are given by:

$$V_S(q) = \frac{2\pi e^2}{\epsilon\epsilon_0 q}, \quad (2.76)$$

$$V_D(q) = -\frac{2\pi e^2 e^{-qd}}{\epsilon\epsilon_0 q}, \quad (2.77)$$

with d the interlayer distance, ϵ_0 the vacuum electric permittivity and ϵ is the dielectric insulator permittivity. Then,

$$\Pi_0(q, \omega) = \begin{pmatrix} \Pi_0^N(q, \omega) & \Pi_0^A(q, \omega) \\ \Pi_0^A(q, \omega) & \Pi_0^N(q, \omega) \end{pmatrix} \quad (2.78)$$

where $\Pi_0^{ee}(q, \omega) = \Pi_0^{hh}(q, \omega) = \Pi_0^N(q, \omega)$ is the normal polarization function and $\Pi_0^{eh}(q, \omega) = \Pi_0^{he}(q, \omega) = \Pi_0^A(q, \omega)$ is the anomalous polarization function. Replacing Eq. (2.74), Eq. (2.75), and Eq. (2.78) in Eq. (2.73) one gets:

$$V_S^{sc}(q, \omega) = \frac{V_S(q) - \Pi_0^N(q, \omega)\mathcal{A}_q}{1 - 2(\Pi_0^N(q, \omega)V_S(q) + \Pi_0^A(q, \omega)V_D(q)) + \mathcal{B}_q\mathcal{A}_q} \quad (2.79)$$

$$V_D^{sc}(q, \omega) = \frac{V_D(q) + \Pi_0^A(q, \omega)\mathcal{A}_q}{1 - 2(\Pi_0^N(q, \omega)V_S(q) + \Pi_0^A(q, \omega)V_D(q)) + \mathcal{B}_q\mathcal{A}_q} \quad (2.80)$$

where $\mathcal{A}_q = V_S(q)^2 - V_D(q)^2$ and $\mathcal{B}_q = \Pi_0^N(q, \omega)^2 - \Pi_0^A(q, \omega)^2$.

Diagrammatically it means that with the Random Phase approximation, all the orders of only the ring diagrams are taken into account in the proper polarization. In Appendix A the Feynman diagrams up to second order for the screened interlayer and intralayer interaction are reported.

To self-consistently solve the gap and number equation, Eqs. (2.66)-(2.69), $V_S(p - q)$ and $V_D(q - k)$ are replaced with the static screened intralayer interaction $V_S^{sc}(p - q, 0)$ and the static screened interlayer interaction $V_D^{sc}(q - k, 0)$ respectively.

The zero-order polarization function can be evaluated [134] as:

$$\Pi_0^{\lambda\lambda'}(r, t) = i\theta(t)\langle[n_\lambda(r, t), n_{\lambda'}(0, 0)]\rangle, \quad (2.81)$$

where $\langle[n_\lambda(r, t), n_{\lambda'}(0, 0)]\rangle$ is the expectation value of the commutator $[n_\lambda(r, t), n_{\lambda'}(0, 0)] = n_\lambda(r, t)n_{\lambda'}(0, 0) - n_{\lambda'}(0, 0)n_\lambda(r, t)$.

The Fourier expansion of the density operators is:

$$n_\lambda(r, t) = \frac{1}{S} \sum_q e^{iqr} n_\lambda(q, t), \quad (2.82)$$

where, for $\lambda = e$:

$$n_e(q, t) = \sum_k c_k^\dagger(t) c_{k+q}(t), \quad (2.83)$$

and for $\lambda = h$

$$n_h(q, t) = \sum_k d_k^\dagger(t) d_{k+q}(t), \quad (2.84)$$

where c^\dagger, c are the fermionic creation and annihilation operators of electrons in the electron-doped layer and d^\dagger, d are the fermionic creation and annihilation operators of holes in the hole-doped layer. Replacing Eq. (2.82) in Eq. (2.81), one gets:

$$\Pi_0^{\lambda\lambda'}(r, t) = i\theta(t) \frac{1}{S^2} \sum_{q, q'} e^{iqr} \langle[n_\lambda(q, t); n_{\lambda'}(q', 0)]\rangle. \quad (2.85)$$

The Fourier expansion of the zero-order polarization function is:

$$\Pi_0^{\lambda\lambda'}(r, t) = \frac{1}{S} \sum_q e^{iqr} \Pi_0^{\lambda\lambda'}(q, t). \quad (2.86)$$

Thus, by comparing Eq. (2.85) with Eq. (2.86), it appears that the Fourier transform of the zero-order polarization function is:

$$\Pi_0^{\lambda\lambda'}(q, t) = i\theta(t) \frac{1}{S} \sum_{q'} \langle [n_\lambda(q, t); n_{\lambda'}(q', 0)] \rangle. \quad (2.87)$$

We introduce the density retarded Green's function $G_{n_\lambda(q,t), n_{\lambda'}(q',0)}^R = i\theta(t) \langle [n_\lambda(q, t); n_{\lambda'}(q', 0)] \rangle$ (times -1), so that

$$\Pi_0^{\lambda\lambda'}(q, t) = \frac{1}{S} \sum_{q'} G_{n_\lambda(q,t), n_{\lambda'}(q',0)}^R. \quad (2.88)$$

The retarded Green's function can be evaluated using its equation of motion [171]:

$$i\partial_t G_{A,B}^R(t) = \delta(t) \langle [A; B] \rangle + G_{[A;H],B}^R(t), \quad (2.89)$$

where A and B are generic bosonic operators and H is the non-interacting Hamiltonian. In this case, A and B are the bosonic density operators of the two layers.

To simplify the notation, we will from here omit on the time index t . All the operators evaluated in k and q are implicitly evaluated in t , while all the operators in k' and q' are implicitly evaluated at zero time.

The equations of motion of the electron-electron and electron-hole retarded two-body density Green's functions are

$$i\partial_t G_{n_e(q), n_e(q')}^R = \delta(t) \langle [n_e(q); n_e(q')] \rangle + G_{[n_e(q); H_0], n_e(q')}^R, \quad (2.90)$$

$$i\partial_t G_{n_e(q), n_h(q')}^R = \delta(t) \langle [n_e(q); n_h(q')] \rangle + G_{[n_e(q); H_0], n_h(q')}^R. \quad (2.91)$$

From these equation we can obtain $G_{n_e(q), n_e(q')}^R$ and $G_{n_e(q), n_h(q')}^R$ to evaluate the zero-order polarization functions $\Pi_0^N(q, t)$ and $\Pi_0^A(q, t)$ respectively.

We report the calculation of the zero-order polarization functions in the normal state of the exciton bilayer system in Appendix B. This gives insights into the Green's function equation of motion approach. In the next section, we extend the calculation to the superfluid case.

2.4 Polarization functions with Green's function equation of motion in exciton superfluid phase

In the superfluid phase, electrons and holes are bound together and form a coherent macroscopic state, thus the creation or destruction of particles in one layer strongly affects the density response of the particles in the other layer. This effect is accounted for when evaluating both the normal and the anomalous polarization in the superfluid phase.

To describe the superfluid exciton phase we introduce the Bogoliubov transformations of the electron and hole creation and annihilation operators:

$$c_k = u_k \alpha_k - v_k \beta_{-k}^\dagger \quad (2.92)$$

$$c_k^\dagger = u_k \alpha_k^\dagger - v_k \beta_{-k} \quad (2.93)$$

$$d_k = v_k \alpha_{-k}^\dagger + u_k \beta_k \quad (2.94)$$

$$d_k^\dagger = v_k \alpha_{-k} + u_k \beta_k^\dagger \quad (2.95)$$

where α, α^\dagger (β, β^\dagger) are the quasi-particle (quasi-anti-particle) annihilation and creation operators respectively. The u_k, v_k are the Bogoliubov amplitudes defined as:

$$u_k^2 = \frac{1}{2} \left(1 + \frac{\xi(k)}{E(k)} \right), \quad (2.96)$$

$$v_k^2 = \frac{1}{2} \left(1 - \frac{\xi(k)}{E(k)} \right), \quad (2.97)$$

$$E(k) = \sqrt{\xi(k)^2 + \Delta(k)^2}. \quad (2.98)$$

The quasi-particle operators are fermionic operators and the only anticommutators which are different from zero are:

$$\{\alpha_k^\dagger; \alpha_{k'}\} = \delta(k, k') \quad (2.99)$$

$$\{\beta_k^\dagger; \beta_{k'}\} = \delta(k, k'). \quad (2.100)$$

The non-interacting electron-hole Hamiltonian correspond to the BCS Hamiltonian H_{BCS} in terms of the Bogoliubov operators:

$$H_{BCS} = \sum_k E(k) (\alpha_k^\dagger \alpha_k + \beta_k^\dagger \beta_k) \quad (2.101)$$

Normal Polarization in the superfluid state

The normal polarization function in the superfluid phase is:

$$\Pi_0^N(q, t) = i\theta(t) \frac{1}{S} \sum_{q'} \langle [n_e(q, t); n_e(q', 0)] \rangle \quad (2.102)$$

$$\begin{aligned} &= i\theta(t) \frac{1}{S} \sum_{q'} \sum_{k, k'} \langle [c_{k+q}^\dagger c_k; c_{k'+q'}^\dagger c_{k'}] \rangle \\ &= i\theta(t) \frac{1}{S} \sum_{q'} \sum_{k, k'} \langle [(u_{k+q} \alpha_{k+q}^\dagger - v_{k+q} \beta_{-k-q}) (u_k \alpha_k - v_k \beta_{-k}^\dagger); \\ &\quad (u_{k'+q'} \alpha_{k'+q'}^\dagger - v_{k'+q'} \beta_{-k'-q'}) (u_{k'} \alpha_{k'} - v_{k'} \beta_{-k'}^\dagger)] \rangle. \end{aligned} \quad (2.103)$$

2.4. Polarization functions with Green's function equation of motion in exciton superfluid phase

Expanding the products inside the commutator, results in:

$$\begin{aligned} \Pi_0^N(q, t) = i\theta(t) \frac{1}{S} \sum_{q'} \sum_{k, k'} \quad (2.104) \\ u_{k+q} u_k u_{k'+q'} u_{k'} \langle [\alpha_{k+q}^\dagger \alpha_k; \alpha_{k'+q'}^\dagger \alpha_{k'}] \rangle - u_{k+q} u_k u_{k'+q'} v_{k'} \langle [\alpha_{k+q}^\dagger \alpha_k; \alpha_{k'+q'}^\dagger \beta_{-k'}^\dagger] \rangle \\ - u_{k+q} u_k v_{k'+q'} u_{k'} \langle [\alpha_{k+q}^\dagger \alpha_k; \beta_{-k'+q'} \alpha_{k'}] \rangle + u_{k+q} u_k v_{k'+q'} v_{k'} \langle [\alpha_{k+q}^\dagger \alpha_k; \beta_{-k'-q'} \beta_{-k'}^\dagger] \rangle \\ - u_{k+q} v_k u_{k'+q'} u_{k'} \langle [\alpha_{k+q}^\dagger \beta_k^\dagger; \alpha_{k'+q'}^\dagger \alpha_{k'}] \rangle + u_{k+q} v_k u_{k'+q'} v_{k'} \langle [\alpha_{k+q}^\dagger \beta_k^\dagger; \alpha_{k'+q'}^\dagger \beta_{-k'}^\dagger] \rangle \\ + u_{k+q} v_k v_{k'+q'} u_{k'} \langle [\alpha_{k+q}^\dagger \beta_{-k}^\dagger; \beta_{-k'+q'} \alpha_{k'}] \rangle - u_{k+q} v_k v_{k'+q'} v_{k'} \langle [\alpha_{k+q}^\dagger \beta_k^\dagger; \beta_{-k'-q'} \beta_{-k'}^\dagger] \rangle \\ - v_{k+q} u_k u_{k'+q'} u_{k'} \langle [\beta_{-k-q} \alpha_k; \alpha_{k'+q'}^\dagger \alpha_{k'}] \rangle + v_{k+q} u_k u_{k'+q'} v_{k'} \langle [\beta_{-k-q} \alpha_k; \alpha_{k'+q'}^\dagger \beta_{-k'}^\dagger] \rangle \\ + v_{k+q} u_k v_{k'+q'} u_{k'} \langle [\beta_{-k-q} \alpha_k; \beta_{-k'+q'} \alpha_{k'}] \rangle - v_{k+q} u_k v_{k'+q'} v_{k'} \langle [\beta_{-k-q} \alpha_k; \beta_{-k'-q'} \beta_{-k'}^\dagger] \rangle \\ + v_{k+q} v_k u_{k'+q'} u_{k'} \langle [\beta_{-k-q} \beta_k^\dagger; \alpha_{k'+q'}^\dagger \alpha_{k'}] \rangle - v_{k+q} v_k u_{k'+q'} v_{k'} \langle [\beta_{-k-q} \beta_k^\dagger; \alpha_{k'+q'}^\dagger \beta_{-k'}^\dagger] \rangle \\ - v_{k+q} v_k v_{k'+q'} u_{k'} \langle [\beta_{-k-q} \beta_{-k}^\dagger; \beta_{-k'+q'} \alpha_{k'}] \rangle + v_{k+q} v_k v_{k'+q'} v_{k'} \langle [\beta_{-k-q} \beta_k^\dagger; \beta_{-k'-q'} \beta_{-k'}^\dagger] \rangle. \end{aligned}$$

Each expectation value can be written as a retarded Green's function, leading to 16 Green's functions equations of motion, Eq. (2.89).

Using the quasi-particle commutator rules, the commutators $[\alpha_{k+q}^\dagger \alpha_k; \beta_{-k'-q'} \beta_{-k'}^\dagger] = [\beta_{-k-q} \alpha_k; \beta_{-k'-q'} \alpha_{k'}] = [\beta_{-k'-q'} \beta_{-k'}^\dagger; \alpha_{k'+q}^\dagger \alpha_k] = [\alpha_{k+q}^\dagger \beta_{-k}^\dagger; \alpha_{k'+q}^\dagger \beta_{-k'}^\dagger] = 0$, and their expectation values are zero.

Then, for the conservation of the number of particles, the expectation values of the terms in which the same operator appears an odd number of times are also zero.

Thus:

$$\begin{aligned} \Pi_0^N(q, t) = i\theta(t) \frac{1}{S} \sum_{q'} \sum_{k, k'} \quad (2.105) \\ u_{k+q} u_k u_{k'+q'} u_{k'} \langle [\alpha_{k+q}^\dagger \alpha_k; \alpha_{k'+q'}^\dagger \alpha_{k'}] \rangle - u_{k+q} u_k u_{k'+q'} v_{k'} \langle [\alpha_{k+q}^\dagger \alpha_k; \alpha_{k'+q'}^\dagger \beta_{-k'}^\dagger] \rangle \\ - u_{k+q} u_k v_{k'+q'} u_{k'} \langle [\alpha_{k+q}^\dagger \alpha_k; \beta_{-k'+q'} \alpha_{k'}] \rangle + u_{k+q} u_k v_{k'+q'} v_{k'} \langle [\alpha_{k+q}^\dagger \alpha_k; \beta_{-k'-q'} \beta_{-k'}^\dagger] \rangle \\ - u_{k+q} v_k u_{k'+q'} u_{k'} \langle [\alpha_{k+q}^\dagger \beta_k^\dagger; \alpha_{k'+q'}^\dagger \alpha_{k'}] \rangle + u_{k+q} v_k u_{k'+q'} v_{k'} \langle [\alpha_{k+q}^\dagger \beta_k^\dagger; \alpha_{k'+q'}^\dagger \beta_{-k'}^\dagger] \rangle \\ + u_{k+q} v_k v_{k'+q'} u_{k'} \langle [\alpha_{k+q}^\dagger \beta_{-k}^\dagger; \beta_{-k'+q'} \alpha_{k'}] \rangle - u_{k+q} v_k v_{k'+q'} v_{k'} \langle [\alpha_{k+q}^\dagger \beta_k^\dagger; \beta_{-k'-q'} \beta_{-k'}^\dagger] \rangle \\ - v_{k+q} u_k u_{k'+q'} u_{k'} \langle [\beta_{-k-q} \alpha_k; \alpha_{k'+q'}^\dagger \alpha_{k'}] \rangle + v_{k+q} u_k u_{k'+q'} v_{k'} \langle [\beta_{-k-q} \alpha_k; \alpha_{k'+q'}^\dagger \beta_{-k'}^\dagger] \rangle \\ + v_{k+q} u_k v_{k'+q'} u_{k'} \langle [\beta_{-k-q} \alpha_k; \beta_{-k'+q'} \alpha_{k'}] \rangle - v_{k+q} u_k v_{k'+q'} v_{k'} \langle [\beta_{-k-q} \alpha_k; \beta_{-k'-q'} \beta_{-k'}^\dagger] \rangle \\ + v_{k+q} v_k u_{k'+q'} u_{k'} \langle [\beta_{-k-q} \beta_k^\dagger; \alpha_{k'+q'}^\dagger \alpha_{k'}] \rangle - v_{k+q} v_k u_{k'+q'} v_{k'} \langle [\beta_{-k-q} \beta_k^\dagger; \alpha_{k'+q'}^\dagger \beta_{-k'}^\dagger] \rangle \\ - v_{k+q} v_k v_{k'+q'} u_{k'} \langle [\beta_{-k-q} \beta_{-k}^\dagger; \beta_{-k'+q'} \alpha_{k'}] \rangle + v_{k+q} v_k v_{k'+q'} v_{k'} \langle [\beta_{-k-q} \beta_k^\dagger; \beta_{-k'-q'} \beta_{-k'}^\dagger] \rangle. \end{aligned}$$

Only 4 terms remain. The first term being:

$$\begin{aligned} \langle [\alpha_{k+q}^\dagger \alpha_k; \alpha_{k'+q'}^\dagger \alpha_{k'}] \rangle &= \langle \alpha_{k+q}^\dagger \alpha_k \alpha_{k'} \delta(k' + q', k) - \alpha_{k'+q'}^\dagger \alpha_k \delta(k + q, k') \rangle \\ &= \langle \alpha_{k+q}^\dagger \alpha_k \alpha_{k'} \delta(k' + q', k) - \alpha_{k+q}^\dagger \alpha_k \alpha_{k'} \delta(k' + q', k) \rangle \\ &= \langle 0 \rangle = 0. \end{aligned} \quad (2.106)$$

The same happens for the last term in Eq. (2.105), $\langle [\beta_{-k-q} \beta_k^\dagger; \beta_{-k'-q'} \beta_{-k'}^\dagger] \rangle = 0$.

Thus only two terms remain. The normal polarization function in the superfluid phase is given by:

$$\begin{aligned} \Pi_0^N(q, t) = i\theta(t) \frac{1}{S} \sum_{q'} \sum_{k, k'} u_{k+q} v_k v_{k'+q'} u_{k'} \langle [\alpha_{k+q}^\dagger \beta_{-k}^\dagger; \beta_{-k'-q'} \alpha_{k'}] \rangle \\ + v_{k+q} u_k u_{k'+q'} v_{k'} \langle [\beta_{-k-q} \alpha_k; \alpha_{k'+q'}^\dagger \beta_{-k'}^\dagger] \rangle. \end{aligned} \quad (2.107)$$

We rewrite it as:

$$\Pi_0^N(q, t) = \Pi_{0A}^N(q, t) + \Pi_{0B}^N(q, t). \quad (2.108)$$

The two terms of the normal polarization function can be written as retarded Green's function as follows:

$$\Pi_{0A}^N(q, t) = i\theta(t) \frac{1}{S} \sum_{q'} \sum_{k, k'} u_{k+q} v_k v_{k'+q'} u_{k'} \langle [\alpha_{k+q}^\dagger \beta_{-k}^\dagger; \beta_{-k'-q'} \alpha_{k'}] \rangle = \frac{1}{S} \sum_{q'} G_{n_e(q), n_e(q')}^{R,A}, \quad (2.109)$$

$$\Pi_{0B}^N(q, t) = i\theta(t) \frac{1}{S} \sum_{q'} \sum_{k, k'} v_{k+q} u_k u_{k'+q'} v_{k'} \langle [\beta_{-k-q} \alpha_k; \alpha_{k'+q'}^\dagger \beta_{-k'}^\dagger] \rangle = \frac{1}{S} \sum_{q'} G_{n_e(q), n_h(q')}^{R,B}. \quad (2.110)$$

The two retarded Green's functions are evaluated using the Green's function equation of motion:

$$i\partial_t G_{n_e(q), n_e(q')}^{R,A} = \delta(t) \langle [\alpha_{k+q}^\dagger \beta_{-k}^\dagger; \beta_{-k'-q'} \alpha_{k'}] \rangle + G_{[n_e(q); H_{BCS}], n_e(q')}^{R,A}, \quad (2.111)$$

$$i\partial_t G_{n_e(q), n_h(q')}^{R,B} = \delta(t) \langle [\beta_{-k-q} \alpha_k; \alpha_{k'+q'}^\dagger \beta_{-k'}^\dagger] \rangle + G_{[n_e(q); H_{BCS}], n_h(q')}^{R,B}. \quad (2.112)$$

For Eq. (2.111), evaluating the $\delta(t)$ -term:

$$\delta(t) \langle [\alpha_{k+q}^\dagger \beta_{-k}^\dagger; \beta_{-k'-q'} \alpha_{k'}] \rangle = \delta(t) \left(\langle \alpha_{k+q}^\dagger \beta_{-k}^\dagger \beta_{-k'-q'} \alpha_{k'} \rangle - \langle \beta_{-k'-q'} \alpha_{k'} \alpha_{k+q}^\dagger \beta_{-k}^\dagger \rangle \right). \quad (2.113)$$

The two expectation values can be evaluated by rewriting the quasi-particle operators using the creation and annihilation electron (c_k^\dagger, c_k) and hole (d_k^\dagger, d_k) operators [172, 173]. At zero temperature:

$$\delta(t) \langle [\alpha_{k+q}^\dagger \beta_{-k}^\dagger; \beta_{-k'-q'} \alpha_{k'}] \rangle = -\delta(t) \delta(-q', q) \delta(k', k+q). \quad (2.114)$$

The H -term of the $G_{n_e(q), n_e(q')}^{R,A}$ equation of motion Eq. (2.111) is:

$$G_{[n_e(q); H_{BCS}], n_e(q')}^{R,A} = i\theta(t) \left\langle \left[[\alpha_{k+q}^\dagger \beta_{-k}^\dagger; H_{BCS}]; \beta_{-k'-q'} \alpha_{k'} \right] \right\rangle. \quad (2.115)$$

The commutator with H_{BCS} is given by:

$$\begin{aligned}
[\alpha_{k+q}^\dagger \beta_{-k}^\dagger; H_{BCS}] &= \sum_s E_s [\alpha_{k+q}^\dagger \beta_{-k}^\dagger; \alpha_s^\dagger \alpha_s + \beta_s^\dagger \beta_s] \\
&= \sum_s E_s \left([\alpha_{k+q}^\dagger \beta_{-k}^\dagger; \alpha_s^\dagger \alpha_s] + [\alpha_{k+q}^\dagger \beta_{-k}^\dagger; \beta_s^\dagger \beta_s] \right) \\
&= \sum_s E_s \left(-\alpha_s^\dagger \beta_{-k}^\dagger \delta(k+q, s) + \beta_s^\dagger \alpha_{k+q}^\dagger \delta(-k, s) \right) \\
&= \sum_s E_s \left(-\alpha_s^\dagger \beta_{-k}^\dagger \delta(k+q, s) - \alpha_{k+q}^\dagger \beta_s^\dagger \delta(-k, s) \right) \\
&= -E(k+q) \alpha_{k+q}^\dagger \beta_{-k}^\dagger - E(k) \alpha_{k+q}^\dagger \beta_{-k}^\dagger \\
[\alpha_{k+q}^\dagger \beta_{-k}^\dagger; H_{BCS}] &= (-E(k+q) - E(k)) \alpha_{k+q}^\dagger \beta_{-k}^\dagger. \tag{2.116}
\end{aligned}$$

Replacing Eq. (2.116) in the the H -term of Eq.(2.111) one gets:

$$\begin{aligned}
G_{[n_e(q); H_{BCS}], n_e(q')}^{R,A} &= i\theta(t) \left\langle [\alpha_{k+q}^\dagger \beta_{-k}^\dagger; H_{BCS}; \beta_{-k'-q'} \alpha_{k'}] \right\rangle \tag{2.117} \\
&= \sum_{k,k'} i\theta(t) (-E(k+q) - E(k)) \langle [\alpha_{k+q}^\dagger \beta_{-k}^\dagger, \beta_{-k'-q'} \alpha_{k'}] \rangle \\
&= \sum_{k,k'} (-E(k+q) - E(k)) G_{e,e}^{R,A}(k, k', q, q', t)
\end{aligned}$$

where $G_{e,e}^{R,A}(k, k', q, q', t) = i\theta(t) \langle [\alpha_{k+q}^\dagger \beta_{-k}^\dagger; \beta_{-k'-q'} \alpha_{k'}] \rangle$. The time derivative term on the left-hand side of Eq. (2.111) corresponds to Eq. (B.21). Thus the equation of motion of $G_{e,e}^{R,A}(k, k', q, q', \omega)$ states:

$$\begin{aligned}
G_{ee}^{R,A}(k, k', q, q', \omega) \omega &= -\delta(q, -q') \delta(k', k+q) u_{k+q} v_k v_{k'+q'} u_{k'} \\
&\quad + G_{ee}^{R,A}(k, k', q, q', \omega) (-E(k) - E(k+q)) \\
G_{ee}^{R,A}(k, k', q, q', \omega) (\omega + E(k) + E(k+q)) &= -\delta(q, -q') \delta(k', k+q) u_{k+q} v_k v_{k'+q'} u_{k'} \\
G_{ee}^{R,A}(k, k', q, q', \omega) &= -\frac{\delta(q, -q') \delta(k', k+q) u_{k+q} v_k v_{k'+q'} u_{k'}}{\omega + E(k) + E(k+q)}. \tag{2.118}
\end{aligned}$$

Following the same procedure for Eq. (2.112):

$$G_{ee}^{R,B}(k, k', q, q', \omega) = \frac{\delta(q, -q') \delta(k, k'+q') u_{k+q} v_k v_{k'+q'} u_{k'}}{\omega - E(k) - E(k+q)} \tag{2.119}$$

Replacing Eq. (2.118) in Eq. (2.109) and Eq. (2.119) in Eq. (2.110) the normal polarization function $\Pi_0^N(q, \omega)$, (Eq. (2.108)) becomes:

$$\begin{aligned}
\Pi_0^N(q, \omega) &= \Pi_{0,A}^N(q, \omega) + \Pi_{0,B}^N(q, \omega) = \frac{1}{S} \sum_{q'} \sum_{k,k'} \left(G_{ee}^{R,A}(k, k', q, q', \omega) + G_{ee}^{R,B}(k, k', q, q', \omega) \right) \\
&= \frac{1}{S} \sum_{q'} \sum_k \left(\frac{\delta(q, -q') u_{k+q}^2 v_k^2}{\omega + i\eta + E(k) + E(k+q)} - \frac{\delta(q, -q') u_k^2 v_{k+q}^2}{\omega + i\eta - E(k) - E(k+q)} \right) \\
\Pi_0^N(q, \omega) &= \frac{1}{S} \sum_k \left(\frac{u_k^2 v_{k+q}^2}{\omega + i\eta - E(k) - E(k+q)} - \frac{u_{k+q}^2 v_k^2}{\omega + i\eta + E(k) + E(k+q)} \right). \tag{2.120}
\end{aligned}$$

This is the zero-order normal polarizability at zero temperature in the superfluid phase of an electron-hole bilayer system.

Anomalous Polarization in the superfluid state

The anomalous polarization function in the superfluid phase is:

$$\begin{aligned}
 \Pi_0^A(q, t) &= i\theta(t) \frac{1}{S} \sum_{q'} \langle [n_e(q, t); n_h(q', 0)] \rangle \\
 &= i\theta(t) \frac{1}{S} \sum_{q'} \sum_{k, k'} \langle [c_{k+q}^\dagger c_k; d_{k'+q'}^\dagger d_{k'+}] \rangle \\
 &= i\theta(t) \frac{1}{S} \sum_{q'} \sum_{k, k'} \langle [(u_{k+q} \alpha_{k+q}^\dagger - v_{k+q} \beta_{-k-q}) (u_k \alpha_k - v_k \beta_{-k}^\dagger), \\
 &\quad (v_{k'+q'} \alpha_{-k'-q'} - u_{k'+q'} \beta_{k'+q'}^\dagger) (v_{k'} \alpha_{-k'}^\dagger + u_{k'} \beta_{k'}^\dagger)] \rangle. \tag{2.121}
 \end{aligned}$$

The procedure is the same as for the normal polarizability. The product of the commutator once again results in 16 terms of expectation values. The commutators in which the same operators appear an odd number of times are and the zero expectation values are cancelled, remaining with only two terms different from zero:

$$\begin{aligned}
 \Pi_0^A(q, t) &= -i\theta(t) \frac{1}{S} \sum_{q'} \sum_{k, k'} v_{k+q} u_k u_{k'+q'} u_{k'} \langle [\beta_{-k-q} \alpha_k^\dagger; \beta_{-k'-q'}^\dagger \alpha_{-k'}^\dagger] \rangle \\
 &\quad + u_{k+q} v_k v_{k'+q'} u_{k'} \langle [\alpha_{-k-q}^\dagger \beta_{-k}; \alpha_{-k'-q'} \beta_{k'}] \rangle \\
 &= \Pi_{0A}^A(q, t) + \Pi_{0B}^A(q, t). \tag{2.122}
 \end{aligned}$$

As for the normal polarization, the anomalous polarization function can be separated in two terms $\Pi_{0A}^A(q, t)$ and $\Pi_{0B}^A(q, t)$. They can be rewritten by introducing a retarded Green's function as follows:

$$\Pi_{0A}^A(q, t) = i\theta(t) \frac{1}{S} \sum_{q'} \sum_{k, k'} v_{k+q} u_k u_{k'+q'} u_{k'} \langle [\beta_{-k-q} \alpha_k^\dagger; \beta_{-k'-q'}^\dagger \alpha_{-k'}^\dagger] \rangle = \frac{1}{S} \sum_{q'} G_{n_e(q), n_e(q')}^{R,A}, \tag{2.123}$$

$$\Pi_{0B}^A(q, t) = i\theta(t) \frac{1}{S} \sum_{q'} \sum_{k, k'} u_{k+q} v_k v_{k'+q'} u_{k'} \langle [\alpha_{-k-q}^\dagger \beta_{-k}; \alpha_{-k'-q'} \beta_{k'}] \rangle = \frac{1}{S} \sum_{q'} G_{n_e(q), n_e(q')}^{R,B}. \tag{2.124}$$

The evaluation of the two retarded Green's functions using the Green's function equation of motion is analogous to the case of the normal polarization function.

The anomalous polarization function $\Pi_0^A(q, t)$ results in:

$$\Pi_0^A(q, t) = \frac{1}{S} \sum_k \left(\frac{u_{k+q} v_{k+q} u_k v_k}{\omega + i\eta - E(k) - E(k+q)} - \frac{u_{k+q} v_{k+q} u_k v_k}{\omega + i\eta + E(k) + E(k+q)} \right). \tag{2.125}$$

The expressions for $\Pi_0^N(q, t)$ (Eq. (2.120)) and $\Pi_0^A(q, t)$ (Eq. (2.125)) are substituted in Eq. (2.80) and Eq. (2.79) to obtain the screened interlayer and intralayer interactions. Those are then used to evaluate the gap and number equations of the system to obtain the behaviour of the gap energy, density and single-particle chemical potential of the

2.4. Polarization functions with Green's function equation of motion in exciton superfluid phase

bilayer exciton system including density fluctuations in the interactions between the particles. Details about the numerical resolution of the gap and number equations are in Appendix.C.

Chapter 3

Josephson Effect in exciton bilayer systems

In this chapter, we explore the static Josephson effect in an electron-hole superfluid bilayer Transition Metal Dichalcogenides (TMD) heterostructure at zero temperature. We focus on designing a bilayer Josephson junction to control the energy of the potential barrier and discuss experimental techniques for its fabrication. We analyze the superfluid characteristics and crossover physics for a rectangular Josephson junction, determining the superfluid properties and the critical current across junctions with varying potential barrier heights. In the low potential barrier region, we investigate the BCS-BEC crossover physics of the Josephson current, finding a maximum critical velocity when excitations transition from bosonic to fermionic. Notably, we identify for the first time in a semiconductor system an experimental way to locate the boundary between the BEC and the crossover regime of the BCS-BEC crossover phenomenon. In the high potential barrier region, we solve the exciton pair tunnelling problem to study the Josephson current. Our results demonstrate good agreement between the outcomes of both barrier regions as they converge. The results reported in this chapter have been published in Ref. [146].

In the first chapter, we have reviewed the main experimental techniques and the materials used to probe the presence of a macroscopic superfluid phase in exciton bilayer systems. However, to date, these works have been able to establish the existence of a strongly correlated excitonic phase but not to make definitive claims for the existence of a superfluid state. This would require observation of dissipationless currents and additional measurements of phase coherence. It is particularly challenging because the excitons are neutral.

In conventional superconductors, the Josephson effect is widely used to establish the presence of superconductivity. The Josephson effect consists of a coherent dissipationless flow of pairs without a driving potential, between two superconductors separated by an insulating barrier (Josephson junction), Fig. 1.10. The Josephson effect establishes the presence of a quantum coherent macroscopic state, and thus the existence of a superconducting or superfluid state.

In this chapter, as a proof-of-concept, we investigate for the first time in exciton bilayers the static Josephson effect paradigm at zero temperature throughout the BCS-BEC crossover. The study is based on a realistic and feasible experimental proposal for the fabrication of an exciton bilayer Josephson junction and for the measurement of a Josephson current in a bilayer junction.

3.1 Experimental proposal

In the exciton bilayer Josephson junction the left and right superconductors in Fig. 1.10 are replaced with a left and a right exciton bilayer system.

We want to study the static Josephson effect throughout the BCS-BEC crossover and the behaviour of the Josephson critical current in different regimes of potential barrier height. It has been shown that interesting insights related to the BCS-BEC crossover physics occur when the Josephson current is studied as a function of the potential barrier height [110].

In conventional superconductors, one of the most used experimental techniques to create a junction between two materials is the Electron-Beam Lithography (EBL). Electron-beam lithography consists of scanning a focused beam of electrons to draw custom shapes on a surface covered with an electron-sensitive film [174]. For bilayer systems, the grooves created by the EBL are naturally filled up by the dielectric that surrounds the two layers [2, 10, 90]. The dielectric used to separate the conducting layers and the metal gates is commonly hexagonal Boron Nitrate (hBN) and since hBN is an insulator, this will result in an infinite and non-tunable potential barrier.

To overcome this issue, here we propose an alternative and feasible Josephson junction bilayer configuration in which it is possible to control the potential barrier height, Fig. 3.1(a).

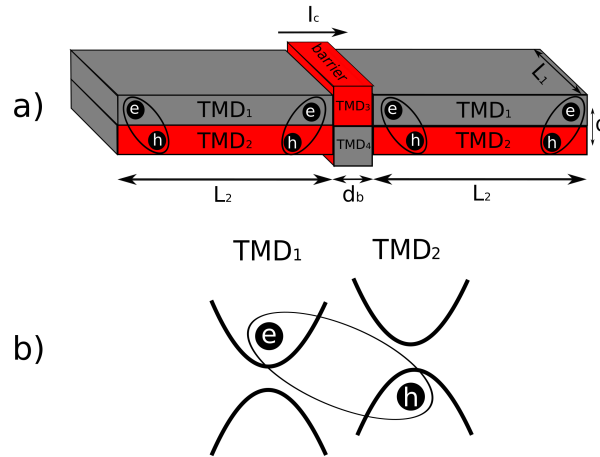


FIGURE 3.1: (a) Schematic of Josephson junction with the different layers labelled TMD_1 – TMD_4 . d is layer separation, d_b the barrier thickness, and L_1 and L_2 the transverse and longitudinal layer lengths. Electron-hole pairs are shown. (b) Energy band alignments at the type-II TMD_1/TMD_2 interface.

The device consists of a left and a right exciton bilayer system obtained from the vertical stacking of two different TMD monolayers, TMD_1 and TMD_2 . They are separated by a barrier region made of two different undoped TMD monolayers vertically stacked, TMD_3 and TMD_4 , and attached to the left and right bilayer system with lateral stitching. The advantages of this proposed configuration are:

- The doped TMD_1 and TMD_2 of the vertical stacking can be chosen to have a type-II interface, with the edges of the conduction and valence band at different energies (Fig. 3.1(b)). This keeps the electrons and holes spatially separate without the necessity for an insulating barrier.
- The bilayer junction can be fabricated using a combination of lateral stitching and vertical stacking of TMD heterostructures [98, 175–177]. The potential barrier height

3.1. Experimental proposal

of the junction is determined by the difference in energy of the conduction (valence) bands in the doped TMDs and the undoped TMDs of the barrier [178]. The barrier height V_0 can be varied by suitable material choice of TMDs. Table 3.1 gives examples. As a final example, $\text{WS}_2|\text{WSe}_2\text{---MoSe}_2|\text{WSe}_2$, the barrier is inserted only in the electron monolayer, a configuration which may be more straightforward to fabricate.

TMD ₁ TMD ₂	—	TMD ₃ TMD ₄	a_B^* [nm]	Ry^* [meV]	ϵ_B [meV]	V_0 [ϵ_B]
MoS ₂ MoSe ₂	—	MoSe ₂ WSe ₂	1.3	100	140	0.04
MoS ₂ WSe ₂	—	MoTe ₂ WTe ₂	1.7	77	108	0.05
WS ₂ WSe ₂	—	MoTe ₂ MoTe ₂	1.8	71	99	0.10
MoS ₂ WS ₂	—	WS ₂ MoSe ₂	1.7	77	108	0.20
MoSe ₂ MoTe ₂	—	MoS ₂ MoSe ₂	1.1	116	162	0.33
MoS ₂ MoSe ₂	—	WTe ₂ WSe ₂	1.3	100	140	0.71
WS ₂ WSe ₂	—	MoSe ₂ WSe ₂	1.9	71	99	0.33

TABLE 3.1: Material parameters: effective Bohr radii a_B^* , effective Rydberg Ry^* , exciton binding energies ϵ_B and barrier heights V_0 .

For lateral stitching, there are two possible techniques: two-step edge epitaxy and lithographic patterning. The edge epitaxy technique relies on the growth of a TMD crystal on the active edge of a dissimilar TMD crystal. The resulting lateral heterostructure is characterized by a sharp junction, of the order of the angstrom [175]. The disadvantage is that this method works, with an acceptable quality of the resulting junction, only with specific shapes: triangles and hexagonal samples. The procedure is facilitated if the two TMDs differ only for the Chalcogen atom, as shown in Fig. 3.2.

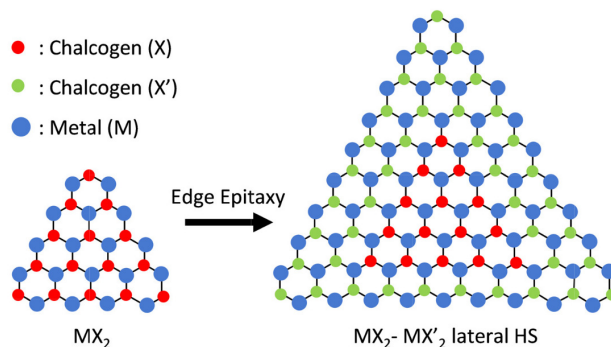


FIGURE 3.2: Schematic illustration of the two-step edge epitaxy for the synthesis of $\text{MX}_2 - \text{MX}'_2$ lateral heterostructure [175].

The other technique is the lithographic patterning. In this case, a portion of the TMD layer is covered with a mask and the uncovered part is subjected to the lithographic process in which atoms are replaced (Fig. 3.3).

The main advantage of lithographic patterning is the possibility of having junctions of arbitrary shapes. The disadvantage is that the junctions are not as sharp as with the edge epitaxy. Indeed, this method is characterized by an intermediate region of a few nanometers in which there is a mix between the TMD₁ and TMD₂ atoms. This is mainly due to the mask that does not perfectly cover the TMD.

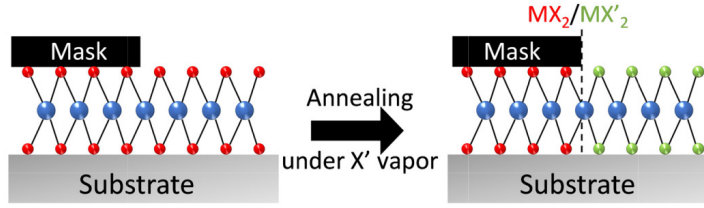


FIGURE 3.3: Schematic illustration of the lithographic patterning for the synthesis of $\text{MX}_2\text{-MX}'_2$ lateral heterostructure [175].

The vertical heterostructure can be obtained through chemical vapour deposition (CVD). In its simplest form, metal oxides are vaporized at high temperatures to react with a chalcogen vapour that is provided via the mild annealing of a powder source, as shown in Fig. 3.4.

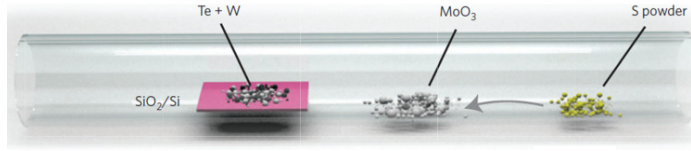


FIGURE 3.4: Schematic representation of a furnace used for the CVD growth of vertical WS_2/MoS_2 heterostructures using solid-phase metal precursors and S powders [175].

A possible way to fabricate the bilayer Josephson junction is to start with the lateral stitching $\text{TMD}_2\text{-TMD}_4\text{-TMD}_2$ for one layer, and then use it as a substrate for the chemical vapour deposition. The TMD_2 regions can be covered with a mask and then CVD depositing TMD_3 only on the TMD_4 region. For the TMD_1 deposition just repeat the procedure covering only the TMD_4 region. In this way, combining the lateral and the vertical heterostructures it is possible to obtain the bilayer Josephson junction reported in Fig. 3.1(a).

The critical Josephson current can be measured using the method of Anderson [179] and Shapiro [180]. A stable dissipationless exciton current is injected in the device using in a counter-flow configuration [60] with two independent currents flowing in the two layers in opposite directions. Then, the voltage drop across the barrier in one of the two layers is measured. If the current injected is a dissipationless coherent current and it is less than the superfluid critical current I_c the voltage drop is zero. Increasing the current, when the I_c value is overcome the superfluidity suddenly disappears and the voltage drop across the barrier jumps to a finite value V_0 , characteristic of the electron current in a metal in the normal state.

3.2 Model of exciton superfluid system in the presence of a potential barrier

We consider a generic TMD bilayer with equal electron and hole densities $n_e = n_h = n$, equal effective masses $m_e^* = m_h^* = m^* = 0.5m_e$, dielectric constant $\epsilon = 5.5\epsilon_0$ and inter-layer distance $d = 0.46a_B^*$. The binding energy of the electron-hole pair in the vacuum evaluated solving the hydrogen-like Schrödinger equation is $\epsilon_B = 1.42 \text{ Ry}^*$. We use effective Rydbergs Ry^* for the energy scale, and effective Bohr radii a_B^* for the length scale.

In this chapter we investigate the Josephson effect as a proof of concept without the intralayer correlations, to get a first look at the Josephson current behaviour for different potential barrier heights.

We solved the zero temperature gap and number equation, as derived in Sec. 2.2, considering an RPA-screened interlayer interaction (Eq. (2.80)) throughout the BCS-BEC crossover:

$$\Delta_0(k) = -\frac{1}{S} \sum_q V_D^{sc}(|q-k|) \frac{\Delta_0(q)}{2E(q)}, \quad (3.1)$$

$$n_0 = \frac{g_s g_v}{S} \sum_p \frac{1}{2} \left(1 - \frac{\zeta(p)}{E(p)} \right). \quad (3.2)$$

where $g_s g_v = 2$, for single-particle parabolic bands $\varepsilon_k = \hbar^2 k^2 / 2m^*$ [98, 181]. The excitation energy is $E(k) = \sqrt{\zeta_k^2 + \Delta_k^2}$, with $\zeta_k = \varepsilon_k - \mu_s$ and μ_s the single-particle chemical potential.

We consider sufficiently wide barriers, $d_b > \zeta$, where $\zeta = \hbar / m^* v_c$ is the superfluid healing length [118, 182]. We will provide an estimation of the numerical value of this quantity in the next section. The characteristic length with which the superfluid phase answers to the bilayer exciton-barrier interface is negligible with respect to the extension of the rest of the barrier, in which the effect of the barrier will be constant. In the barrier region, under this condition, we can use the Thomas-Fermi approximation, i.e. the single-particle chemical potential μ_s^b and the superfluid chemical potential μ_{sf}^b are reduced compared with their values outside the barrier,

$$\begin{aligned} \mu_s^b &= \mu_s - V_0, \\ \mu_{sf}^b &= \mu_{sf} - 2V_0 = 2(\mu_s - V_0) + \varepsilon_B. \end{aligned} \quad (3.3)$$

Using μ_s^b in the dispersion relation $\zeta(k)$ in Eq. (3.1) and Eq. (3.2) gives the superfluid gap Δ_k^b and the density n^b inside the barrier region.

Figure 3.5(a) shows for different barrier heights V_0 in the low barrier region, the superfluid density in the barrier n^b as a function of the μ_s outside the barrier, which we remember can be changed experimentally tuning the particle density through external metal gates. The BEC regime is characterised by negative values of μ_s . As μ_s increases and becomes positive, the system enters the BCS-BEC crossover regime, but μ_s remains well below the Fermi energy. Only in the weak-coupled BCS limit would μ_s approach the Fermi energy. However, for sufficiently large μ_s , strong screening of the electron-hole pair interaction in the superfluid outside the barrier region suppresses the superfluidity leading to a first-order phase transition in the mean-field approximation [46] (the shaded regions in Fig. 3.5).

The colour-coded dots indicate the value $\mu_s = -\varepsilon_B / 2 + V_0$ below which n^b is zero. It means that below this value of μ_s the potential barrier is too high and the excitons do not have enough energy to penetrate the barrier, we define this regime as *high potential barrier region*.

The $V_0 = 0$ curve in Fig. 3.5(a) gives as a reference the superfluid density n in the absence of a barrier. This reaches a maximum at the value $\mu_s = 0.31 \text{ Ry}^*$ for density $n = n^b = 0.105(a_B^*)^{-2}$. This defines the onset density n_0 for the superfluidity.

Figure 3.5(b) shows the maximum of the superfluid gap Δ^b inside the barrier as a function of μ_s . The curve for $V_0 = 0$, also gives the maximum of the superfluid gap Δ_k in the superfluid regions outside any barrier and, like n , this gap vanishes when μ_s

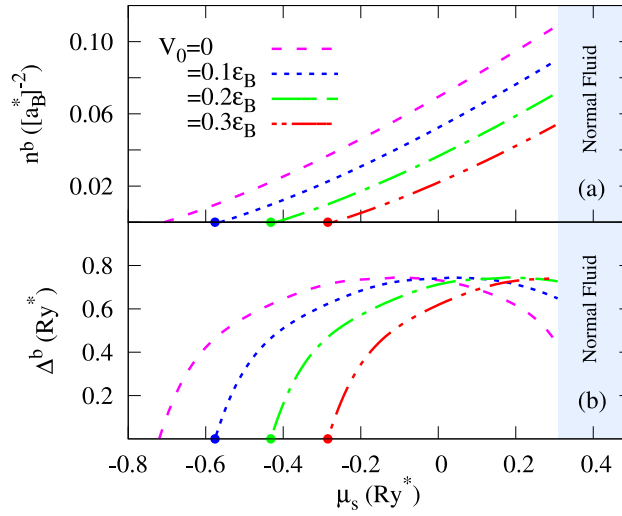


FIGURE 3.5: (a) Density n^b inside the barrier as a function of the single-particle chemical potential μ_s outside barrier. V_0 is barrier height and ϵ_B is the exciton binding energy. (b) Superfluid gap Δ^b inside the barrier.

reaches $-\epsilon_B/2$. For $V_0 > 0$, Δ^b for the barrier vanishes at the same value of μ_s at which n^b vanishes. As V_0 increases, we find a suppression of the gap energy for $\mu_s < 0$, in the BEC regime, and an amplification of the Δ^b for $\mu_s > 0$, in the crossover-BCS regime. This is due to the screening. In the BCS-crossover regime, at high density, the detrimental effect screening is important. In the barrier, the density is reduced, so the screening is weakened. In the BEC regime, we do not see this effect because here the screening is already negligible outside the barrier region. Above the onset density, the strong screening suppresses the superfluidity and the system enters the normal fluid area.

3.3 Josephson critical current

We investigate the Josephson critical current in the two opposite barrier regions.

Low potential barrier region

For a low potential barrier region, $V_0 < \mu_{sf}/2$, the density in the barrier is different from zero and the injected exciton current can flow through the barrier with density n^b . In this case, the barrier acts as an impurity that probes the current, like an electric resistance in a circuit. The exciton superfluid flows over the barrier and can be described by the simple hydrodynamic relation:

$$I_c^b = n^b L_1 v_c^b. \quad (3.4)$$

where L_1 is the transverse length of the junction and v_c is the superfluid critical velocity of the system.

The Landau criterion gives the critical velocity of the superfluid [19],

$$v_c = \min_k \frac{\mathcal{E}_k}{\hbar k}. \quad (3.5)$$

In the simplest picture, there are two types of excitation energy \mathcal{E}_k in this system: Anderson-Bogoliubov modes [135] associated with bosonic behaviour of the pairs, and the fermionic modes associated with pair-breaking excitations [118].

3.3. Josephson critical current

In the bosonic excitation branch, \mathcal{E}_k is given by the dispersion relation $\mathcal{E}_k = \sqrt{\hbar^2 c_{sf}^2 k^2 + \varepsilon_k^2}$ [118, 183], where $c_{sf} = \sqrt{\mu_{sf}/2m}$ [184] is the speed of sound, with superfluid chemical potential $\mu_{sf} = 2\mu_s + \varepsilon_B$. From Eq. (3.5), the critical velocity for bosonic excitations is thus the speed of sound,

$$v_c^{(BEC)} = c_{sf} = \sqrt{\frac{\mu_{sf}}{2m}}. \quad (3.6)$$

For single-particle fermionic excitations $\mathcal{E}_k = E(k) = \sqrt{\varepsilon_k^2 + \Delta_k^2}$, and the critical velocity is the pair-breaking (p-b) velocity [118],

$$v_c^{(p-b)} = \min_k \frac{\sqrt{(\varepsilon_k - \mu_s)^2 + \Delta_k^2}}{\hbar k} \quad (3.7)$$

is numerically evaluated for given values of μ_s and Δ_k to determine the value of $k = k_{\min}$ that minimises Eq. (3.7) (details of the calculation of the Landau critical velocity in Appendix D).

The critical velocity v_c^b in the barrier is the lesser of $v_c^{b(BEC)}$ and $v_c^{b(p-b)}$, obtained from Eq. (3.6) and Eq. (3.7) with μ_{sf}^b and Δ_k^b . As the density is increased and the superfluid regimes are scanned from BEC to BCS-BEC crossover to BCS, the critical velocity should switch from $v_c^{(BEC)}$ to $v_c^{(p-b)}$, whichever is the lesser.

With the critical velocity, we can evaluate the healing length ξ to determine the d_b for which is possible to apply the Thomas-Fermi approximation.

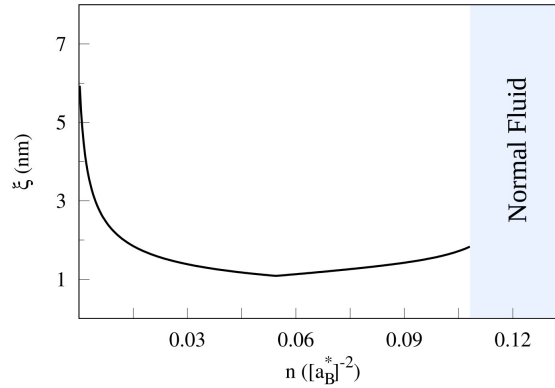


FIGURE 3.6: The healing length ξ as a function of the density n for the TMD bilayer system we are considering.

Fig. 3.6 shows that, similar to the ultracold atom gas case, the ξ has a minimum between the low-density BEC regime and the crossover onset density [185]. However, in contrast with the ultracold atom gas, the largest healing length is in the BEC regime. This is because the screening suppresses the superfluid phase before it reaches the BCS regime, where the healing length increases exponentially. For our TMD bilayer system, the max healing length is $\xi_{max} = 6nm$. We take a barrier width of $d_b = 15nm$, more than double ξ_{max} , to safely use the Thomas-Fermi approximation.

High potential barrier region

For high potential barriers, $V_0 \geq \mu_{sf}/2$, $\mu_s^b < -\varepsilon_B/2$ and $n^b = 0$. The excitons do not have enough energy to cross the barrier V_0 and the supercurrent is given purely by quantum tunnelling of the electron-hole pairs [186, 187].

$$\hbar I_c^b = n_c t_{sf}(\mu_{sf}) L_1 L_2. \quad (3.8)$$

$n_c = \mathcal{C}n$ is the density of the superfluid condensate, with \mathcal{C} the condensate fraction of the superfluid state, which can be calculated as [188, 189]

$$\mathcal{C} = \frac{\sum_k u_k^2 v_k^2}{\sum_k v_k^2} = \frac{1}{2n} \sum_k \frac{\Delta_k^2}{E(k)^2}. \quad (3.9)$$

The Eq. (3.9) is calculated from the two-body density matrix and in the BEC regime it corresponds to the fraction of bosonic excitons in the ground state [190]. Replacing in Eq. (3.9) Δ_k^b , n^b and μ_s^b we obtain the condensate fraction \mathcal{C}^b in the barrier region for the low potential barrier.

The transfer matrix element in (3.8) [186],

$$t_{sf}(\mu_{sf}) = f(V_0/\mu_{sf}) \frac{\mu_{sf}}{k_{\mu_{sf}} L_1} e^{-k_{\mu_{sf}} d_b}, \quad (3.10)$$

is related to the probability for an electron-hole pair to tunnel across the barrier, where $k_{\mu_{sf}}^{-1} = \hbar/\sqrt{2m(V_0 - \mu_{sf})}$ is the wave-function decay length in the barrier. The expression for $f(V_0/\mu_{sf})$ is derived in Ref. [186],

$$f(V_0/\mu_{sf}) = \left[1 - \frac{V_0}{\mu_{sf}} - \sqrt{\left(\frac{V_0}{\mu_{sf}}\right)^2 - 1} \right]^2. \quad (3.11)$$

So for $V_0 > \mu_{sf}/2$, the final expression for the critical current is,

$$I_c^b = \frac{n_c \mu_{sf} f(V_0/\mu_{sf}) e^{-k_{\mu_{sf}} d_b} L_2}{\hbar k_{\mu_{sf}}}. \quad (3.12)$$

Figure 3.7(a) shows the critical current in the barrier I_c^b as a function of the density n outside the barrier. The coloured dots again mark the value of n at which n_b drops to zero and the switch occurs from predominantly flow over to tunnelling. Figure 3.7(b) shows in detail the critical current in the tunnelling region. We took a safety interval around the coloured dots, corresponding to $V_0 = \mu_{sf}$, in which neither the low potential barrier current, described by Eq. (3.4), nor the high potential barrier current Eq. (3.12) work. The high potential barrier current is seen to connect smoothly (dashed lines) with the critical current in the flow-over region. We recall that the existence of a non-zero tunnelling current in this region is accepted as a clear signature of superfluidity. The flattening of I_c^b at high densities reflects the drop in Δ_k^b from the strong screening (Fig. 3.5(b)). We note that I_c^b is everywhere less than the critical current outside the barrier $I_c = nL_2 v_c$, shown by the $V_0 = 0$ curve. For this reason, the overall critical current in the system is given by I_c^b . Thus the BCS-BEC crossover physics in the barrier region controls the transport properties of the entire device.

3.3. Josephson critical current

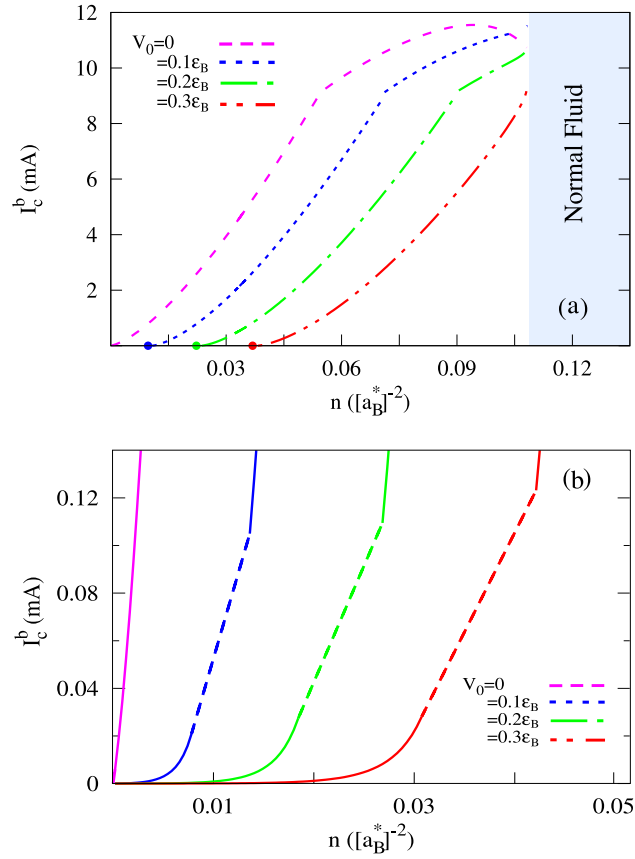


FIGURE 3.7: (a) Critical current in the barrier I_c^b (Eq. (3.4)) for barrier height V_0 , as a function of density n . (b) Details of I_c^b at very low densities; solid lines in the upper part are a zoom-in of the panel (a), solid lines in the lower part are obtained with Eq. (3.12), dashed lines interpolate high-barrier and low barrier results.

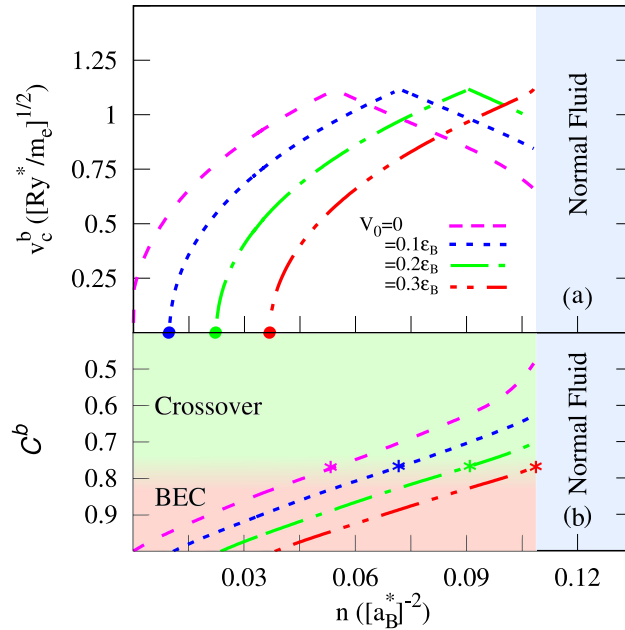


FIGURE 3.8: (a) Critical velocity v_c^b in barrier (Eq. ((3.5)). (b) Condensate fraction C^b in the barrier (Eq. (3.9)). The asterisk symbols in panel (b) match the position of the maximum of the critical velocity v_c^b in panel (a).

Figure 3.8(a) shows the critical velocity v_c^b across the barrier. The maxima in v_c^b result from the switch from Anderson-Bogoliubov bosonic excitations to single-particle fermionic excitations, $v_c^{(p-b)}$ increasing with density while $v_c^{(BEC)}$ decreases with density [113].

As expected, the position of the maxima is sensitive to the barrier height. Fig. 3.8(b) shows that the maximum of v_c^b for each value of V_0 matches the density at which the condensate fraction $C^b = 0.8$. Remarkably, this value also agrees with the conventional criterion used to identify the crossover to BEC boundary given by the vanishing of the single-particle chemical potential [43, 191].

It is an attractive concept and relevant for experiments, that the switchover from bosonic excitations to single-particle fermionic excitations lines up with the BEC and BCS-BEC crossover regime boundary. In contrast to the condensate fraction which is not observable, the critical velocity $v_c^b = I_c^b/n$ is a directly experimentally measurable quantity in these electron-hole Josephson devices: $I_c^b = I_c$, the overall critical current of the system, and the density n is precisely controlled by gate potentials. This remarkable result provides a way of experimentally locating the BCS-BEC crossover boundary in 2D exciton systems.

Figure 3.9, shows the nature of the driving mechanisms of I_c^b for different V_0 and n . The density n is capped at the superfluid onset density, n_b . For very small V_0 , as we increase density, we go from bosonic excitations to fermionic pair-breaking excitations. By increasing V_0 , a region of tunnelling of electron-hole pairs appears at small n . When $V_0 > 0.3\epsilon_B$, strong screening preempts v_c^b from reaching the maximum, so there are no pair-breaking fermionic excitations.

For high potential barriers, $V_0 > 0.7\epsilon_B$, there are no bosonic excitations, and only tunnelling through the barrier remains.

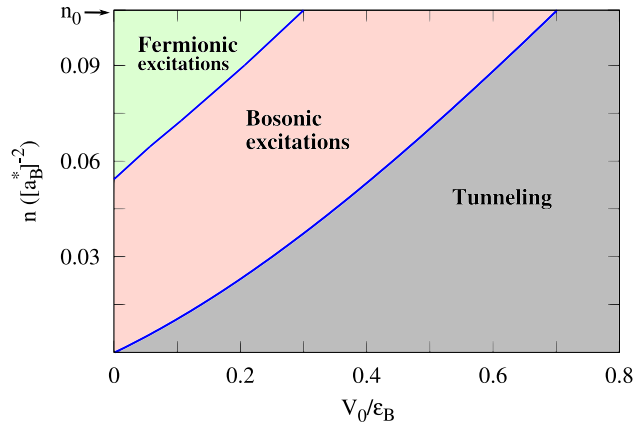


FIGURE 3.9: Driving mechanisms for the Josephson critical current at different barrier heights V_0 . In the fermionic excitation area, the critical current is determined by the pair-breaking branch, in the bosonic excitation area it is determined by the Anderson-Bogoliubov branch. The tunnelling area corresponds to the high-potential barrier region.

3.4 Conclusions

We have demonstrated that measurements of the critical current across a Josephson-junction barrier can yield significant additional information on electron-hole superfluid properties in a double-layer TMD heterostructure. The barrier can be fabricated and its height adjusted by suitable combinations of TMD layers.

The additional information is as follows.

- The existence of a Josephson effect below a critical tunnelling current is *per se* a direct signature of superfluidity. We note that this could be used to distinguish between a phase of excitons in a normal or superfluid state. Up to now, this has required painstaking analysis to merge Coulomb drag resistance and counterflow experimental data [192].
- For low barriers, the crossover physics in the barrier region controls the transport properties of the entire device.
- One can experimentally observe the maximum of the critical velocity at the density where excitations switch from bosonic to fermionic, the density in this system controlling the coupling strength. This maximum can be used to identify the boundary separating the BEC and BCS-BEC crossover regimes of the electron-hole superfluidity, and in fact, remarkably, the density at the maximum matches the density at which the condensate fraction passes through 0.8.

Chapter 4

Effects of intralayer correlations on electron-hole bilayer superfluidity

In this chapter, we investigate the intralayer correlations acting within the layers in the superfluid phase of electron-hole spatially separated layers. In this system, superfluidity is predicted to be almost exclusively confined to the BEC and crossover regimes where the electron-hole pairs are well localized. We show that the system is in the weak intralayer correlation region and the Hartree-Fock is an excellent approximation to treat intralayer correlations. We find in the BEC regime that the effect of the intralayer correlations on superfluid properties is negligible, but in the BCS-BEC crossover regime, the superfluid gap is significantly weakened by the intralayer correlations. This is caused by the intralayer correlations boosting the number of low-energy particle-hole excitations that drive the screening. We further find that the intralayer correlations suppress the predicted phenomenon in which the average pair size passes through a minimum as the crossover regime is traversed. The results we present here have been published in Ref. [44].

Theoretical investigations of excitonic superfluidity in two-layer systems have mainly focused on the interlayer electron-hole correlations needed to generate the electron-hole pairs. Reference [75] was the first attempt to include the effect of intralayer correlations on superfluidity in this system by including an unscreened repulsive intralayer interaction term in the Hamiltonian. However, there is no comparison of results with and without these correlations, so the role of the intralayer correlation is not yet clear. In addition, Ref. [46] showed that screening plays a central role in exciton superfluidity, particularly at high density where the intralayer correlation is expected to be stronger. Thus intralayer correlation should be included side by side with screening. Finally, Refs. [12, 104] show Quantum Monte Carlo (QMC) simulations where all correlations, and in fact all vertex corrections, are included. These can yield no information about the vertex corrections separate contributions, nor where in the phase diagram the intralayer correlations become significant.

In this chapter, we show that the Hartree-Fock approximation is a valid approximation to treat the intralayer repulsive interaction in electron-hole bilayer superfluids. Then, we investigate the effect of the intralayer correlation on the superfluid properties as a function of the density, benchmarking the results with QMC simulations in the case of double-bilayer graphene. Finally, we explore the effect of intralayer correlation exploring the BCS-BEC crossover by fixing the density and tuning the interlayer distance.

4.1 Hartree-Fock correlations in bilayer exciton system

Superfluidity of spatially indirect excitons has been predicted at low density, where the average separation between the excitons is much greater than the layer spacing separating the electrons and holes. The excitons are then well approximated by particles with dipole moments perpendicular to the layers and mutually interacting through weak repulsive dipole-dipole interactions acting parallel to the layers [11, 106].

For a dipolar system, at low density, the kinetic energy effects exceed the dipole-dipole correlations, and the system is in the region of weak correlations [131]. At high density, the dipole system enters the strong correlation region in which the dipole-dipole correlations exceed the kinetic energy [193].

This is in striking contrast to Wigner crystallization in double-layer coulombic systems, where at low densities the intralayer correlations from the Coulomb interactions are dominant over kinetic energy effects, and the system is in the region of strong correlations [105], while at high density is in the weak correlation region [134].

Here we want to identify the regions of intralayer correlations for an exciton bilayer. We evaluate the expectation value of the kinetic energy $\langle K \rangle$ and of the intralayer repulsive interaction $\langle V_S^{sc} \rangle$ [131]:

$$\langle K \rangle = \frac{1}{S} \sum_{\lambda} \sum_k \tilde{\zeta}_{\lambda}(k) n(k), \quad (4.1)$$

$$\langle V_S^{sc} \rangle = \frac{1}{2S} \sum_{\lambda} \sum_{k,q} V_S^{sc}(k-q) n(q) n(k), \quad (4.2)$$

with $\tilde{\zeta}_k = \varepsilon_k - \mu_s$ and $n(k)$ density of state. We use the RPA self-consistent screened intralayer interaction V_S^{sc} , Eq. (2.79).

For equal electron and hole layers, the sum over the layer index $\lambda = e, h$ gives equal contributions:

$$\langle K \rangle = \frac{2}{S} \sum_k \tilde{\zeta}_{\lambda}(k) n(k), \quad (4.3)$$

$$\langle V_S^{sc} \rangle = \frac{1}{S} \sum_{k,q} V_S^{sc}(k-q) n(q) n(k). \quad (4.4)$$

We consider a Double bilayer graphene with single-particle parabolic bands with $\varepsilon_k = \hbar^2 k^2 / 2m^*$, with equal effective masses $m^* = m_e^* = m_h^* = 0.04$. For the spin and valley degeneracy, we consider $g_s g_v = 2$. We take hBN as the insulator between the layers with dielectric constant $\epsilon = 2$. We consider equal electron and hole layer densities, $n = n_e = n_h$, corresponding to an average interparticle spacing in the layers of $r_0 = (\pi n)^{-1/2}$.

We evaluate Eqs. (4.3)-(4.4) both in the normal and superfluid state as a function of the density. In the superfluid state, we solve the gap and number equations of the system at zero temperature (Eq. (2.66)-(2.70)) without the intralayer correlation term in $\tilde{\zeta}(k)$. We obtain the behaviour of the density of states $n(k)$, the chemical potential μ_s and the screened intralayer interaction V_S^{sc} (Eq. (2.79)) as a function of the density. Because of strong screening, there is a maximum onset density for the superfluidity that corresponds to $r_0 \simeq a_B^*$.

Figure 4.1 shows the ratio between the kinetic energy $\langle K \rangle$ and the intralayer interaction $\langle V_S^{sc} \rangle$ expectation values as a function of the intralayer distance r_0 . In the superfluid regime, for $r_0 / r_{on} > 1$, $\langle K \rangle$ is larger than $\langle V_S^{sc} \rangle$, the system is in the superfluid state with weak correlations region. As r_0 approaches r_{on} , at onset density, the interlayer attractive

interaction is strongly suppressed by the screening and the particle-particle intralayer Coulomb interaction takes over the exciton-exciton dipole interaction. Above the onset density $r_0/r_{on} < 1$, when the superfluidity suddenly disappears, the ratio $\langle K \rangle / \langle V_S^{sc} \rangle >$ increases to greater than 1, resembling a Coulomb-like behaviour at large density. The exciton bilayer system is in the normal state characterized by a weak correlations region.

We conclude that for a DBG, in the density interval where superfluidity is predicted [43, 46], the system is always in the weak correlation region. In this region, an expansion of the corrections due to the intralayer correlations will be dominated by the Hartree-Fock contribution [194].

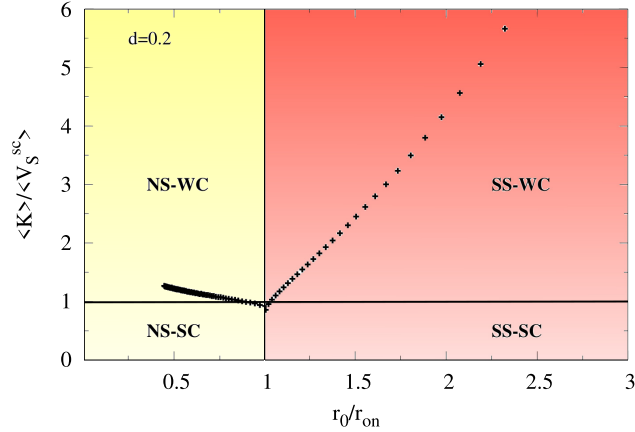


FIGURE 4.1: The ratio between the kinetic energy $\langle K \rangle$ and the intralayer interaction $\langle V_S^{sc} \rangle$ expectation values as a function of the intralayer distance r_0 for a fixed interlayer distance $d = 0.2$. r_0 is in unit of the onset interparticle distance r_{on} . The four regions identify the Normal State with Weak Correlation (NS-WC), Superfluid State with Weak Correlation (SS-WC), Normal State with Strong Correlation (NS-SC), and Superfluid State with Strong Correlation (SS-SC).

We have shown in Chap. 2 that with the inclusion of the Hartree-Fock term the coupled mean-field equations for the superfluid gap Δ_k and layer density n are given by:

$$\Delta(k) = -\frac{1}{S} \sum_{k'} V_D^{sc}(k-k') \frac{\Delta(k')}{2E^{HF}(k')}, \quad (4.5)$$

$$n = \frac{g_s g_v}{S} \sum_k \frac{1}{2} \left(1 - \frac{\epsilon_k - \mu_s}{E^{HF}(k)} \right). \quad (4.6)$$

where $E^{HF}(k) = \sqrt{\zeta_k^{HF^2} + \Delta_k^2}$ is the excitation energy, $\zeta_k^{HF} = \epsilon_k - \mu_s - \Sigma(k)$ with $\Sigma(k) = \frac{1}{S} \sum_p V_S^{sc}(p-k)n_p$, and the density of states $n_k = \frac{1}{2}(1 - \zeta_k^{HF}/E_k^{HF})$ [131, 195]. We considered screened RPA interlayer and intralayer interactions, Eqs. (2.79)-(2.80).

We express lengths in units of the effective Bohr radius, $a_B^* = \epsilon a_0 m_e / m_r^* = 5.3$ nm, where $m_r^* = m^*/2$ is the reduced mass. Energies are expressed in effective Rydberg $Ry^* = 68$ meV.

Figure 4.2(a) shows the resulting superfluid energy gap Δ_k for a layer separation $d = 0.2$.

The intralayer distance r_0 can be tuned using gate voltage exploring the BCS-BEC crossover. We span the full range for superfluidity: $r_0 = 3.0$ deep BEC regime, $r_0 = 2.0$ crossover regime, $r_0 = 1.5$ close to onset density. As the onset density is approached, we

see that the Hartree-Fock correlations have a strong effect on the superfluidity, reducing the gap Δ_k by as much as a factor of 2 (Fig. 4.2(a)).

Figure 4.2(b) demonstrates that this suppression of Δ_k comes from the effect of the Hartree-Fock correlations weakening the self-consistent electron-hole screened interaction, $V_D^{sc}(q)$. The weakening is due to the Hartree-Fock corrections boosting the number of the low-energy particle-hole excitations that drive the screening (see Fig. 4.2(c)). The effect of the intralayer correlations on the superfluidity weakens with decreasing density, and for $r_0 \gtrsim 3$ the correlations have negligible effect.

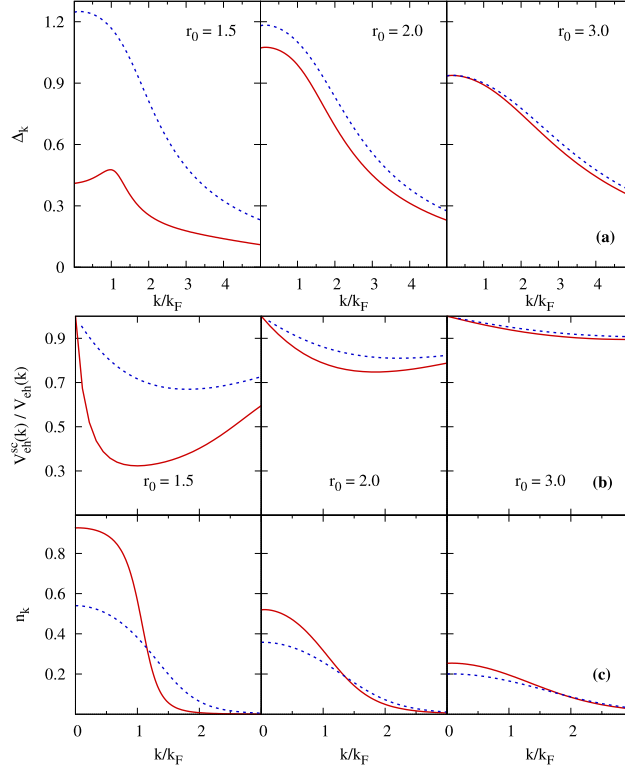


FIGURE 4.2: (a) Superfluid gap Δ_k in effective Rydberg Ry^* units at densities with average interparticle spacing r_0 . Layer separation $d = 0.2$. Solid red: Δ_k within the mean field including intralayer correlations. Dashed blue: Δ_k within the mean-field but neglecting intralayer correlations. (b) Ratio of self-consistent screened electron-hole attraction $V_{eh}^{sc}(k)$ to the bare attraction $V_{eh}^{eh}(k)$ for the same densities. (c) Corresponding density of states n_k .

Figure 4.3 compares our results with Diffusion Quantum Monte Carlo (DQMC) numerical simulations [43] with the same physical parameters.

Figure 4.3(a) shows that including the Hartree-Fock correlations significantly improves the agreement with DQMC for both the height and position of the maximum of the superfluid peak Δ_{max} .

Figures 4.3(b) and (c) compare the condensate fraction CF and the QMC single-particle chemical potential μ_s (see Appendix E), respectively. We see that the Hartree-Fock corrections are significant and move these quantities closer to the benchmark DQMC results.

Note that the condensate fraction in Ref. [43] is a quantity that does not rely on any fitting procedure or model, therefore it offers an unfiltered way to compare the qualitative and the quantitative effects of the different correlations.

DQMC shows a brief entrance into the BCS regime, specified by $CF < 0.2$, whereas our onset density preempts entry into the BCS regime. This is associated with static

screening underestimating the onset density. Corrections from dynamical screening have been shown to increase this density [196].

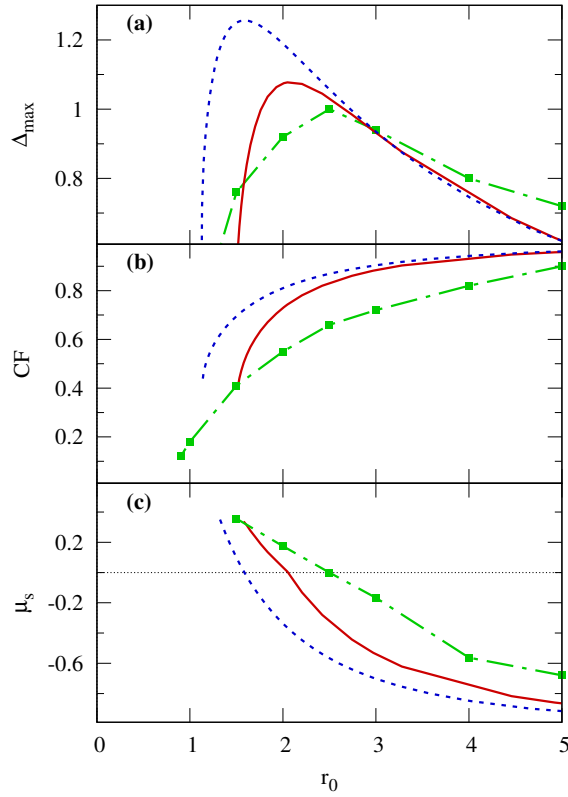


FIGURE 4.3: (a) Maximum superfluid gap Δ_{max} as function of r_0 , the average inter-particle distance within a layer. Solid red: Δ_{max} within mean-field with intralayer correlations. Dashed blue: Δ_{max} within the mean-field but without intralayer correlations. Shown for comparison (dash-dot green), the Δ_{max} from Diffusion Quantum Monte Carlo numerical simulations [43]. (b) The corresponding condensate fraction CF . (c) The corresponding single-particle chemical potential μ_s .

During the last decade, different materials with different interlayer distances have been found to host stable exciton systems. The smallest separation experimentally attained to date, in units of their effective Bohr radii, are: in Gallium Arsenide (GaAs) double quantum wells $d \simeq 1.0$ (10 nm) [56, 197, 198], in double bilayer graphene (DBG) $d \simeq 0.2$ (1 nm) [1], and in double layer Transition Metal Dichalcogenide (TMD) $d \simeq 0.45$ (0.6 nm) [2, 3].

In Fig. 4.4 we report the ratio between the expectation value of the kinetic energy and intralayer interaction for those interlayer distances d . As d increases, the ratio $\langle K \rangle / \langle V_S^{sc} \rangle$ decreases because the intralayer interaction V_S^{sc} is less screened, and so it is stronger. This results in the system being able to enter the strong correlations region $\langle K \rangle / \langle V_S^{sc} \rangle < 1$ in the superfluid state close to onset density.

By increasing the density above the onset density, the ratio $\langle K \rangle / \langle V_S^{sc} \rangle$ increases, and the system goes from normal state strong correlations to normal state weak correlations region. This means that there is a density interval around the onset density in which the Hartree-Fock approximation is not a good approximation for the intralayer correlations, neither for the superfluid nor for the normal state.

We find that with the inclusion of the Hartree-Fock intralayer correlations the onset density is reduced, and this reduction increases as d increases, as reported in Fig. 4.5.

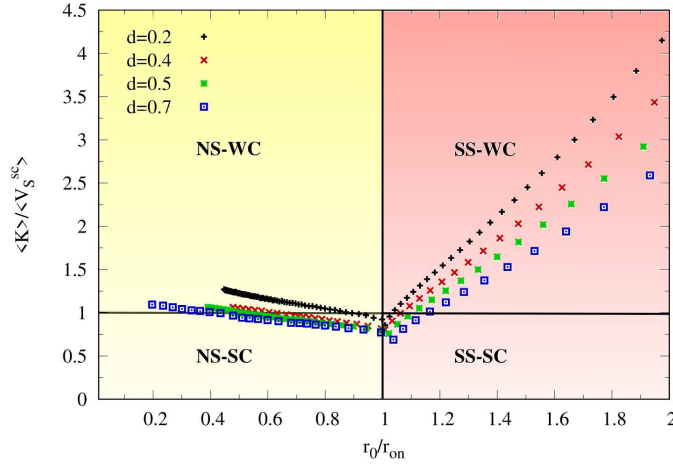


FIGURE 4.4: The ratio between the kinetic energy $\langle K \rangle$ and the intralayer interaction $\langle V_S^{sc} \rangle$ expectation values as a function of the intralayer distance r_0 for different interlayer distances: $d = 0.2$ (black points), $d = 0.4$ (red points), $d = 0.5$ (green points), $d = 0.7$ (blue points). Here the interparticle and interlayer distances are in units of the onset interlayer distance r_{on} .

Figure 4.5 maps out the superfluidity and its regimes at very low temperatures in the r_0 - d phase space with the inclusion of Hartree-Fock correlations.

The boundary between the BEC and the BCS-BEC crossover regimes as a function of the interlayer distance in Fig. 4.5(a), corresponds to when the chemical potential μ_s changes sign from negative to positive (Fig. 4.3(b)) [191, 199]. Fig. 4.5(b) shows that this boundary corresponds to $\Delta_{max}/E_F \simeq 5$.

Figure 4.5 shows that the inclusion of intralayer correlations strongly reduces the region of the $r_0 - d$ space in which superfluidity survives. This leads to the whole superfluid phase, from low density up to the onset density, being always in the weak correlations regions $\langle K \rangle / \langle V_S^{sc} \rangle > 1$.

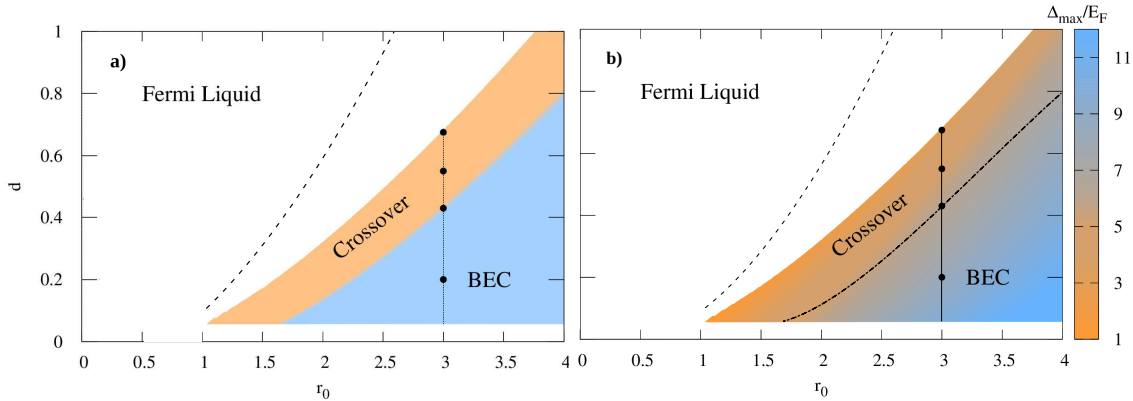


FIGURE 4.5: a) BEC and BCS-BEC crossover regimes are individuated when the single-particle chemical potential μ_s changes sign as a function of the layer separation d and average interparticle spacing r_0 . The BCS regime is preempted by strong screening that suppresses superfluidity at small r_0 and large d . b) Max gap energy Δ_{max} divided by the Fermi energy E_F . The black dash-dotted line delimits the boundary between the BEC and the crossover regime reported in panel (a). In both panels marked are the points in r_0 - d phase space used in Fig. 4.4 and Fig. 4.6. The black dashed line in both panels is the boundary of the superfluid phase without the intralayer correlations.

We compare in Fig. 4.6(a) for a fixed value of the layer interparticle spacing $r_0 = 3$, the evolution of the superfluid gap energy Δ_k when the Hartree-Fock correlations within the layers are either included or neglected, for different layer separations d . The corresponding (r_0-d) points are marked on the phase diagram, Fig. 4.5. Figure 4.6(b) compares the corresponding ratios of screened electron-hole attraction $V_D^{sc}(k)$ to the bare attraction $V_D(k)$.

The layer spacing $d = 0.2$ lies deep in the BEC regime and Fig. 4.6(b) confirms that screening is indeed negligible there.

Since the Hartree-Fock corrections primarily affect the screening, the correlations have almost no effect on Δ_k for $d = 0.2$. However, $d = 0.4$ lies on the BCS-BEC crossover boundary, and we see at that point that screening is no longer negligible, and as a consequence, Δ_k starts to develop a sensitivity to the Hartree-Fock corrections. As d is further increased and the crossover regime is traversed, both the screening and Δ_k become increasingly sensitive to the Hartree-Fock corrections. By $d = 0.7$, the correlations boost the low-lying density of states so much that the screening is strongly enhanced. This in turn strongly suppresses Δ_k . $d = 0.7$ is close to the superfluid threshold where the screening kills the superfluidity.

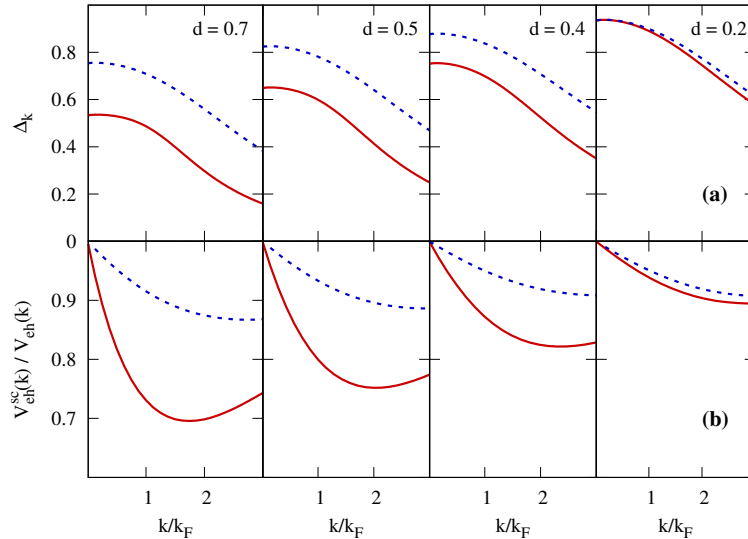


FIGURE 4.6: (a) Superfluid gap $\Delta(k)$ for a fixed density corresponding to $r_0 = 3$, at different d points in the BEC and BCS-BEC crossover regimes (refer Fig. 4.5). Solid red: $\Delta(k)$ within mean-field with intralayer correlations included. Dashed blue: $\Delta(k)$ within mean-field but neglecting intralayer correlations. (b) Ratio of self-consistent screened electron-hole attraction $V_D^{sc}(k)$ to the bare attraction $V_D(k)$ for the same r_0-d points spanning the BEC and BCS-BEC crossover regimes.

Figure 4.7 compares, with intralayer correlations included or neglected, the spatial size of the electron-hole pairs [191, 200],

$$\xi_{pair} = \left[\frac{\sum_{\mathbf{k}} |\nabla_{\mathbf{k}} u_{\mathbf{k}} v_{\mathbf{k}}|^2}{\sum_{\mathbf{k}} u_{\mathbf{k}}^2 v_{\mathbf{k}}^2} \right]^{1/2}, \quad (4.7)$$

as a function of r_0 for layer separation $d = 0.2$.

Without the intralayer correlations, starting from the low-density BEC regime, ξ_{pair} initially decreases as the density increases. In the BEC regime, the pairs act as well-spaced

composite bosons interacting primarily through exchange, thus, as the interparticle spacing decreases, exchange effects strengthen causing the pairs to shrink [201]. In contrast, in the crossover regime, the bosonic nature of the pairs is lost because there is a significant overlap of the single-fermion wave functions. Thus ξ_{pair} will grow exponentially as the density is further increased. Reference [201] pointed out that this competing behaviour leads to a minimum in ξ_{pair} . In Fig. 4.7 this minimum is clearly visible when intralayer correlations are omitted.

However, we find that when intralayer correlations are included, the resulting build-up of screening strength with increasing density greatly weakens the shrinkage of ξ_{pair} and effectively eliminates the minimum. Then at higher densities, the very strong screening further weakens the superfluidity, causing the ξ_{pair} to grow exponentially. ξ_{pair} diverges at the onset density for superfluidity. For $d > 0.2$, there is no minimum when intralayer correlations are included, and the minimum without correlations rapidly weakens. Our results can be compared with the Cooper pair radii from Diffusion Quantum Monte Carlo (DQMC) reported in Ref. [43]. We found that the inclusion of intralayer correlations improves the agreement with the results for the Cooper pair radius from DQMC.

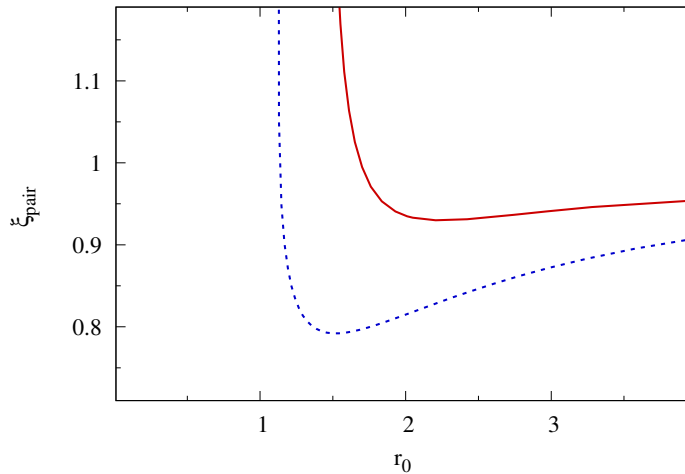


FIGURE 4.7: The pair size of the exciton ξ_{pair} as a function of r_0 , the average interparticle spacing in each layer. The layer separation is $d = 0.2$. Solid red: within mean-field with intralayer correlations included. Dashed blue: within mean-field but neglecting intralayer correlations.

4.2 Conclusions

We have demonstrated that the primary effect of the Hartree-Fock correlations on the superfluid properties of an exciton bilayer system is an increase in the strength of screening caused by a boost in the density of the low-lying states. Screening plays a crucial role in determining superfluid properties because the pairing interaction is long-range [45, 46], and we find that the strength of the screening can be as much as doubled by the Hartree-Fock corrections. Effects of screening on the superfluidity are negligible in the deep BEC regime [48] and therefore Hartree-Fock has minimal effect in that regime, but in the BCS-BEC crossover regime, where screening plays a crucial role in determining the superfluid properties, the increased screening strength results in:

4.2. Conclusions

- A diminution of the superfluid gap Δ by up to a factor of two within the BCS-BEC crossover regime, leading to a better agreement with the DQMC simulations.
- A shift to lower densities of the boundary between the BEC and crossover regimes.
- A disappearance of the minimum in the electron-hole pair-size as a function of density.

Chapter 5

Density Collective Modes

In this chapter, we explore collective modes in the exciton bilayer system as a fingerprint of the presence of the superfluid exciton phase. We focus on collective modes originated by density fluctuations treated with Random-Phase approximation. We compare results in the normal state and superfluid state to identify unambiguous fingerprints of the presence of the superfluid phase in the bilayer exciton system. In addition, we discuss the main differences between the collective modes associated with the long-range Coulomb interaction in an exciton bilayer with respect to and the collective modes associated with the contact interaction in cold atom gases. Finally, we qualitatively discuss the collective modes originating from fluctuations in the amplitude and phase of the superfluid order parameter.

The experimental investigation of collective modes has been widely used in superconductors and ultracold gas atoms to study how systems respond to external perturbations. A variety of collective modes associated with the perturbation of different quantities of the system has been found. Different collective modes appear and characterize different phases of the system. Thus collective modes are a powerful tool that can be used as an unambiguous fingerprint of exciton superfluidity in a bilayer system.

A recent study [142] described density collective modes in a bilayer exciton superfluid using a "quasi-localized particle approximation," where electrons and holes are highly localized. They identified acoustic and optic modes similar to those found in the normal state of the exciton bilayer. However, these are gapped in the superfluid phase. This approximation is valid in low-density and large interlayer distance regimes with weak interactions. Similar results were found in an exciton solid bilayer system using the same approximation, where excitons are organized in a crystal structure [145].

We propose here a complete description of density collective modes in the bilayer exciton system in the superfluid phase through the BCS-BEC crossover. We use the superfluid model reported in Chapter 1 without any restriction on the localization of electrons and holes. We compare the results in the superfluid phase and in the normal state looking for unambiguous fingerprints of the normal-superfluid phase transition.

5.1 Exciton bilayer density response function

We investigate the collective modes originated by density fluctuations.

In Chap. 2 we have evaluated the screened interlayer and intralayer interactions to account for the effect of density fluctuations in the bilayer exciton system. Using these screened interactions in the gap and number equation, rather than the bare ones, significantly impacts the gap energy, the single-particle chemical potential, and the density behaviour [44, 46–48, 202, 203].

In Sec. 2.3 we have reported how from the RPA Dyson equation for the screened interaction $W^{RPA}(q, \omega)$ (Eq. (2.72)) it is possible to get the RPA screened interaction Eq. (2.73).

Equation (2.72) can be rewritten also with the dressed polarization function $\Pi^{RPA}(q, \omega)$ [134]:

$$W^{RPA}(q, \omega) = V(q) + V(q)\Pi^{RPA}(q, \omega)V(q). \quad (5.1)$$

Comparing Eq. (2.72) and Eq. (5.1) one gets:

$$\Pi^{RPA}(q, \omega) = \frac{\Pi_0(q, \omega)}{1 - \Pi_0(q, \omega)V(q)}. \quad (5.2)$$

This is the RPA polarization function corresponding to the density response function of the system [158].

In a bilayer exciton system of equal electrons and holes, we have:

$$\Pi^{RPA}(q, \omega) = \begin{pmatrix} \Pi_{ee}^{RPA}(q, \omega) & \Pi_{eh}^{RPA}(q, \omega) \\ \Pi_{eh}^{RPA}(q, \omega) & \Pi_{ee}^{RPA}(q, \omega) \end{pmatrix}, \quad (5.3)$$

The diagonal element $\Pi_{ee}^{RPA}(q, \omega)$ is the electron-electron response function which describes the particle density response in one layer due to a density perturbation in the same layer. The off-diagonal element $\Pi_{eh}^{RPA}(q, \omega)$ is the electron-hole response function which describes the particle density response in one layer due to a density perturbation in the opposite layer. The $V(q)$ is the 2×2 bare interaction matrix and $\Pi_0(q, \omega)$ is the 2×2 zero-order polarization function matrix defined as:

$$V(q) = \begin{pmatrix} V_S(q) & V_D(q) \\ V_D(q) & V_S(q) \end{pmatrix}, \quad (5.4)$$

$$\Pi_0(q, \omega) = \begin{pmatrix} \Pi_0^N(q, \omega) & \Pi_0^A(q, \omega) \\ \Pi_0^A(q, \omega) & \Pi_0^N(q, \omega) \end{pmatrix}, \quad (5.5)$$

where $V_S(q)$ and $V_D(q)$ are the bare intralayer repulsive and interlayer attractive interaction and $\Pi_0^N(q, \omega)$ and $\Pi_0^A(q, \omega)$ are the normal and anomalous zero order polarization:

$$\Pi_0^N(q, \omega) = \frac{1}{S} \sum_k \frac{u_k^2 v_{k+q}^2}{\omega - E(k) - E(k+q)} - \frac{u_{k+q}^2 v_k^2}{\omega + E(k) + E(k+q)}, \quad (5.6)$$

$$\Pi_0^A(q, \omega) = \frac{1}{S} \sum_k \frac{u_{k+q} v_{k+q} u_k v_k}{\omega - E(k) - E(k+q)} - \frac{u_{k+q} v_{k+q} u_k v_k}{\omega + E(k) + E(k+q)}, \quad (5.7)$$

where u_k and v_k are the Bogoliubov amplitudes defined in Eq. (2.96)-(2.97).

Replacing Eq. (5.3), Eq. (5.4) and Eq. (5.5) in Eq. (5.2) one gets:

$$\Pi_{ee}^{RPA}(q, \omega) = \frac{\Pi_0^N(q, \omega) - V_S(q)\mathcal{B}(q, \omega)}{1 - 2(\Pi_0^N(q, \omega)V_S(q) + \Pi_0^A(q, \omega)V_D(q)) + \mathcal{A}(q)\mathcal{B}(q, \omega)}, \quad (5.8)$$

$$\Pi_{eh}^{RPA}(q, \omega) = \frac{V_D(q)\mathcal{B}(q, \omega) + \Pi_0^A(q, \omega)}{1 - 2(\Pi_0^N(q, \omega)V_S(q) + \Pi_0^A(q, \omega)V_D(q)) + \mathcal{A}(q)\mathcal{B}(q, \omega)}, \quad (5.9)$$

where $\mathcal{B}(q, \omega) = \Pi_0^N(q, \omega)^2 - \Pi_0^A(q, \omega)^2$ and $\mathcal{A}(q) = V_S(q)^2 - V_D(q)^2$.

The poles in the electron-electron and the electron-hole RPA response functions reveal the presence of collective modes. These modes represent a coordinated motion of

particles characterized by a certain momentum q and energy ω , in response to a density perturbation acting on the system [194]. The energy spectra of the density collective modes are obtained by looking for combinations of $[q, \omega]$ to make the denominator of the response functions zero.

In a system with equal electron and hole layers, the electron-electron and the electron-hole response functions share the same denominator. The energy spectra of the density collective modes are given by:

$$1 - 2(\Pi_0^N(q, \omega)V_S(q) + \Pi_0^A(q, \omega)V_D(q)) + \mathcal{A}(q)\mathcal{B}(q, \omega) = 0. \quad (5.10)$$

The collective modes are stable if there is a real solution $\omega(q)$ of Eq. (5.10). If there is a complex $\Omega(q) = \omega(q) + i\Gamma(q)$ the collective mode associated is unstable, and $\Gamma(q)$ is the damping parameter which characterises the lifetime of the collective modes.

Note that both the normal $\Pi_0^N(q, \omega)$ and the anomalous $\Pi_0^A(q, \omega)$ superfluid polarization functions, Eqs. (5.6) and (5.7), have poles for real ω . The region in the $(\omega - q)$ space where these zero-order polarization functions have poles is known as the amplitude excitation or continuum region.

In Appendix F is reported how the normal polarization $\Pi_N(q, \omega)$, Eq. (F.2), has poles in the normal exciton state for $\omega = E(k + q) - E(k)$.

In the normal state, the continuum is defined by the geometry of the Fermi surfaces of the two Fermi liquids and accounts for the possible excitation energies of quasi-particle/quasi-anti-particle pairs. A perturbation with $\omega(q)$ in the normal state promotes a particle from an occupied state (which then remains empty, referred to as the quasi-anti-particle) with wave vector k to an empty state with wave vector $k + q$ (the quasi-particle) [131].

In the BEC superfluid regime, most electron-hole pairs are condensed in the system ground state. A density perturbation with energy ω and momentum q can excite an entire electron-hole pair from the ground state. If the perturbation energy is sufficiently high, the exciton breaks, promoting the electron to an energy state $E(k)$ and the hole to a state $E(k + q)$, or vice versa. Therefore, the normal and anomalous polarization functions have poles when the perturbation energy ω equals $E(k) + E(k + q)$.

In both cases, the excitations have a finite lifetime, ultimately resulting in the recombination of the quasi-particle and quasi-anti-particle with photon emission in the normal state or the reformation of the exciton pair in the ground state for the superfluid case. Within the continuum, the polarization functions are complex.

Since Eq. (5.10) is invariant under the change Ω to $-\Omega$ we impose $Re[\Omega] = \omega > 0$. The branch cut in which the zero-order polarization functions diverge is given by $\omega \in C_q = \{E(q + k) + E(k), k \in R^2\}$, originating from the denominator $\omega - E(k) - E(k + q)$ of the polarization functions. The behaviour of the dispersion relation $E(k)$, and thus the position of the continuum in the energy spectrum $\omega(q)$, depends on the system location within the BCS-BEC crossover region.

5.1.1 Density collective modes in BEC regime

We consider the same system of the previous chapter with the interlayer distance $d = 0.2a_B^*$ and we set the interparticle distance $r_0 = 3a_B^*$, in the BEC. As shown in the previous chapter, intralayer correlations are negligible in the deep BEC regime for this $(d - r_0)$. Thus, $\zeta(k) = \varepsilon(k) - \mu_s$ with $\varepsilon(k) = \hbar^2 k^2 / 2m^*$.

We rewrite the normal and anomalous polarization functions, Eq. (F.2)-(5.7), in the superfluid exciton phase replacing the sum over k with the integral:

$$\Pi_0^N(q, \omega) = \frac{1}{\pi} \int dk k \int_0^{2\pi} d\theta \frac{u_k^2 v_{k+q}^2}{\omega - E(k) - E(k, q, \theta)} - \frac{u_{k+q}^2 v_k^2}{\omega + E(k) + E(k, q, \theta)}, \quad (5.11)$$

$$\Pi_0^A(q, \omega) = \frac{1}{\pi} \int dk k \int_0^{2\pi} d\theta \frac{u_{k+q} v_{k+q} u_k v_k}{\omega - E(k) - E(k, q, \theta)} - \frac{u_{k+q} v_{k+q} u_k v_k}{\omega + E(k) + E(k, q, \theta)}, \quad (5.12)$$

where $E(k, q, \theta) = E(\sqrt{k^2 + q^2 + 2kq\cos(\theta)})$. The polarization functions are in the unit of the 2D density of states per unit volume at the Fermi surface of a non-interacting system $N_0 = m_e/2\pi\hbar^2$, the momenta k and q in unit of the Fermi wavevector k_F and the energies $E(k)$, ω in unit of the Fermi energy ε_F .

We minimize $E(k, q, \theta) + E(k)$ as a function of k and θ finding the boundary $\bar{\omega}$ of the pair-breaking excitation area.

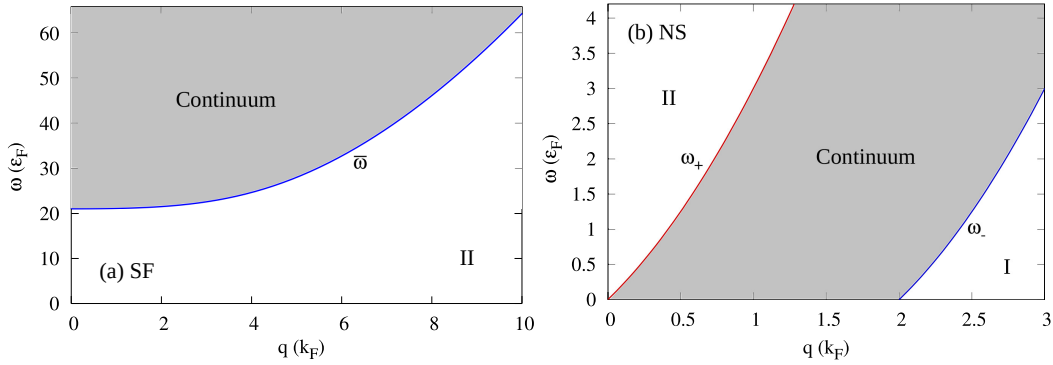


FIGURE 5.1: The pair-breaking continuum region (grey area) is shown for the interlayer distance $d = 0.2a_B^*$ in the exciton deep BEC superfluid state (SF) at the interparticle distance $r_0 = 3a_B^*$ (a) and the normal state (NS) at the interparticle distance $r_0 = 0.5a_B^*$ (b). In the BEC regime, the boundary is defined by the energy $\bar{\omega}$. In the normal state, the top and bottom boundaries are defined by the energies ω_+ and ω_- , respectively.

In Fig. 5.1, we show the pair-breaking continuum region (grey area) for the exciton deep BEC superfluid state and the normal state. In the superfluid phase for $\omega > \bar{\omega}$ the system is in the pair-breaking region and it has no upper boundary, (Fig. 5.1(a)) In contrast, in the normal state, (Fig. 5.1(b)), the continuum has a bottom (ω_-) and an upper (ω_+) energy boundary.

In the normal state, the zero temperature Fermi step functions in the numerator of the normal polarization function $\Pi_0^N(q, \omega)$, Eq. (F.3), impose a cut-off to the integral in k . For a fix q and $\omega > \omega_+$ or $\omega < \omega_-$, there is no value of k for which the denominator of the normal polarization Eq. (F.3) is zero.

In contrast, in the superfluid state, the Bogoliubov amplitudes smoothly approach zero for large momenta in the numerator of the superfluid polarisation functions. There is no cutoff on the integral and thus for any q and ω , there is always a value of k and θ for which the denominator of the normal and anomalous polarization functions is zero.

Figure 5.2 shows the real and imaginary part of the normal polarization function $\Pi_0^N(q, \omega)$ for $q = k_F$.

The imaginary part of the polarization function is zero for $\omega < \bar{\omega}$, while the real part is negative. Entering the pair-breaking excitation region the imaginary part presents maximum and the real part becomes suddenly positive, then they both decrease for large

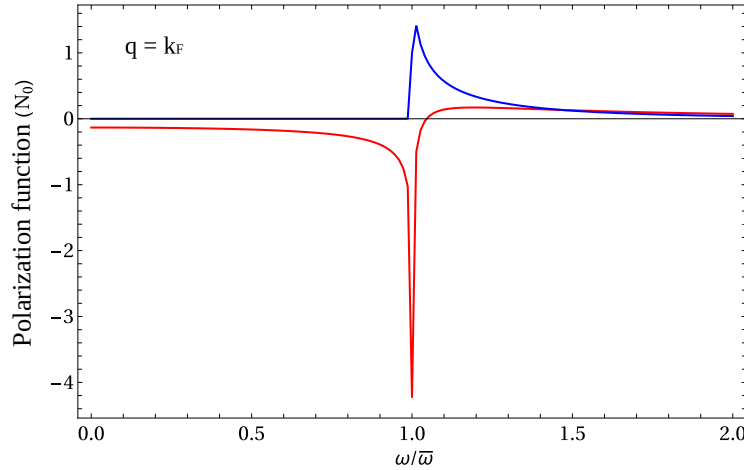


FIGURE 5.2: Real (red solid line) and imaginary (blue solid line) component of the normal polarization function $\Pi_0^N(\omega, q)$ as a function of ω for $q = k_F$. $N_0 = m/2\pi\hbar^2$ is the 2D density of states unit volume at the Fermi surface and $\bar{\omega}$ is the energy boundary of the superfluid continuum.

ω . This behaviour is similar to the one reported in Fig. F.2 for the normal polarization function $\Pi_0^N(q, \omega)$ in the normal state for $q > 2k_F$ where there is a stable excitation region of the $(\omega - q)$ space which precedes the continuum. The difference is that in the normal state for $q > 2k_F$, when $\omega > \omega_+$, the imaginary part is zero while the normal part remains positive.

In Appendix F we show how in the normal state there are stable collective modes only if $\Pi_0^N(q, \omega) > 0$. This happens if $\omega > \omega_+$, so in the region of the $(\omega - q)$ space above the continuum region.

In the superfluid phase, it is possible to show that Eq. (5.10) has real stable solutions only if $\Pi_0^N(q, \omega) - \Pi_0^A(q, \omega) > 0$.

The normal and anomalous polarization functions in the BEC regime cancel out each other as a function of q and ω . For $\omega < \bar{\omega}$ the difference $\Pi_0^N(q, \omega) - \Pi_0^A(q, \omega)$ is very small and slightly negative, making it impossible to have a real solution for Eq. (5.10).

In the BEC region, there are no real values of $[\omega, q]$ for which Eq. (5.10) is solved (Fig. 5.3), thus there are no stable density collective modes outside the continuum.

The effect of density fluctuations on the screening interaction is negligible because the excitons are well-spaced (large r_0) and they interact minimally with each other [147]. Consequently, density fluctuations do not induce a stable collective response in the system.

5.1.2 Density collective modes in the Crossover regime

Increasing the density and entering the crossover regime of the BCS-BEC crossover, the interlayer and intralayer interactions are significantly affected by density fluctuations and the screening process [44].

Setting $d = 0.2a_B^*$ and $r_0 = 1.5a_B^*$ the system is in the crossover regime close to onset density. We have shown in the previous chapter that the effect of the intralayer correlations is important as onset density is approached. Thus, $\zeta(k) = \varepsilon(k) - \mu_s - \Sigma(k)$, where $\Sigma(k) = 1/S \sum_{k'} V_S^{sc}(k - k')n(k')$ is the Hartree-Fock correlation energy. We evaluate the boundary of the pair-breaking excitation area in the crossover regime, including the intralayer correlations.

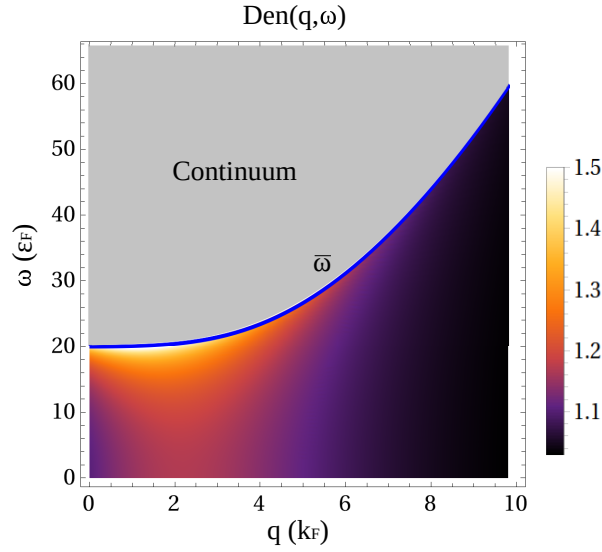


FIGURE 5.3: Heat map of the denominator $Den(q, \omega)$ of the normal and anomalous polarization function, Eq. (5.10), outside the continuum, $\omega < \bar{\omega}$, as a function of the momentum q and energy ω in the BEC regime.

Figure 5.4(a) shows that the intralayer correlation lowers $\bar{\omega}$ because the gap energy is significantly suppressed near the onset density when the intralayer correlations are included. The recess of $\bar{\omega}$ around k_F reflects the fact that the system is in the crossover-BCS regime and so the gap energy $\Delta(k)$ has a maximum around k_F . For $q < 2k_{min}$, where k_{min} is the momentum in which $E(k)$ has a minimum, $\bar{\omega}(q) = 2\Delta(q)$ like in ultracold gas atoms [204].

The normal polarization function $\Pi_0^N(q, \omega)$ for $\omega < \bar{\omega}$ is negative and keeps decreasing as q or ω increases. The difference between the normal and the anomalous polarization function, $\Pi_0^N(q, \omega) - \Pi_0^A(q, \omega)$ is negative and increases in modulus as q and ω increase (Fig. 5.4(b)). In the crossover regime, as in the BEC regime, there are no real solutions for Eq. (5.10) outside the continuum (Fig. 5.4(c)) and no maximum in the density response function.

This is strikingly different from what we find in the normal state, where the optic and acoustic modes appear outside the continuum (See Appendix F) [144]. In the BEC and crossover regime, the superfluid phase always features a large order parameter $\Delta(k) > \varepsilon_F$. It is because of this large energy gap in the single-particle excitation spectra, that low-energy excited states are inaccessible for the optic and acoustic modes found in the normal state. The macroscopic coherent phase of condensed excitons halts the propagation of stable density collective modes. The disappearance of the acoustic and optic branch outside the continuum lowering the density is a striking signal of the transition from normal to superfluid phase in the exciton bilayer system.

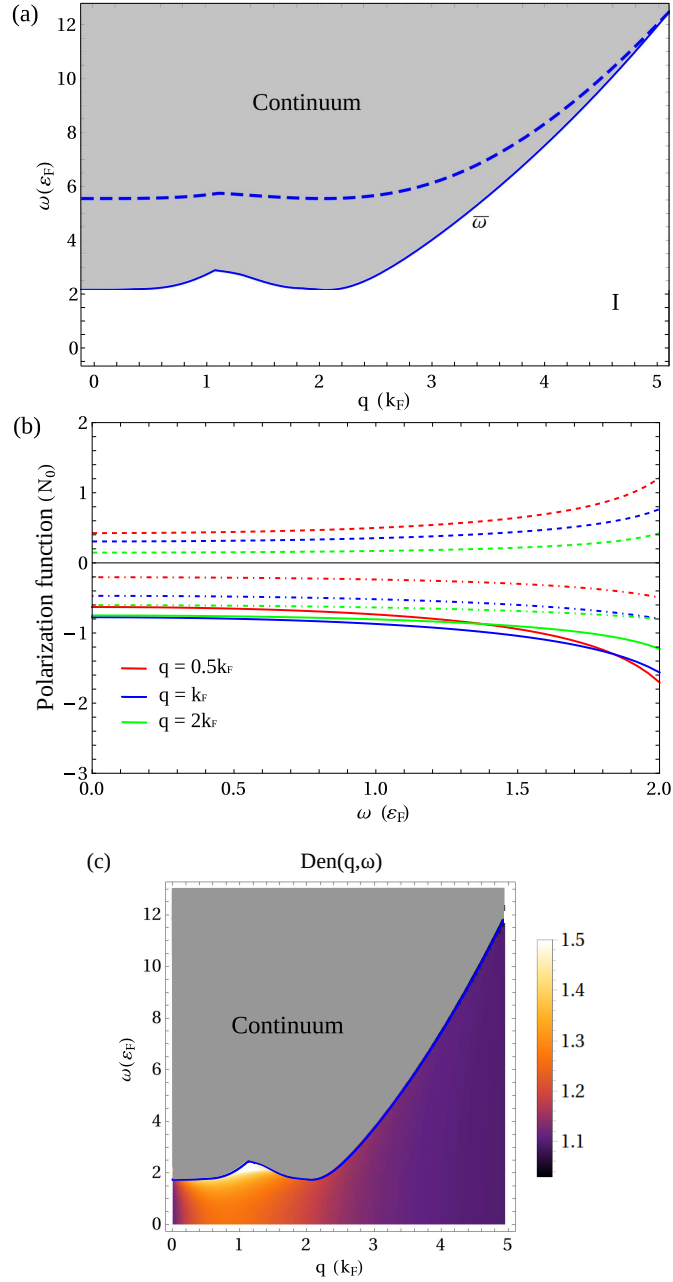


FIGURE 5.4: (a) Boundary of the continuum (grey area) in the $(\omega - q)$ space with the inclusion of the intralayer correlations (red solid line) and without (blue dashed line). (b) The normal polarization functions Π_0^N (solid lines), the anomalous polarization function Π_0^A (dashed lines) and the difference $\Pi_0^N - \Pi_0^A$ (dashed-dotted lines) with the inclusion of intralayer correlations for three different values of q : $q = 0.5k_F$ (red), $q = k_F$ (blue) and $q = 2k_F$ (green). (c) Heat map of the denominator $Den(q, \omega)$ of the normal and anomalous polarization function, Eq. (5.10), outside the continuum, $\omega < \bar{\omega}$, as a function of the momentum q and energy ω in the crossover-BCS regime. Here $d = 0.2a_B^*$ and $r_0 = 1.5a_B^*$ with $\Delta_{max} = \epsilon_F$.

5.2 Differences and analogies with cold atoms

We found no stable density collective modes in the superfluid phase of an exciton bilayer system. To properly discuss these results, we must recall some features related to the presence of collective modes in the density response function in ultracold gas atoms.

On collective modes in ultracold gas atoms

Superfluid ultracold atom systems are characterized by attractive contact interactions between fermions, leading to Cooper pair formation [205]. The collective modes, associated with amplitude and phase perturbations of the order parameter and with density perturbations, have been extensively studied throughout the BCS-BEC crossover using linear response theory [206].

These collective modes in ultracold gas atoms are identified by evaluating the amplitude, phase, and density response functions, using the gap energy and chemical potential derived from the gap and number equations, while including fluctuations in the order parameter and density.

Fluctuations of the order parameter can be incorporated through a path-integral approach [133, 137], where Gaussian fluctuations are represented as $\Delta(q) = \Delta_0 + \delta(q)e^{i\theta(q)}$, with Δ_0 as the mean-field energy gap, $\delta(q)$ as the amplitude fluctuation, and $\theta(q)$ as the phase fluctuation of the superfluid order parameter. Alternatively, these fluctuations can be included in the BCS Hamiltonian via driven fields that couple with the amplitude and phase of the order parameter and the particle density [139, 207].

It is crucial to note that the density response function is sensitive to phase and amplitude fluctuations, but the reverse is not true [204]. This is evident from the amplitude-density, phase-density, and density-density response functions (Eq. 43-46 in Ref. [204]). By considering only the matrix elements deriving from density fluctuations, the amplitude and phase response functions disappear but the opposite is not true. Density fluctuations do not affect the amplitude and phase response functions because of the RPA and the form of the normal and anomalous polarization functions.

In a 3D system within the BCS regime, the density response function shows a maximum outside the continuum, resulting from the coupling of the phase and density response functions and related to stable Anderson-Bogoliubov modes [135, 136].

In a 3D neutral system [133], the Anderson-Bogoliubov modes is gapless, $\omega_\theta(q = 0) = 0$. For a charged system, because of the presence of a repulsive Coulomb interaction between the fermions [139, 140], the phase mode acquires a gap $\omega_\theta(0) = \omega_{pl}$, where $\omega_{pl} = \sqrt{2\pi\hbar^2 ne^2 / m^* \epsilon \epsilon_0}$ is the plasma frequency, constant in q for 3D systems. In a 2D neutral system the gapless nature of the Anderson-Bogoliubov modes is preserved [208]. However, a study of this mode in a 2D charged system is missing. Because, in 2D systems the plasma frequency $\omega_{pl} = \sqrt{2\pi q \hbar^2 ne^2 / m^* \epsilon \epsilon_0}$ is zero at $q = 0$ (Fig. F.3), it is reasonable to say that also the 2D Anderson-Bogoliubov mode for a charged system is gapless in the crossover-BCS regime. One expects this to appear in the density response function for small q and ω outside the continuum.

On collective modes in exciton bilayer systems

In exciton bilayer systems, the density response functions $\Pi_{ee}^{RPA}(q, \omega)$ and $\Pi_{eh}^{RPA}(q, \omega)$ evaluated in Sec. 5.1 take into account only density fluctuations. The resulting gap energy, single-particle chemical potential and density do not include the effect of the order parameter fluctuations. As a net result, there are no poles in the denominator or maximum

in the density response function. Thus, there is no trace of stable Anderson-Bogoliubov modes outside the continuum just considering density fluctuations.

By including fluctuations of the order parameter phase $\theta(q)$, we expect the appearance of acoustic Anderson-Bogoliubov modes. In ultracold gas atoms, there is a smooth passage from the first sound collective mode in the normal state at $T > T_c$ to the Anderson-Bogoliubov mode in the superfluid phase at $T < T_c$. They both coincide with the hydrodynamic sound of the system given by $mc_s^2 = nd\mu/dn$. We have demonstrated that in electron-hole bilayer systems, due to the screening, the propagation of the acoustic and optic collective modes in the normal state is halted by the presence of a macroscopic superfluid order parameter. The disappearance of the optic branch characterizes the transition from normal to superfluid phase in electron-hole systems.

In addition, in contrast with the contact interaction of cold atom systems, the finite-range interlayer Coulomb interaction $V_{eh}(q)$ in the gap equation, strongly depends on the screening and thus on the particle density. For this reason, the amplitude of the exciton order parameter $\Delta(q)$ is sensitive to density fluctuations near onset density even with the Random Phase Approximation. We expect the presence of unstable amplitude collective modes in the continuum.

In the continuum, the energy of the collective modes acquires an imaginary part $\Omega(q) = \omega(q) + i\Gamma(q)$. Approaching the real axis of the Ω complex plane the normal and the anomalous response functions show non-analytical behaviour. The Nozières analytic continuation method is generally adopted [132] to solve the non-analyticity problem. In Appendix B we show how to perform this analytic continuation in the normal state. In the superfluid state, this procedure has been applied only for a contact interaction case [133, 139]. The investigation of the behaviour of collective modes in the continuum is beyond the scope of the present study, and we leave it for future works.

5.3 Conclusions

We have investigated density collective modes in the superfluid phase of an exciton bilayer system.

In the normal state, at high density, exciton bilayer systems respond to small external density perturbations through low-energy optic and acoustic density collective modes. However, as the density decreases and the system enters the superfluid phase, the response changes significantly.

The superfluid exciton phase features large gap energy $\Delta(k)$ in the single-particle dispersion, preventing the propagation of stable acoustic and optic density collective modes.

In contrast with ultracold gas atoms, the long-range attractive interaction between electrons and holes in exciton bilayers likely causes a coupling between density fluctuations and the order parameter amplitude response function, resulting in unstable amplitude collective modes in the continuum at the transition from normal to superfluid phase.

Both the absence of the acoustic and optic modes outside the continuum and the appearance of amplitude modes in the continuum can be experimentally detected and thus, can be regarded as unambiguous signatures of the superfluid phase in the exciton bilayer system.

Conclusions

Chapter 6

Conclusion and Future perspectives

6.1 Conclusion

We have developed a theoretical model to describe the exciton bilayer system at zero temperature, with screening and intralayer correlations included. With this method, we have identified and investigated fingerprints of superfluidity in the exciton bilayer system. We focused on two very different phenomena:

- The Josephson effect. This simultaneously probes the presence of a dissipationless current and a macroscopic coherent state through the transport properties of the system.
- The density collective modes. These describe the collective response of the system to an external density perturbation. The behaviour of the collective modes strongly depends on the phase in which the system is.

In **Chapter 2**, through a path-integral approach, we have calculated the gap and number equations at zero temperature. These describe the behaviour of the gap energy of the superfluid phase, the single-particle chemical potential, and the particle density of a bilayer exciton system. We have included in the model the intralayer correlations, using the Hartree-Fock approximation which inserts an additional term in the single-particle dispersion relation of the system. In Sec. 2.3 we have reported the calculation to include the screening with a self-consistent Random-Phase-Approximation in the interlayer and intralayer interactions. We showed, for the first time, the derivation of the anomalous and normal polarization functions in the superfluid phase using a Green function equation of motion approach.

In **Chapter 3** we report our proposal for experimentally measuring, in an exciton-bilayer Josephson junction, the neutral exciton Josephson current. The junction linking the two superfluid bilayer exciton systems is designed with a potential barrier which is tunable in height. We provide pointers for the practical fabrication of the proposed junction in a system of double monolayer Transition Metal Dichalcogenides. The device could be fabricated with a combination of lateral stitching and vertical stacking of the Transition Metal Dichalcogenide monolayers. The Josephson current measurement itself could use the Shapiro method.

We studied separately the *high potential* and *low potential regions*. For low potentials, the excitons have sufficient energy to pass through the barrier region, and here we have solved the gap and number equations with a potential barrier included. With increasing potential barrier height, we find that the gap energy in the BEC regime is suppressed but, because of screening, the gap energy in the crossover-BCS regime is amplified.

In the low potential-barrier region, the exciton superfluid flows over the barrier and can be described by the simple hydrodynamic relation $I_c^b = n^b L_1 v_c^b$. The superfluid critical velocity in the barrier v_c^b is evaluated according to the Landau criterion. However in

the high potential-barrier region, the excitons have insufficient energy to cross the barrier, so the supercurrent is given purely by quantum tunnelling of the electron-hole pairs. The high potential-barrier current and the critical current in the low potential-barrier region are found to connect smoothly.

In studying the superfluid critical velocity as a function of density, we found a maximum. It is remarkable that the density at the maximum exactly matches the density at which the chemical potential changes sign and the condensate fraction passes through the value of 0.8, well-known indicators of the boundary separating the BEC and BCS-BEC crossover regimes. Thus for electron-hole superfluidity, this maximum can be used to locate this boundary. One can experimentally observe the maximum of the critical velocity which occurs at the density where excitations switch from bosonic to fermionic. For this system, the density controls the coupling strength.

In **Chapter 4**, we investigated the effect of intralayer correlations in exciton bilayer systems. In the superfluid phase where the system is dilute the nature of the interactions between the widely spaced excitons is dipolar. Hence at these low densities the intralayer correlations are weak, making the Hartree-Fock approximation excellent. Increasing the density, the correlations become stronger. However, the development of screening prevents entrance into the strong correlation region. When the density exceeds the onset density, the screening completely suppresses superfluidity making the system normal. At high densities in the normal state, the pairs break up and the intralayer interactions are no longer dipolar. Thus the correlations become weak at high density and the Hartree-Fock approximation is again valid.

We demonstrate that the primary effect of the Hartree-Fock correlations on the superfluid properties in the exciton bilayer system is an increase in the strength of screening. This is caused by a boost in the density of low-lying states. Effects of screening on the superfluidity are negligible in the deep BEC regime [48] and therefore Hartree-Fock has minimal effect in that regime. However, in the BCS-BEC crossover regime where screening plays a crucial role in determining the superfluid properties, we find that the strength of the screening can be as much as doubled by the Hartree-Fock corrections and that this increase in the screening strength results in a diminution of the superfluid gap by up to a factor of two. With Hartree-Fock included, there is good agreement with results from diffusion Monte Carlo numerical simulations also in the BCS-BEC crossover regime. The Hartree-Fock intralayer correlations shift the boundary between the BEC and BCS-BEC crossover regimes to lower densities, and they eliminate a predicted minimum in the electron-hole pair size as a function of density.

In **Chapter 5** we explored the low-temperature behaviour of the density collective modes to identify unambiguous fingerprints of the transition from the normal state to the superfluid.

In the normal state at high densities, low-energy optic and acoustic density collective modes characterise the response of exciton bilayer systems to small external density perturbations. Lowering the density and entering the superfluid phase, the response of the system changes dramatically.

The superfluid exciton phase is characterized by the presence of a large gap energy in the single-particle energy dispersion relation, since static screening blocks access to exciton superfluidity in the BCS regime where the gap energy is much smaller than the Fermi energy. The large energy gap in the BEC and BCS-BEC crossover regimes makes the low-energy excited states inaccessible for density fluctuations, so a macroscopic coherent phase of condensed excitons blocks the propagation of stable density collective modes.

In contrast with ultracold gas atoms, the long-range attractive interaction between electrons and holes in exciton bilayers likely causes a coupling between density fluctuations and the order parameter amplitude response function, resulting in unstable pair-breaking amplitude collective modes in the continuum at the transition from normal to superfluid phase. Both the absence of the acoustic and optic modes outside the continuum and the appearance of pair-breaking amplitude modes in the continuum can be experimentally detected and thus, can be regarded as unambiguous signatures of the superfluid phase in the exciton bilayer system.

6.2 Future Prospectives

In this Thesis, we have opened the way for systematic studies in exciton bilayer systems, of the Josephson effect and of collective modes in order to definitively probe the existence of superfluidity. In carrying out our investigations of these two phenomena, we have paid particular attention to suitable materials and experimental techniques to validate the results. The recently predicted very rich phase diagram (Fig. 1.9) makes our investigation of fingerprints of exciton bilayer superfluidity results even more timely.

Regarding further exploration in the exciton bilayer system of the Josephson effect, collective modes and other quantum many-body phenomena, there is a great deal still to be done, discovered and clarified. Below are possible research lines we plan to pursue in the future.

1st Research Line: Superfluid order parameter collective modes

In Chapter 5 we studied density collective modes. As yet there are no theoretical studies of the order-parameter collective modes. Chapter 5 concluded with a comparison between the results for the long-range interaction bilayer exciton system and contact interaction ultracold gas atoms. We made certain predictions on the behaviour of the order-parameter collective modes in the bilayer exciton system, and one future research line will be to investigate the amplitude and phase order parameter in bilayer excitons at finite temperature using the path-integral approach discussed in Chapter 1.

2nd Research Line: Drag-Josephson measurement

Recently, perfect Coulomb drag measurements have been performed in a double-monolayer-TMD system [6], probing for the presence of stable excitons in the device at temperatures up to 20K. The authors carried out high-quality measurements of the drag current down to 1.5K. They succeeded in limiting the noise effects from interlayer tunnelling and defects in the electrical contacts. We propose combined experiments as follows:

- Perform a Coulomb drag measurement by injecting the driving current I_{drive} in one layer and measuring the drag current in the other layer I_{drag} to probe for the presence of excitons. Drag can distinguish exciton flow from the flow of independent electrons and holes.
- Perform a Josephson effect measurement, to determine the voltage drop across the barrier using the Shapiro method [180]. The Josephson effect identifies the presence of a dissipationless current and the existence of phase coherence

This new combined Josephson and Coulomb drag technique can provide a definitive picture of the phase space regions as a function of density and temperature of (i)

the exciton superfluid, (ii) the exciton normal fluid, and (iii) the decoupled electron and hole normal-liquid state. The superfluid phase is characterized by perfect Coulomb drag ($I_{drive} = I_{drag}$) combined with the existence of a Josephson critical current I_c . Increasing the temperature and approaching the superfluid critical temperature, I_c will decrease. Above the superfluid critical temperature, the system will be in the exciton normal state, and I_c will be zero, while the drag ratio is expected to be $I_{drive} \leq I_{drag}$. Then when the temperature is further increased in the decoupled electron and hole normal liquid state, the excitons are dissociated and the drag ratio will steadily decrease.

3rd Research Line: Pseudogap

An important feature that is investigated in the normal state of superconductors and ultracold atomic gases is the pseudogap phenomenon, a high-temperature precursor of the superconducting or superfluid phase. In this phenomenon, there is a suppression of spectral weight in the single-particle Green function in the excitation spectra above the superfluid critical temperature, in 2D given by T_{BKT} [209]. This suppression resembles a gap opening (pseudogap), even though the system in the normal state as yet does not possess global coherence. Notwithstanding this, local pairs with finite lifetimes can exist in pockets of superfluidity [210], and they persist up to the mean-field superfluid critical temperature T_{MF} [211]. Above T_{MF} , the excitons lose degeneracy and the system becomes a classical exciton gas.

The theoretical predictions [212] of the opening of a pseudogap in the excitation spectra in superconductors and ultracold atomic gases have been confirmed by ARPES and STM experiments [213]. In exciton bilayers, the existence of such a region in the phase diagram has been predicted [71, 88, 214]. However, there has still not been an in-depth investigation of the pseudogap phenomenon in the normal state of electron-hole systems. This we propose to do.

4nd Research Line: Unified model phase diagram

The supersolid phase recently predicted [7] in the exciton bilayer system has further enriched the predicted rich phase diagram that already contained the superfluid phase, the exciton crystal state, and the Wigner crystal. Different theoretical approaches have been adopted to investigate these phases. There exists as yet no unified theory able to describe this rich exciton bilayer phase diagram.

In Chapter 2-4 we have made a step in this direction by inserting intralayer correlations in the mean-field approach at zero temperature. With this extra term in the Hamiltonian, the superfluid phase as a function of the interlayer distance d and interparticle distance r_0 always lies below the diagonal $r_0 = d$ in the phase space, as would be expected.

As a next step, the model can be extended to treat the normal exciton, the superfluid, and the supersolid phase. For the superfluid exciton phase, we have been using a plane wave expansion of the single-particle wave function. This does not allow for any translational symmetry breaking.

A future research line will use a Bloch wave expansion:

$$\Psi_{\lambda,\tau}(x) = \frac{1}{\sqrt{\beta S}} \sum_{k,n} e^{-i\omega_n\tau + i(k-K)x} \Psi_{\lambda,n}(k-K), \quad (6.1)$$

where K is the reciprocal lattice vector. This allows for the possibility of the existence of periodic electron and hole lattices in the layers. Equation (6.1) for $\Psi_{\lambda,\tau}(x)$ would be

substituted into the partition function Eq. (2.21). To obtain the gap equation, the effective action would be minimised with respect to the gap energy Δ and the reciprocal lattice vector K . The idea is to describe the transition from the superfluid phase characterized by the macroscopic order parameter with $K = 0$ (no periodicity), to a supersolid phase characterized by macroscopic order parameter with $K = 2\pi/a_{SS}$, with a_{SS} the triangular lattice constant predicted in Ref. [7]. We expect the transition from the superfluid to the supersolid phase will be smooth and mediated by a region of the $(r_0 - d)$ diagram characterized by clusters of excitons.

Appendix A

Electron-Hole Feynman Diagrams in Self-Consistent Random Phase Approximation

We treat the Feynman diagrams of screened intralayer and interlayer interaction, up to the second order interaction in the self-consistent Random Phase Approximation.

The self-consistent Dyson equation for the dressed interaction $W(q, \omega)$ is given by:

$$W(q, \omega) = V(q) + V(q)\Pi^*(q, \omega)W(q, \omega). \quad (\text{A.1})$$

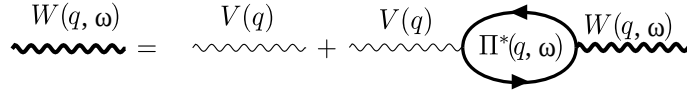


FIGURE A.1: Feynman diagram representation of the Dyson equation. The thick-wavy line represents the dressed interaction $W(q, \omega)$, the thin-wavy line is the bare interaction $V(q)$, and the thick-bubble line is the complete proper polarization $\Pi^*(q, \omega)$.

In the Random-Phase Approximation the Dyson equation becomes:

$$W^{RPA}(q, \omega) = V(q) + V(q)\Pi_0(q, \omega)W^{RPA}(q, \omega). \quad (\text{A.2})$$

We want to show the RPA Feynman diagrams up to second-order interactions, so we expand $W^{RPA}(q, \omega)$ to second-order:

$$W^{RPA}(q, \omega) = V(q) + V(q)\Pi_0(q, \omega)(V(q) + \cancel{V(q)\Pi_0(q, \omega)W^{RPA}(q, \omega)}), \quad (\text{A.3})$$

$$W^{RPA}(q, \omega) = V(q) + V(q)\Pi_0(q, \omega)V(q). \quad (\text{A.4})$$

We study a two-component system in which $W(q, \omega)$, $\Pi(q, \omega)$ and $V(q)$ are 2×2 matrices defined as:

$$V(q) = \begin{pmatrix} V_S(q) & V_D(q) \\ V_D(q) & V_S(q) \end{pmatrix} \quad (\text{A.5})$$

$$\Pi_0(q, \omega) = \begin{pmatrix} \Pi_0^N(q, \omega) & \Pi_0^A(q, \omega) \\ \Pi_0^A(q, \omega) & \Pi_0^N(q, \omega) \end{pmatrix} \quad (\text{A.6})$$

$$W(q, \omega) = \begin{pmatrix} V_S^{sc}(q, \omega) & V_D^{sc}(q, \omega) \\ V_D^{sc}(q, \omega) & V_S^{sc}(q, \omega) \end{pmatrix} \quad (\text{A.7})$$

Using these 2×2 matrices in Eq.(A.4) one gets:

$$\begin{aligned} V_S^{sc}(q, \omega) &= V_S(q) + V_S(q)\Pi_0^N(q, \omega)V_S(q) + V_D(q)\Pi_0^A(q, \omega)V_S(q) + V_S(q)\Pi_0^A(q, \omega)V_D(q) \\ &\quad + V_D(q)\Pi_0^N(q, \omega)V_D(q) \end{aligned} \quad (\text{A.8})$$

$$\begin{aligned} V_D^{sc}(q, \omega) &= V_D(q) + V_S(q)\Pi_0^N(q, \omega)V_D(q) + V_D(q)\Pi_0^A(q, \omega)V_D(q) + V_S(q)\Pi_0^A(q, \omega)V_S(q) \\ &\quad + V_D(q)\Pi_0^N(q, \omega)V_S(q) . \end{aligned} \quad (\text{A.9})$$

In Fig. A.2 we report the Feynman diagrams for the interaction terms of Eq. (A.8) and Eq. (A.9) for the screened interlayer and intralayer interaction.

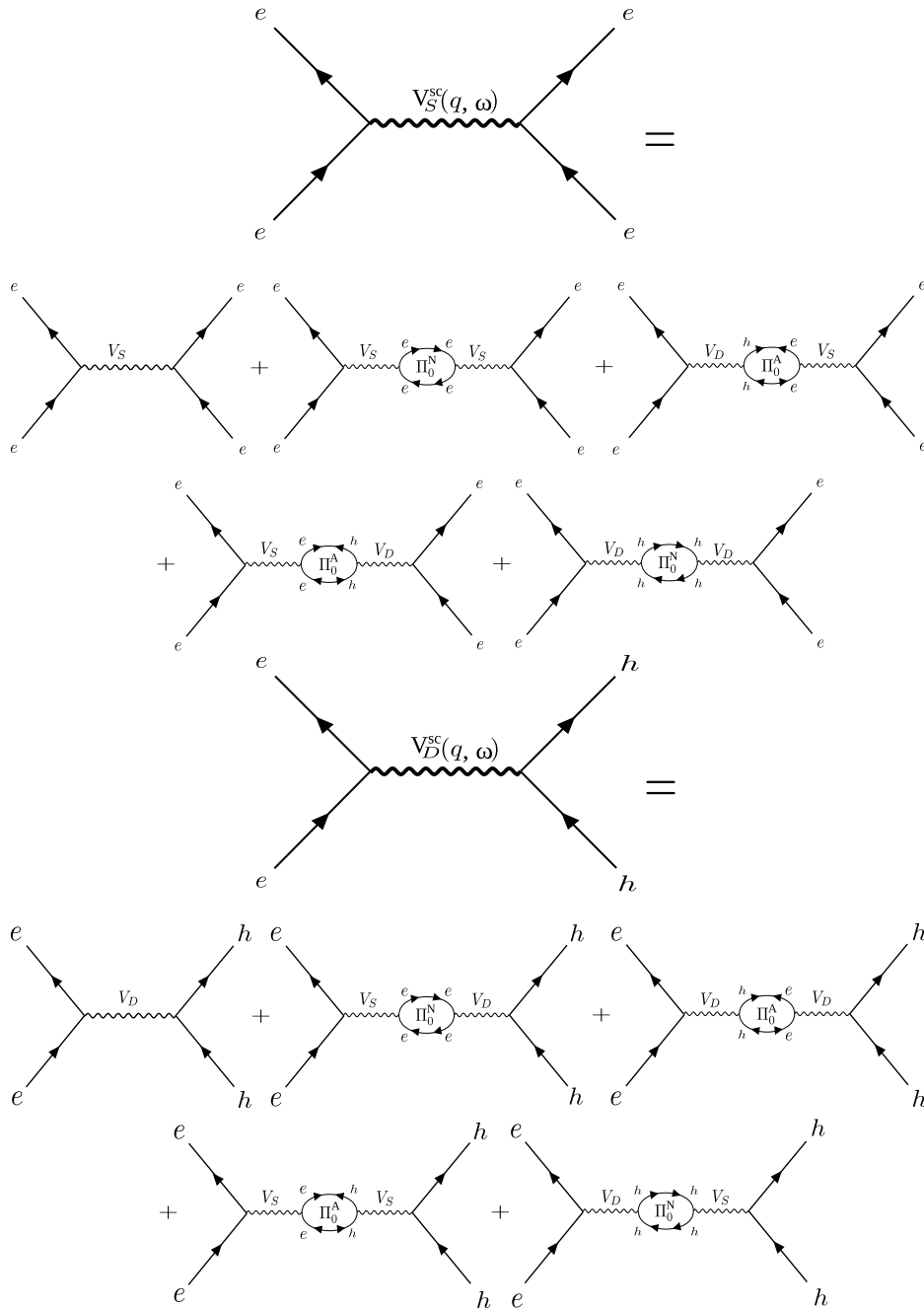


FIGURE A.2: First and second-order Feynman diagrams for the repulsive intralayer $V_S^{\text{SC}}(q, \omega)$ and the attractive intralayer $V_D^{\text{SC}}(q, \omega)$.

Appendix B

Polarization function with Green's function equation of motion in normal state

The Hamiltonian of the electron-hole bilayer system, in the normal state, in second quantization is:

$$H_0 = \sum_k E(k) c_k^\dagger c_k + \sum_k E(k) d_k^\dagger d_k \quad (\text{B.1})$$

where $E(k) = \hbar k^2 / 2m - \mu_s$. We consider equal electron and hole layers, $E^e(k) = E^h(k) = E(k)$.

In the normal state the only anticommutators different from zero of the creation (c^\dagger, d^\dagger) and annihilation (c, d) operators are:

$$\{c_k^\dagger, c_{k'}\} = \delta(k - k'), \quad (\text{B.2})$$

$$\{d_k^\dagger, d_{k'}\} = \delta(k - k'). \quad (\text{B.3})$$

The electron-electron Green's function equation of motion, Eq. (2.90):

$$i\partial_t G_{n_e(q), n_e(q')}^R = \delta(t) \langle [n_e(q); n_e(q')] \rangle + G_{[n_e(q); H_0], n_e(q')}^R, \quad (\text{B.4})$$

is composed of three terms.

We evaluate each term of Green's function equation of motion separately.

The $\delta(t)$ -term of Eq. (B.4) in the normal state is:

$$\delta(t) \langle [n_e(q); n_e(q')] \rangle = \delta(t) \sum_{k, k'} \langle [c_{k+q}^\dagger c_k; c_{k'+q'}^\dagger c_{k'}] \rangle. \quad (\text{B.5})$$

The commutator of fermionic operators $[c_{k+q}^\dagger c_k; c_{k'+q'}^\dagger c_{k'}]$ follows the general rule of commutators:

$$[AB; CD] = A[B; C]D + [A; C]BD + CA[B; D] + C[A; D]B \quad (\text{B.6})$$

$$[A; B] = \{A; B\} - 2BA \quad (\text{B.7})$$

where A and B are fermionic operators. The right-hand side commutator in Eq. (B.5) reads:

$$\begin{aligned} & [c_{k+q}^\dagger c_k; c_{k'+q'}^\dagger c_{k'}] \\ &= c_{k+q}^\dagger [c_k; c_{k'+q'}^\dagger] c_{k'} + [c_{k+q}^\dagger; c_{k'+q'}^\dagger] c_k c_{k'} + c_{k'+q'}^\dagger c_{k+q}^\dagger [c_k; c_{k'}] + c_{k'+q'}^\dagger [c_{k+q}^\dagger; c_{k'}] c_k \end{aligned}$$

$$\begin{aligned}
&= c_{k+q}^\dagger \left(\delta(k, k' + q') - 2c_{k'+q'}^\dagger c_k \right) c_{k'} - 2c_{k'+q'}^\dagger c_{k+q}^\dagger c_k c_{k'} - 2c_{k'+q'}^\dagger c_{k+q}^\dagger c_{k'} c_k \\
&\quad + c_{k'+q'}^\dagger \left(\delta(k + q, k') - 2c_{k'}^\dagger c_{k+q}^\dagger \right) c_k \\
&= c_{k+q}^\dagger c_{k'} \delta(k, k' + q') + c_{k'+q'}^\dagger c_k \delta(k + q, k') - 2c_{k+q}^\dagger c_{k'+q'}^\dagger c_k c_{k'} - 2c_{k'+q'}^\dagger c_{k+q}^\dagger c_k c_{k'} \\
&\quad - 2c_{k'+q'}^\dagger c_{k+q}^\dagger c_{k'} c_k - 2c_{k'+q'}^\dagger c_{k'}^\dagger c_{k+q}^\dagger c_k \\
&= c_{k+q}^\dagger c_{k'} \delta(k, k' + q') + c_{k'+q'}^\dagger c_k \delta(k + q, k') - \cancel{2c_{k+q}^\dagger c_{k'+q'}^\dagger c_k c_{k'}} + \cancel{2c_{k+q}^\dagger c_{k'+q'}^\dagger c_k c_{k'}} \\
&\quad - 2c_{k'+q'}^\dagger c_{k+q}^\dagger c_{k'} c_k - 2c_{k'+q'}^\dagger c_{k'}^\dagger c_{k+q}^\dagger c_k \tag{B.8}
\end{aligned}$$

$$\begin{aligned}
&= c_{k+q}^\dagger c_{k'} \delta(k, k' + q') + c_{k'+q'}^\dagger c_k \delta(k + q, k') - 2c_{k'+q'}^\dagger c_{k+q}^\dagger c_{k'} c_k - 2c_{k'+q'}^\dagger c_{k'}^\dagger c_{k+q}^\dagger c_k \\
&= c_{k+q}^\dagger c_{k'} \delta(k, k' + q') + c_{k'+q'}^\dagger c_k \delta(k + q, k') - 2c_{k'+q'}^\dagger c_{k+q}^\dagger c_{k'} c_k \\
&\quad - 2c_{k'+q'}^\dagger \left(\delta(k', k + q) - c_{k+q}^\dagger c_{k'} \right) c_k \\
&= c_{k+q}^\dagger c_{k'} \delta(k, k' + q') - c_{k'+q'}^\dagger c_k \delta(k + q, k') - \cancel{2c_{k'+q'}^\dagger c_{k+q}^\dagger c_{k'} c_k} + \cancel{2c_{k'+q'}^\dagger c_{k+q}^\dagger c_{k'} c_k} \\
&= c_{k+q}^\dagger c_{k'} \delta(k, k' + q') - c_{k'+q'}^\dagger c_k \delta(k + q, k') . \tag{B.9}
\end{aligned}$$

The expectation value of Eq. (B.9) is:

$$\begin{aligned}
\langle c_{k+q}^\dagger c_{k'} \delta(k, k' + q') - c_{k'+q'}^\dagger c_k \delta(k + q, k') \rangle &= \langle c_{k+q}^\dagger c_{k'} \delta(k, k' + q') \rangle - \langle c_{k'+q'}^\dagger c_k \delta(k + q, k') \rangle \\
&= \langle c_{k+q}^\dagger c_{k-q'} \rangle - \langle c_{k+q+q'}^\dagger c_k \rangle \\
&= \delta(q, -q') (f(E(k+q)) - f(E(k))) ,
\end{aligned}$$

where we used the definition $\langle c_k^\dagger c_k \rangle = f(E(k)) = 1/(e^{E(k)/k_B T} + 1)$ of the Fermi-Dirac statistics distribution function.

The $\delta(t)$ -term of Eq. (2.90) results in:

$$\delta(t) \langle [n_e(q); n_e(q')] \rangle = \sum_k \delta(t) \delta(q, -q') (f(E(k+q)) - f(E(k))) . \tag{B.10}$$

The H -term on the right-hand side of Eq. (B.4) is:

$$G_{[n_e(q,t); H_0], n_e(q',0)}^R(t) = i\theta(t) \langle [n_e(q, t); H_0], n_e(q', 0) \rangle . \tag{B.11}$$

As for the $\delta(t)$ -term we first evaluate the commutator between the electron density operator $n_e(q, t)$ and the Hamiltonian H_0 reported in Eq. (B.1):

$$[n_e(q, t); H_0(t)] = \sum_{k,s} [c_{k+q}^\dagger c_k; E(s)(c_s^\dagger c_s + d_s^\dagger d_s)] , \tag{B.12}$$

which can be separated into two commutators:

$$[n_e(q, t); H_0(t)] = A + B , \tag{B.13}$$

where:

$$A = \sum_{k,s} [c_{k+q}^\dagger c_k; E(s) c_s^\dagger c_s], \quad (\text{B.14})$$

$$B = \sum_{k,s} [c_{k+q}^\dagger c_k; E(s) d_s^\dagger d_s]. \quad (\text{B.15})$$

Working out A:

$$\begin{aligned} A &= \sum_{k,s} [c_{k+q}^\dagger c_k; E(s) (c_s^\dagger c_s)] \quad (\text{B.16}) \\ &= \sum_{k,s} E(s) [c_{k+q}^\dagger c_k; c_s^\dagger c_s] \\ &= \sum_{k,s} E(s) \left(c_{k+q}^\dagger [c_k; c_s^\dagger] c_s + [c_{k+q}^\dagger; c_s^\dagger] c_k c_s + [c_s^\dagger; c_{k+q}^\dagger] c_k c_s + c_s^\dagger [c_{k+q}^\dagger; c_s] c_k \right) \\ &= \sum_{k,s} E(s) \left(c_{k+q}^\dagger (\delta(k,s) - 2c_s^\dagger c_k) c_s - 2c_s^\dagger c_{k+q}^\dagger c_k c_s - 2c_{k+q}^\dagger c_s^\dagger c_k c_s + c_s^\dagger (\delta(k+q,s) - 2c_s c_{k+q}^\dagger) c_k \right) \\ &= \sum_{k,s} E(s) \left(c_{k+q}^\dagger c_s \delta(k,s) + c_s^\dagger c_k \delta(k+q,s) - \cancel{2c_{k+q}^\dagger c_s^\dagger c_k c_s} + \cancel{2c_{k+q}^\dagger c_s^\dagger c_k c_s} - 2c_{k+q}^\dagger c_s^\dagger c_k c_s \right. \\ &\quad \left. - 2c_s^\dagger c_s c_{k+q}^\dagger c_k \right) \\ &= \sum_{k,s} E(s) \left(c_{k+q}^\dagger c_s \delta(k,s) + c_s^\dagger c_k \delta(k+q,s) - 2c_{k+q}^\dagger c_s^\dagger c_k c_s - 2c_s^\dagger c_s c_{k+q}^\dagger c_k \right) \\ &= \sum_{k,s} E(s) \left(c_{k+q}^\dagger c_s \delta(k,s) + c_s^\dagger c_k \delta(k+q,s) - 2c_s^\dagger c_{k+q}^\dagger c_s c_k - 2c_s^\dagger (\delta(s,k+q) - c_{k+q}^\dagger c_s) c_k \right) \\ &= \sum_{k,s} E(s) \left(c_{k+q}^\dagger c_s \delta(k,s) - c_s^\dagger c_k \delta(k+q,s) - \cancel{2c_s^\dagger c_{k+q}^\dagger c_s c_k} + \cancel{2c_s^\dagger c_{k+q}^\dagger c_s c_k} \right) \\ &= \sum_{k,s} E(s) \left(c_{k+q}^\dagger c_s \delta(k,s) - c_s^\dagger c_k \delta(k+q,s) \right) \\ &= \sum_k E(k) c_{k+q}^\dagger c_k - E(k+q) c_{k+q}^\dagger c_k, \end{aligned}$$

$$A = \sum_k (E(k) - E(k+q)) c_{k+q}^\dagger c_k \quad (\text{B.17})$$

For the term B:

$$\begin{aligned} B &= \sum_{k,s} [c_{k+q}^\dagger c_k; E(s) d_s^\dagger d_s] \quad (\text{B.18}) \\ &= \sum_{k,s} E(s) [c_{k+q}^\dagger c_k; d_s^\dagger d_s] \\ &= \sum_{k,s} E(s) \left(c_{k+q}^\dagger [c_k; d_s^\dagger] d_s + [c_{k+q}^\dagger; d_s^\dagger] c_k d_s + d_s^\dagger c_{k+q}^\dagger [c_k; d_s] + d_s^\dagger [c_{k+q}^\dagger; d_s] c_k \right) = \\ &= \sum_{k,s} E(s) \left(-2c_{k+q}^\dagger d_s^\dagger c_k d_s - 2d_s^\dagger c_{k+q}^\dagger c_k d_s - 2d_s^\dagger c_{k+q}^\dagger d_s c_k - 2d_s^\dagger d_s c_{k+q}^\dagger c_k \right) = \\ &= \sum_{k,s} E(s) \left(\cancel{-2c_{k+q}^\dagger d_s^\dagger c_k d_s} + \cancel{2c_{k+q}^\dagger d_s^\dagger c_k d_s} + \cancel{2d_s^\dagger d_s c_{k+q}^\dagger c_k} - \cancel{2d_s^\dagger d_s c_{k+q}^\dagger c_k} \right) = 0 \\ B &= 0 \quad (\text{B.19}) \end{aligned}$$

Then Eq. (B.11) becomes:

$$\begin{aligned}
 G_{[n_e(q);H_0],n_e(q')}^R &= -i\theta(t)\langle [n_e(q);H_0], n_e(q') \rangle \\
 &= \sum_{k,k'} i\theta(t) (E(k) - E(k+q)) \langle c_{k+q}^\dagger c_k, c_{k'+q}^\dagger c_{k'} \rangle \\
 &= \sum_{k,k'} (E(k) - E(k+q)) G_{ee}^R(k, k', q, q', t)
 \end{aligned} \tag{B.20}$$

where $G_{ee}^R(k, k', q, q', t) = i\theta(t)\langle c_{k+q}^\dagger c_k, c_{k'+q}^\dagger c_{k'} \rangle$.

To evaluate the imaginary-time partial derivative term in the left-side of Eq. (B.4) we perform the time Fourier expansion of the retarded Green's function:

$$\begin{aligned}
 G_{n_e(q),n_e(q')}^R &= \sum_{k,k'} G_{ee}^R(k, k', q, q', t) \\
 &= \sum_{\omega} \sum_{k,k'} e^{-i\omega t} G_{ee}^R(k, k', q, q', \omega)
 \end{aligned} \tag{B.21}$$

Thus, the time-partial derivative term reads:

$$\begin{aligned}
 i\partial_t G_{n_e(q),n_e(q')}^R &= i\partial_t \left(\sum_{\omega} \sum_{k,k'} e^{-i\omega t} G_{ee}^R(k, k', q, q', \omega) \right) \\
 &= \sum_{\omega} \sum_{k,k'} i\partial_t \left(e^{-i\omega t} G_{ee}^R(k, k', q, q', \omega) \right) \\
 &= \sum_{\omega} \sum_{k,k'} \omega e^{-i\omega t} G_{ee}^R(k, k', q, q', \omega)
 \end{aligned} \tag{B.22}$$

After replacing Eq. (B.22) in the time-partial derivative term, Eq. (B.10) in the δ -term and Eq. (B.20) in the H -term of Eq. (B.4), the equation of motion of the electron-electron retarded Green's function reads:

$$\begin{aligned}
 \sum_{\omega} \sum_{k,k'} \omega e^{-i\omega t} G_{ee}^R(k, k', q, q', \omega) &= \sum_{k,k'} \delta(t)\delta(q, -q') (f(\epsilon_{k+q}) - f(\epsilon_k)) \\
 &\quad + \sum_{\omega} \sum_{k,k'} (E(k) - E(k+q)) e^{-i\omega t} G_{ee}^R(k, k', q, q', \omega)
 \end{aligned} \tag{B.23}$$

The sum $\sum_{k,k'}$ appears in every term, thus:

$$\begin{aligned}
 \sum_{\omega} \omega e^{-i\omega t} G_{ee}^R(k, k', q, q', \omega) &= \delta(t)\delta(q, -q') (f(\epsilon_{k+q}) - f(\epsilon_k)) \\
 &\quad + \sum_{\omega} (E(k) - E(k+q)) e^{-i\omega t} G_{ee}^R(k, k', q, q', \omega) \\
 \sum_{\omega} e^{-i\omega t} G_{ee}^R(k, k', q, q', \omega) (\omega - E(k) + E(k+q)) &= \delta(t)\delta(q, -q') (f(\epsilon_{k+q}) - f(\epsilon_k)) \\
 \sum_{\omega} e^{-i\omega t} G_{ee}^R(k, k', q, q', \omega) (\omega - E(k) + E(k+q)) &= \sum_{\omega} e^{-i\omega t} \delta(\omega)\delta(t)\delta(q, -q') (f(\epsilon_{k+q}) - f(\epsilon_k))
 \end{aligned} \tag{B.24}$$

Now, the sum $\sum_{\omega} e^{-i\omega t}$ appears in every terms, thus:

$$G_{ee}^R(k, k', q, q', \omega) (\omega - E(k) + E(k+q)) = \delta(q, -q') (f(\epsilon_{k+q}) - f(\epsilon_k)) \tag{B.25}$$

$$G_{ee}^R(k, k', q, q', \omega) = \frac{\delta(q, -q')(f(\epsilon_{k+q}) - f(\epsilon_k))}{\omega - E(k) + E(k+q)} \quad (\text{B.26})$$

The last step to obtain the normal polarization function in the normal phase is to perform the time Fourier expansion of Eq. (2.87):

$$\begin{aligned} \Pi_0^N(q, t) &= \frac{1}{S} \sum_{q'} G_{n_e(q,t)n_e(q',0)}^R \\ &= \frac{1}{S} \sum_{q', k, k'} G_{ee}^R(k, k', q, q', t) \\ &= \frac{1}{S} \sum_{\omega, q', k, k'} e^{-i\omega t} G_{ee}^R(k, k', q, q', \omega) \end{aligned} \quad (\text{B.27})$$

Replacing Eq. (B.26) in Eq. (B.27), one gets:

$$\begin{aligned} \Pi_0^N(q, \omega) &= \frac{1}{S} \sum_{k, q'} \frac{\delta(q, -q')(f(\epsilon_{k+q}) - f(\epsilon_k))}{\omega + i\eta - E(k) + E(k+q)} \\ &= \frac{1}{S} \sum_k \frac{f(\epsilon_{k+q}) - f(\epsilon_k)}{\omega + i\eta - E(k) + E(k+q)} \end{aligned} \quad (\text{B.28})$$

where $\omega \rightarrow \omega + i\eta$ is extended to the imaginary space because the polarization function has poles on the real axis. We show how to evaluate the polarization function in this non-analytic branch cut in Appendix G.

The zero temperature, static, normal polarization function in the normal state of an exciton bilayer system is:

$$\Pi_0^N(q) = \frac{1}{S} \sum_k \frac{\theta(\epsilon_F - \epsilon_{k+q}) - \theta(\epsilon_F - \epsilon_k)}{E(k+q) - E(k)} \quad (\text{B.29})$$

where ϵ_F is the Fermi energy. Eq. (B.29) is the Stern-Lindhard function of the non-interacting electron gas [131].

The anomalous polarization function in the normal phase is obtained by evaluating the equation of motion of the electron-hole retarded Green's function, Eq. (2.91). The $\delta(t)$ -term in this case results in:

$$\begin{aligned} \delta(t) \langle [n_e(q); n_h(q')]_- \rangle &= \sum_{k, k'} \delta(t) \langle [c_{k+q}^\dagger c_k; d_{k'+q}^\dagger d_{k'}] \rangle \\ &= \sum_{k, k'} \delta(t) \left(\langle c_{k+q}^\dagger [c_k; d_{k'+q}^\dagger] d_{k'} + [c_{k+q}^\dagger; d_{k'+q}^\dagger] c_k d_{k'} + d_{k'+q}^\dagger c_{k+q}^\dagger [c_k; d_{k'}] + d_{k'+q}^\dagger [c_{k+q}^\dagger; d_{k'}] c_k \rangle \right) \\ &= \sum_{k, k'} \delta(t) \left(\langle -2c_{k+q}^\dagger d_{k'+q}^\dagger c_k d_{k'} - 2d_{k'+q}^\dagger c_{k+q}^\dagger c_k d_{k'} - 2d_{k'+q}^\dagger c_{k+q}^\dagger d_{k'} c_k - 2d_{k'+q}^\dagger d_{k'} c_{k+q}^\dagger c_k \rangle \right) \\ &= \sum_{k, k'} \delta(t) \left(\langle \cancel{2d_{k'+q}^\dagger c_{k+q}^\dagger c_k d_{k'}} - \cancel{2d_{k'+q}^\dagger c_{k+q}^\dagger c_k d_{k'}} + \cancel{2d_{k'+q}^\dagger d_{k'} c_{k+q}^\dagger c_k} - \cancel{2d_{k'+q}^\dagger d_{k'} c_{k+q}^\dagger c_k} \rangle \right) \\ \delta(t) \langle [n_e(q); n_h(q')]_- \rangle &= 0 \end{aligned} \quad (\text{B.31})$$

The $\delta(t)$ -term of the Green's function equation of motion corresponds to the numerator of the polarization function, thus $\Pi_0^A(q, \omega) = 0$ in the normal phase, as expected. There are processes driving a coherent electron-hole response to density fluctuations.

Appendix C

Self-consistent solution of the Gap and Number Equations

At zero temperature the gap and number equations of an electron-hole bilayer system are given by:

$$\Delta(k) = -\frac{1}{S} \sum_q V_D(|q-k|) \frac{\Delta(q)}{2E(q)}, \quad (\text{C.1})$$

$$n = \frac{g_s g_v}{S} \sum_p n(p). \quad (\text{C.2})$$

Where:

$$E(q) = \sqrt{\xi^2(q) + |\Delta(q)|^2}, \quad (\text{C.3})$$

$$\xi(q) = \frac{\hbar^2 q^2}{2m} - \mu_s - \frac{1}{S} \sum_p V_S(|p-q|) n(p), \quad (\text{C.4})$$

$$n(p) = \frac{1}{2} \left(1 - \frac{\xi(p)}{E(p)} \right), \quad (\text{C.5})$$

where g_s and g_v are the spin and valley degeneracy.

The gap and number equations are numerically solved in a self-consistent procedure. The value of the single-particle chemical potential μ_s is fixed and a trial order parameter $\Delta^0(k)$ and density of states $n^0(k)$ is chosen. Then the normal and anomalous polarization functions are computed and used to define the screened interlayer $V_D^0(q)$ and intralayer $V_S^0(q)$ interactions. The right-hand side of the gap equation and number equation are evaluated finding the new profile for $\Delta^1(k)$ and $n^1(k)$. The new gap energy and density of state are then used to update the polarization functions and the screened interactions, $V_S^1(q)$ and $V_S^1(q)$. The updated functions of the gap energy, density of state and screened interactions are then replaced in the right-hand side of the gap and number equation to obtain new profiles. The procedure is iteratively repeated until the gap energy, the density of state and the polarization functions converge.

Appendix D

Superfluid critical velocity

The pair-breaking superfluid critical velocity is defined by the Landau criterion:

$$v_c = \min(k) \frac{E(k)}{k}, \quad (\text{D.1})$$

where $E(k) = \sqrt{(\varepsilon(k) - \mu_s)^2 + \Delta(k)^2}$ is the pair-breaking BCS dispersion relation. To find k_{min} which minimizes the ratio $E(k)/k$ we solve the equation:

$$\begin{aligned} \left. \frac{dE(k)/k}{dk} \right|_{k_{min}} &= 0 \\ \left(\frac{dE(k)}{dk} k - E(k) \right) \frac{1}{k^2} &= 0 \\ \frac{1}{2} \left((\varepsilon(k)^2 - \mu_s)^2 + \Delta(k)^2 \right)^{-1/2} \left(2(\varepsilon(k) - \mu_s) \frac{d\varepsilon(k)}{dk} + 2\Delta(k) \frac{d\Delta(k)}{dk} \right) k - E(k) &= 0 \\ \frac{1}{2} \left(2(\varepsilon(k) - \mu_s) \frac{d\varepsilon(k)}{dk} + 2\Delta(k) \frac{d\Delta(k)}{dk} \right) k - E(k)^2 &= 0, \end{aligned}$$

where, replacing

$$\frac{d\varepsilon(k)}{dk} = \frac{\hbar k}{m} = \frac{2\varepsilon(k)}{k}. \quad (\text{D.2})$$

one obtains,

$$\begin{aligned} (\varepsilon(k) - \mu_s) 2\varepsilon(k) + \Delta(k) k \frac{d\Delta(k)}{dk} - E(k)^2 &= 0 \\ 2\varepsilon(k)^2 - 2\varepsilon(k)\mu_s + \Delta(k) k \frac{d\Delta(k)}{dk} - [(\varepsilon(k) - \mu_s)^2 + \Delta(k)^2] &= 0 \\ 2\varepsilon(k)^2 - 2\varepsilon(k)\mu_s + \Delta(k) k \frac{d\Delta(k)}{dk} - \varepsilon(k)^2 - \mu_s^2 + 2\varepsilon(k)\mu_s - \Delta(k)^2 &= 0 \\ \varepsilon(k)^2 + \Delta(k) k \frac{d\Delta(k)}{dk} - \mu_s^2 - \Delta(k)^2 &= 0. \end{aligned}$$

In a system with contact interaction, Δ is k -independent and the solution of Eq. (D) is analytical. In the exciton system with finite-range interaction, $\Delta(k)$ depends on k , and the solution for k of Eq. (D) can be derived analytically. We find that k_{min} decreases as the density n increases. Close to the onset density, k_{min} approaches the Fermi wave-vector k_F . This is a reasonable result since moving toward the BCS regime, the condensed excitons are mostly localized around the Fermi surface, with $k = k_F$.

The critical velocity throughout the BCS-BEC crossover corresponds to $E_{k_{min}}/k_{min}$ with k_{min} obtained from the solution of Eq. (D) as a function of the density n .

Appendix E

Chemical potential with intralayer correlations

The single-particle chemical potential μ of a many-body fermionic system is the minimum energy required to add or remove a particle of the system. In BCS theory, introducing the Bogoliubov transformation, the chemical potential is the energy $\varepsilon(\bar{k}) = \hbar^2 \bar{k}^2 / 2m^*$ evaluated in the momentum \bar{k} in which the Bogoliubov amplitudes $v_{\bar{k}}^2$ and $u_{\bar{k}}^2$ are equals,

$$u_{\bar{k}}^2 = \frac{1}{2} \left(1 + \frac{\zeta(k)}{E(k)} \right) \quad (\text{E.1})$$

$$v_{\bar{k}}^2 = \frac{1}{2} \left(1 - \frac{\zeta(k)}{E(k)} \right) \quad (\text{E.2})$$

$$E(k) = \sqrt{\zeta(k)^2 + \Delta(k)^2} \quad (\text{E.3})$$

The Bogoliubov amplitude $v_{\bar{k}}^2$ represents the particle-excitation density, while $u_{\bar{k}}^2$ is the vacancy-excitation density. It is possible to prove that the equality $v_{\bar{k}}^2 = u_{\bar{k}}^2$ implies $\zeta(\bar{k}) = 0$.

Without intralayer correlations, $\zeta(k) = \varepsilon(k) - \mu_s$, thus the equality $v_{\bar{k}}^2 = u_{\bar{k}}^2$ stands when:

$$\begin{aligned} \zeta(\bar{k}) &= 0 \\ \varepsilon(\bar{k}) &= \mu_s \end{aligned} \quad (\text{E.4})$$

and $\mu = \varepsilon(\bar{k}) = \mu_s$.

Including intralayer correlations, the single-particle dispersion relation becomes $\zeta(k) = \varepsilon(k) - \mu_s - \Sigma(k)$, where $\Sigma(k) = 1/S \sum_{k'} V_N^{sc}(k - k') n(k')$ is the correlation Fock energy. From the condition $\zeta(\bar{k}) = 0$ one gets:

$$\mu = \varepsilon(\bar{k}) = \mu_s + \Sigma(\bar{k}) \quad (\text{E.5})$$

The chemical potential μ is shifted respect to μ_s by a factor $\Sigma(\bar{k})$.

Fig. E.1 shows that for $\mu_s = -0.2$, the chemical potential with intralayer correlations is $\mu = 0.38$.

Decreasing the μ_s also the μ decreases, and at a certain negative μ_s the $\mu = 0$. Below this μ_s , there is no \bar{k} in which $v^2(k) = u^2(k)$ and so the definition Eq. (E.5) is no longer valid. In other words, Eq. (E.5) is valid until there is a Fermi surface that guarantees the presence of particle and vacancy excitations. When $\mu < 0$ (BEC regime), most of the pairs are condensed in the lowest energy state $k = 0$ thus our guess is in this regime to define

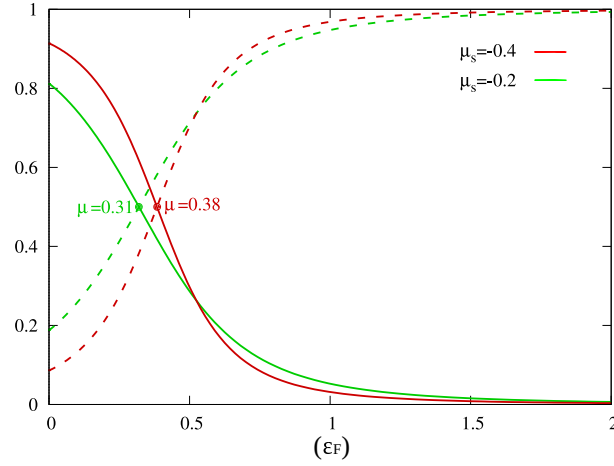


FIGURE E.1: The Bogoliubov amplitudes v_k^2 (solid line) and u_k^2 (dashed line) for $\mu_s = -0.2$ (green curves) and $\mu_s = -0.4$ (red curves).

the chemical potential as:

$$\mu = \mu_s + \Sigma(0) \quad (\text{E.6})$$

The idea is to use Eq. (E.5) for $\mu > 0$ and Eq. (E.6) for $\mu < 0$,

$$\begin{cases} \mu_s + \Sigma(0) \rightarrow \mu \leq 0 \\ \mu_s + \Sigma(\bar{k}) \rightarrow \mu > 0. \end{cases} \quad (\text{E.7})$$

The two branches join at $\mu = 0$.

As proof of the validity of this definition of the chemical potential, we evaluate k_{min} : the wave vector in which $E(k)$ has the minimum. The value of k_{min} tracks the collapse of the Fermi surface. In the BEC, $\mu < 0$, $k_{min} = 0$. By increasing the density, the first value for which $k_{min} \neq 0$ is when the chemical potential becomes positive [43]. This condition is satisfied using our definition of μ instead of μ_s .

The μ_s in $\xi(k)$ is the single-particle chemical potential of the non-interacting system while the μ we define here is the single-particle chemical potential of the system including the effect of the intralayer correlations. This latter is the one evaluated in Ref. [43].

Appendix F

Density collective modes in exciton bilayer normal state

The RPA electron-electron and electron-hole response functions of a bilayer system in the normal states are obtained by setting to zero $\Pi_0^A(q, \omega)$ in Eqs. (5.8)-(5.9):

$$\Pi_{ee}^{RPA}(q, \omega) = \frac{\Pi_0^N(q, \omega) - V_S(q)\Pi_0^N(q, \omega)^2}{1 - 2\Pi_0^N(q, \omega)V_S(q) + (V_S(q)^2 - V_D(q)^2)\Pi_0^N(q, \omega)^2} \quad (\text{F.1})$$

$$\Pi_{eh}^{RPA}(q, \omega) = \frac{V_D(q)\Pi_0^N(q, \omega)^2}{1 - 2\Pi_0^N(q, \omega)V_S(q) + (V_S(q)^2 - V_D(q)^2)\Pi_0^N(q, \omega)^2} \quad (\text{F.2})$$

where $\Pi_0^N(q, \omega)$ is the 2D dynamic Lindhard function, Eq. (B.29):

$$\Pi_0^N(q, \omega) = \frac{1}{S} \sum_k \frac{\theta(k_F - k) - \theta(k_F - |k + q|)}{\omega + \xi(k) - \xi(k + q)} \quad (\text{F.3})$$

The electron-electron and the electron-hole response function have the same denominator because we are considering equal electron and hole layers. Thus, the energy spectra of the density collective modes in the normal exciton bilayer phase are obtained by solving the following equation:

$$1 - 2\Pi_0^N(q, \omega)V_S(q) + (V_S(q)^2 - V_D(q)^2)\Pi_0^N(q, \omega)^2 = 0. \quad (\text{F.4})$$

$\Pi_0^N(q, \omega)$ has poles making impossible to solve Eq. (F.4) in the poles region. The polarization function $\Pi_0^N(q, \omega)$ diverges in the interval in the real axis for $\omega \in C_q = \{\xi(q + k) - \xi(k), k \in R^2\}$.

In the normal state the boundaries of the brunch cut are given by the following relation [131]:

$$\max(0, \omega_-(q)) < \omega < \omega_+(q) \quad (\text{F.5})$$

$$\hbar\omega_{\pm} = \frac{\hbar^2 q^2}{2m} \pm \hbar v_F q \quad (\text{F.6})$$

where $v_F = \hbar k_F / m^*$ is the Fermi velocity.

The $\omega(q)$ region enclosed between $\omega_-(q)$ and $\omega_+(q)$ is called "continuum". A perturbation with $\omega(q)$ in the continuum induces a promotion of a particle from an occupied state (which then remains empty and is referred to as the quasi-anti-particle) with wave-vector k to an empty one with wave vector $k + q$, quasi-particle, that is not stable. This excitation is characterized by a lifetime and eventually results in the recombination of

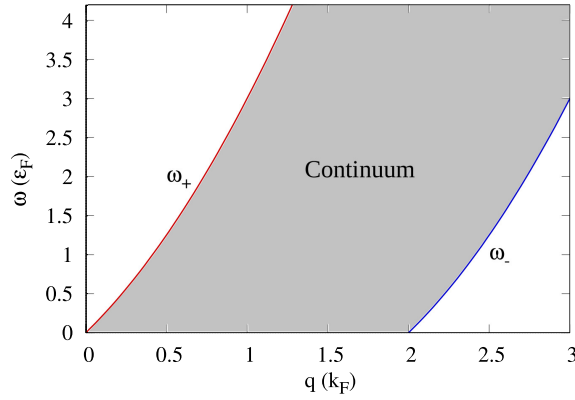


FIGURE F.1: The continuum region (grey area) in the exciton normal state. The top and bottom boundaries of the continuum are defined by the energies ω_+ and ω_- , respectively.

the quasi-particle and quasi-anti-particle, with the emission of a photon of energy $\hbar v_F q$. Possible collective modes in the continuum are unstable.

For $q < 2k_F$ (left panel in Fig. F.2), the imaginary part of the polarization is different from zero for $0 < \omega < \omega_+$, and it is characterized by the "shark tail" shape [131]. For $q > 2k_F$ the lower boundary of the continuum region moved up to ω_+ different from zero. As reported in the right panel of Fig. F.2 there is a small interval close to zero frequency in which the imaginary part of the polarization is zero.

It is possible to prove that Eq. (F.4) has real solutions only if $\Pi_0^N(q, \omega) > 0$. Stable collective modes must be searched only for $\omega > \omega_+$. In Ref. [144, 215] stable collective modes have been found at very low density, $r_s > 20$, for $\omega < \omega_-$.

The intralayer correlations are vital for observing collective modes below the continuum area. At low density in the normal state, the system experiences strong correlations, making the Hartree-Fock approximation insufficient. A T-matrix approach or quasi-localized-charge approximation is used to account for these correlations. Unlike Ref. [144, 215], which considered the bilayer exciton system in the normal state, we also account for the presence of a superfluid exciton phase. In a bilayer exciton system, the normal state only occurs at high density (weak correlation region), while at low density, the ground state is the superfluid phase. Although we have included the Hartree-Fock term in our formalism, it showed no significant effects, since at high density the Hartree-Fock correlation energy is much smaller than the Fermi energy and thus negligible (Fig. 4.1).

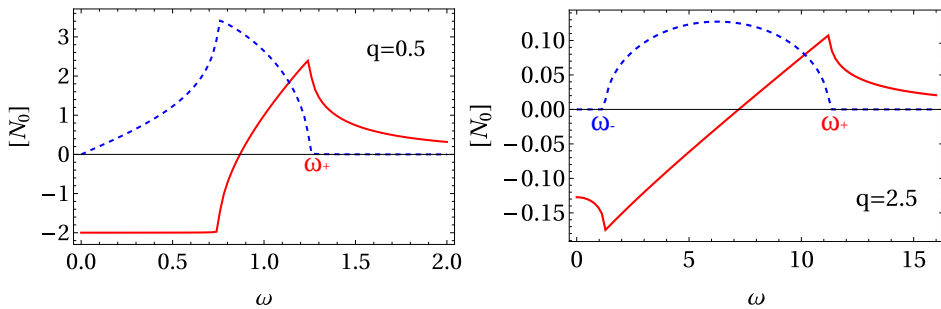


FIGURE F.2: The real (red solid line) and imaginary part (blue dashed line) of the zero-order normal polarization function $\Pi_0^N(q, \omega)$ in units of the 2D density of states N_0 as a function of ω for $q = 0.5k_F$ (left panel) and $q = 2.5k_F$ (right panel).

We solve Eq. (F.4) outside the continuum, for $\omega > \omega_+$ as a function of q .

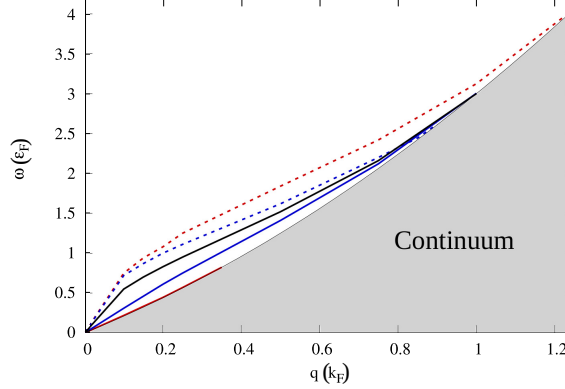


FIGURE F.3: Energy spectra of the acoustic (solid line) and optic (dashed lines) collective modes as a function of the momentum for different interlayer distance: $d = 0.2$ (red curves) and $d = 1.0$ (blue curves). The black solid line is the energy spectra of the plasma mode for an isolated electron single layer.

There are two different branches of solutions for Eq. (F.4) as a function of the momentum q . They correspond to the acoustic and optic density collective modes. In the acoustic branch, the relative electron and hole motion is in phase while in the optic mode is out of phase. In both cases, at a certain q they approach the continuum and disappear, like plasma collective modes in an isolated 2D electron layer [131]. Indeed, as reported in Fig. F.3, increasing the interlayer distance the two branches merge in the plasma branch. Decreasing the d the energy of the acoustic branch decreases and disappears in the continuum at always smaller q . The interlayer interaction is getting stronger so the in-phase electron-hole collective modes require less energy. Analogously, the energy of the optic branch increases. In the long-wave limit ($q \rightarrow 0$) for $d \rightarrow 0$ the optic branch goes as $\hbar\omega_{op} = \sqrt{2}\hbar\omega_{pl}$, where ω_{pl} is the 2D plasma frequency. This is the plasma frequency of a single particle layer with electric charge $2e$ and effective mass $2m^*$. Increasing the density, the energy of the acoustic, optic and plasma collective modes increases, in particular, for small q they go as \sqrt{n} .

The real part of the polarization function becomes positive increasing the ω , before exiting the continuum, Fig. F.2. In the continuum, the normal polarization function, Eq. (F.3), has poles for real frequency ω so it is not possible to find a real solution of Eq. (F.4). Possible solutions of Eq. (F.4) are imaginary, $\Omega(q) = \omega(q) + i\Gamma(q)$ where Γ is the damping parameter and provides information about the lifetime of collective modes in the continuum.

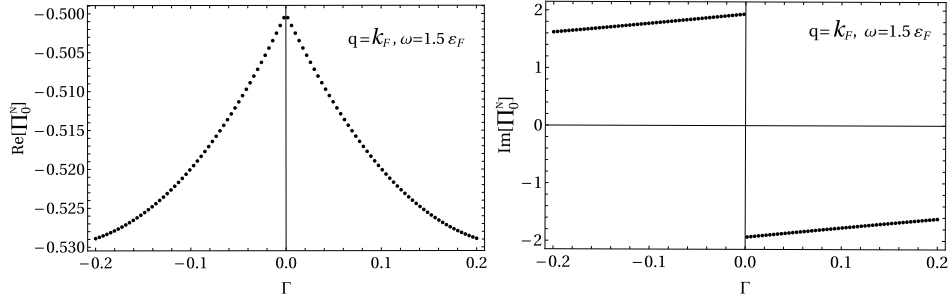


FIGURE F.4: Real (left panel) and imaginary (right panel) of the normal polarization function $\Pi_0^N(q, \omega + i\Gamma)$ for $q = k_F$ and $\omega = 1.5\epsilon_F$ as a function of the damping parameter Γ .

The solution of Eq. (F.4) depends on which direction of the complex Ω plane the real axis is approached. As reported in Fig. F.4, in the continuum there is a jump in the imaginary part and a cusp in the real part of the normal polarization $\Pi_0^N(q, \omega + i\Gamma)$ function at $\Gamma = 0$.

To solve this issue the polarization function is analytically continued. We adopt the Nozières analytic continuation method, explained in Appendix. G, to evaluate an analytical normal polarization function $\Pi_C^N(q, \omega + i\Gamma)$ in the normal state of the bilayer exciton system (see detailed calculation in Appendix G.1). The analytic continuation results in moving the poles from the real axis to the negative imaginary semi-plane of Ω .

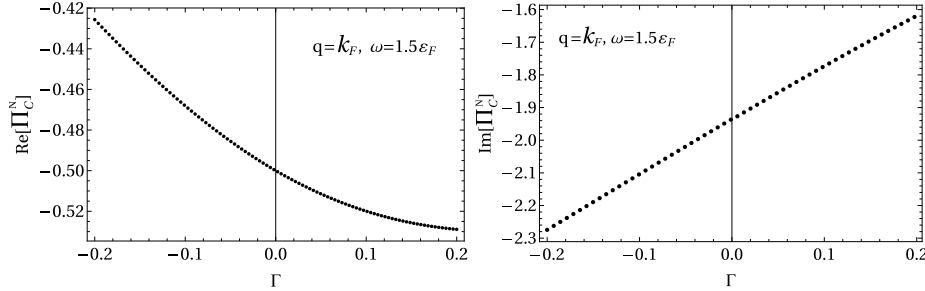


FIGURE F.5: Real (left panel) and imaginary (right panel) of the analytically continued normal polarization function $\Pi_C^N(q, \omega + i\Gamma)$ as a function of the damping parameter Γ for the same momentum q and energy ω of Fig. F.4.

Figure F.5 shows the normal and imaginary part of the analytically continued normal polarization function $\Pi_C^N(q, \omega + i\Gamma)$ for the same q and ω of Fig. F.4. The jump in the imaginary part and the cusp in the real part of the normal polarization function disappeared after the analytic continuation. Replacing the analytically continued normal polarization function $\Pi_C^N(q, \omega + i\Gamma)$ it is possible to search complex solution $\Omega(q) = \omega(q) + i\Gamma(q)$ of Eq. F.4 in the continuum.

We start with $d = 0.2$ and $q = 0.35k_F$, close to the momentum in which the acoustic brunch disappears. No solution of Eq. F.4 exists in the continuum for $q = 0.35k_F$, as reported in Fig. F.6, or for any other momenta q . The real and imaginary parts of Eq. F.4 are zero for some values of ω and Γ separately but never the absolute value.

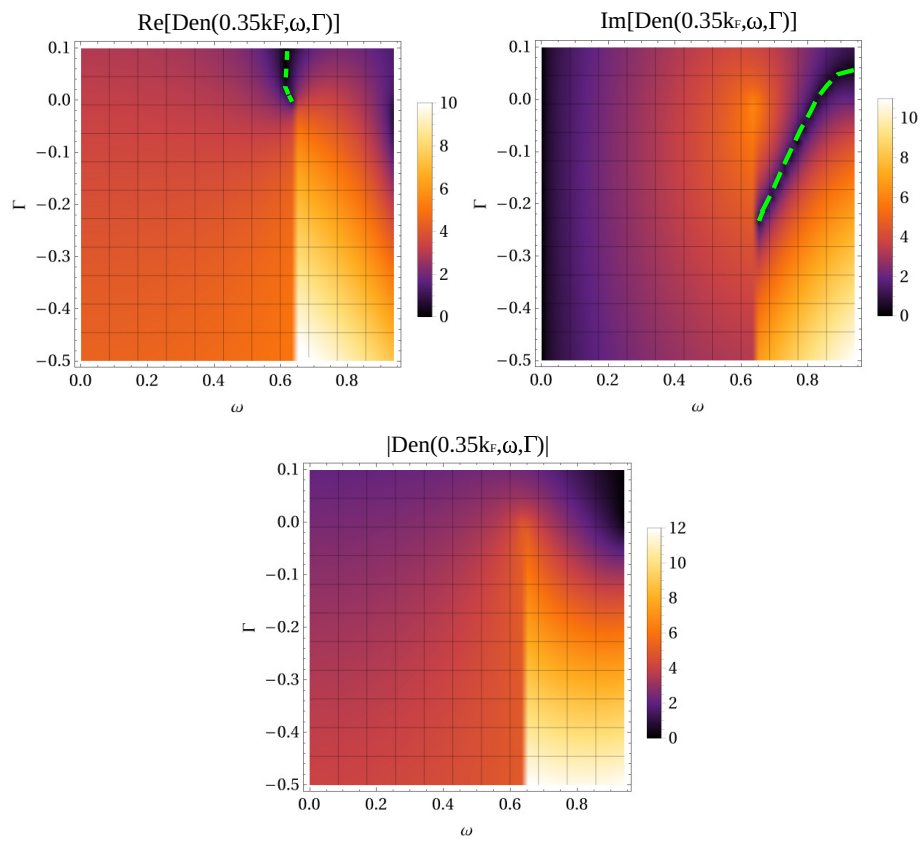


FIGURE F.6: Real (a), imaginary (b) and absolute value (c) of Eq. F.4 for $d = 0.2$ and $q = 0.4k_F$ in the continuum. The green dashed line follows the zeros.

Appendix G

Nozières Analytic Continuation procedure

Let's suppose to have the following function:

$$f(z) = \int_0^{\infty} d\varepsilon \frac{\rho(\varepsilon)}{z - \varepsilon}. \quad (\text{G.1})$$

The $\rho(\varepsilon)$ is called the spectral function with ε real. The $f(z)$ is analytic for complex $z = \omega + i\delta$ while it has a branch cut for real z . For $z = \varepsilon$, $f(z)$ has poles. The value of the function approaching the poles changes depending on whether the branch cut is approached from a positive or negative imaginary semi-plane.

To remove the non-analyticity in the real axis we use here the Nozières analytic continuation procedure [132].

The $f(z)$ in the negative imaginary semi-plane is replaced with:

$$f(\omega - i\delta) \rightarrow f(\omega - i\delta) + (f(\omega + i\delta) - f(\omega - i\delta)). \quad (\text{G.2})$$

In the limit $\delta \rightarrow 0$, the term $f(\omega + i\delta) - f(\omega - i\delta)$ adjusts the function in the proximity of the real branch cut so that $f(z)$ from the negative semi-plane smoothly evolves into $f(z)$ from the positive semi-plane, without any discontinuity. Using Eq. (G.2), the poles are shifted from the real axis to the negative imaginary semi-plane, allowing the function to be evaluated on the real axis. The term $\lim_{\delta \rightarrow 0} f(\omega + i\delta) - f(\omega - i\delta)$ can be evaluated as:

$$\lim_{\delta \rightarrow 0} f(\omega + i\delta) - f(\omega - i\delta) = \lim_{\delta \rightarrow 0} \int_0^{\infty} d\varepsilon \rho(\varepsilon) \left(\frac{1}{\omega + i\delta - \varepsilon} - \frac{1}{\omega - i\delta - \varepsilon} \right). \quad (\text{G.3})$$

Using the following property of the Dirac delta function:

$$\lim_{\delta \rightarrow 0} \frac{1}{x + i\delta} = \frac{1}{x} - i\pi\delta(x), \quad (\text{G.4})$$

then,

$$\begin{aligned} \lim_{\delta \rightarrow 0} f(\omega + i\delta) - f(\omega - i\delta) &= \int_0^{\infty} d\varepsilon \rho(\varepsilon) \left(\frac{1}{\omega - \varepsilon} - i\pi\delta(\omega - \varepsilon) - \frac{1}{\omega - \varepsilon} - i\pi\delta(\omega - \varepsilon) \right) \\ &= -2i\pi \int_0^{\infty} d\varepsilon \rho(\varepsilon) \delta(\omega - \varepsilon) \\ &= -2i\pi\rho(\omega). \end{aligned} \quad (\text{G.5})$$

The Nozierès analytic continuation consists in building the function:

$$f^C(z) = \begin{cases} f(z), & \text{Im}[z] > 0 \\ f(z) - 2i\pi\rho(z), & \text{Im}[z] \leq 0 \end{cases} \quad (\text{G.6})$$

The $\rho(z)$ appearing in Eq. (G.6) is the analytic continuation of $\rho(\omega)$, where [132]:

$$\rho(\omega) = -\frac{\text{Im}[f(\omega + i\delta)]}{\pi}. \quad (\text{G.7})$$

G.1 Analytic Continuation of the Polarization function in the Normal State

The normal polarization function $\Pi_0^N(q, \Omega)$ in the normal exciton state states:

$$\Pi_0^N(q, \Omega) = \frac{1}{(2\pi)^2} \int_0^\infty dk \, 2k \int_0^{2\pi} d\phi \frac{\theta(1-k) - \theta(1 - \sqrt{k^2 + q^2 + 2kq \cos \phi})}{\Omega - q^2 - 2kq \cos \phi}. \quad (\text{G.8})$$

$\Pi_0^N(q, \Omega)$ is in unit of $(Ry^* a_B^2)^{-1}$, the momenta q and k are in unit of k_F while the $\Omega = \omega + i\delta$ is in unit of ε_F .

The $\Pi_0^N(q, \Omega)$ has a branch cut for real Ω . The evaluation of the polarization function in the branch cut can be done by performing the Nozières analytic continuation.

The first step is the evaluation of the spectral function $\rho(\omega)$ using Eq. (G.7):

$$\begin{aligned} \rho(\omega) &= -\frac{\text{Im}[\Pi(q, \omega + i\delta)]}{\pi} \\ &= -\frac{1}{\pi} \text{Im} \left[\frac{1}{(2\pi)^2} \int_0^\infty dk \, 2k \int_0^{2\pi} d\phi \frac{\theta(1-k) - \theta(1 - \sqrt{k^2 + q^2 + 2kq \cos \phi})}{\omega + i\delta - q^2 - 2kq \cos \phi} \right] \\ &= -\frac{1}{\pi} \frac{1}{(2\pi)^2} \text{Im} \left[\int_0^\infty dk \, 2k \int_0^{2\pi} d\phi \frac{\theta(1-k) - \theta(1 - \sqrt{k^2 + q^2 + 2kq \cos \phi})}{\omega + i\delta - q^2 - 2kq \cos \phi} \right]. \end{aligned}$$

Using Eq. (G.4) one gets:

$$\begin{aligned} \rho(\omega) &= -\frac{1}{\pi} \frac{1}{(2\pi)^2} \text{Im} \left[\int_0^\infty dk \, 2k \int_0^{2\pi} d\phi \left(\theta(1-k) - \theta(1 - \sqrt{k^2 + q^2 + 2kq \cos \phi}) \right) \right. \\ &\quad \left. \times \left(\frac{1}{\omega - q^2 - 2kq \cos \phi} - i\pi\delta(\omega - q^2 - 2kq \cos \phi) \right) \right] \\ \rho(\omega) &= \frac{1}{(2\pi)^2} \int_0^\infty dk \, 2k \int_0^{2\pi} d\phi \left(\theta(1-k) - \theta(1 - \sqrt{k^2 + q^2 + 2kq \cos \phi}) \right) \delta(\omega - q^2 - 2kq \cos \phi). \end{aligned} \quad (\text{G.9})$$

We introduce the following property of the Dirac delta function:

$$\delta(g(x)) = \sum_i \frac{\delta(x - x_i)}{|g'(x_i)|}, \quad (\text{G.10})$$

where x_i are the roots of $g(x)$. Thus:

$$\delta(\omega - q^2 - 2kq \cos \phi) = \sum_i \frac{\delta(\cos(\phi) - \phi_i)}{|g'(\phi_i)|}, \quad (\text{G.11})$$

where $g(\phi) = \omega - q^2 - 2kq \cos \phi$ and the root ϕ_i is:

$$\phi_i = \frac{\omega - q^2}{2kq}. \quad (\text{G.12})$$

Then,

$$\begin{aligned} \rho(\omega) &= \frac{1}{(2\pi)^2} \int_0^\infty dk \, 2k \int_0^{2\pi} d\phi \left(\theta(1-k) - \theta(1 - \sqrt{k^2 + q^2 + 2kq \cos \phi}) \right) \frac{\delta(\cos(\phi) - \phi_i)}{|-2kq|} \\ &= \frac{1}{(2\pi)^2} \int_0^\infty dk \, 2k \int_0^{2\pi} d\phi \left(\theta(1-k) - \theta(1 - \sqrt{k^2 + q^2 + 2kq \cos \phi}) \right) \frac{\delta(\cos(\phi) - \phi_i)}{2kq} \\ &= \frac{2}{(2\pi)^2} \int_0^\infty dk \int_0^\pi d\phi \left(\theta(1-k) - \theta(1 - \sqrt{k^2 + q^2 + 2kq \cos \phi}) \right) \frac{\delta(\cos(\phi) - \phi_i)}{q}. \end{aligned} \quad (\text{G.13})$$

Transforming $\cos(\phi) = x$:

$$\rho(\omega) = \frac{2}{(2\pi)^2} \int_0^\infty dk \int_{-1}^1 \frac{dx}{\sqrt{1-x^2}} \left(\theta(1-k) - \theta(1 - \sqrt{k^2 + q^2 + 2kqx}) \right) \frac{\delta(x - \phi_i)}{q}. \quad (\text{G.14})$$

The integral in x is different from zero only if $|\phi_i| < 1$, thus:

$$\left| \frac{\omega - q^2}{2kq} \right| < 1 \quad (\text{G.15})$$

$$k > \left| \frac{\omega - q^2}{2q} \right| = \bar{k}. \quad (\text{G.16})$$

This is the lower limit of integral in k to have $\delta(x - \phi_i) = 1$. Replacing Eq. (G.12) in ϕ_i :

$$\rho(\omega) = \frac{2}{(2\pi)^2} \int_{\bar{k}}^\infty dk \frac{1}{\sqrt{1 - \left(\frac{\omega - q^2}{2kq}\right)^2}} \left(\theta(1-k) - \theta(1 - \sqrt{k^2 + \omega}) \right) \frac{1}{q}. \quad (\text{G.17})$$

This is the spectral function $\rho(\omega)$. The next step is to do the analytic continuation $\omega \rightarrow \Omega$ to the complex plane. To do it we have to see where is analytic.

The denominator of the integrand is zero when:

$$1 - \left(\frac{\omega - q^2}{2kq} \right)^2 = 0 \quad (\text{G.18})$$

$$1 - \frac{(\omega - q^2)^2}{4k^2q^2} = 0 \quad (\text{G.19})$$

$$4k^2q^2 - (\omega - q^2)^2 = 0 \quad (\text{G.20})$$

$$k = \frac{\omega - q^2}{2q}, \quad (\text{G.21})$$

which corresponds to the lower boundary of the k -integral.

The presence of step functions at the numerator of $\rho(\omega)$ provides non-analyticity points. We individuate the k -intervals in which the numerator is different from zero as a function of ω :

$$\begin{cases} \omega \geq 1 \rightarrow 0 < k < 1 \\ \omega < 1 \rightarrow \sqrt{1-\omega} < k < 1 \end{cases} \quad (\text{G.22})$$

Implementing the condition $k > \bar{k}$ one finds that the numerator is constant and equal to 1 in the following cases:

$$q \leq 1 \rightarrow \begin{cases} \omega \leq -q^2 + 2q \rightarrow \sqrt{1-\omega} < k < 1 \\ \omega > -q^2 + 2q \rightarrow \bar{k} < k < 1 \end{cases} \quad (\text{G.23})$$

$$1 < q < 2 \rightarrow \begin{cases} \omega \leq -q^2 + 2q \rightarrow \sqrt{1-\omega} < k < 1 \\ -q^2 + 2q < \omega < q^2 \rightarrow -\bar{k} < k < 1 \\ \omega \geq q^2 \rightarrow \bar{k} < k < 1 \end{cases} \quad (\text{G.24})$$

$$q \geq 2 \rightarrow \begin{cases} \omega \leq q^2 \rightarrow -\bar{k} < k < 1 \\ \omega \geq q^2 \rightarrow \bar{k} < k < 1 \end{cases} \quad (\text{G.25})$$

Those are the $k(q, \omega)$ integration intervals in which the function $\rho(\omega)$ is analytic.

Doing the continuation $\omega \rightarrow \Omega = \omega + i\Gamma$ also the k integration intervals are continued in the imaginary space and the spectral function is analytic following the path reported in Eq. (G.23)-(G.25). This allows the analytic continuation of the polarization function $\rho(\omega) \rightarrow \rho(\Omega)$.

The Nozierès analytic continuation of the normal polarization function is:

$$\Pi_0^C(q, \Omega) = \begin{cases} \Pi_0^N(q, \Omega), & \text{Im}[\Omega] > 0 \\ \Pi_0^N(q, \Omega) - 2i\pi\rho(\Omega), & \text{Im}[\Omega] \leq 0. \end{cases} \quad (\text{G.26})$$

Bibliography

- ¹G. W. Burg, N. Prasad, K. Kim, T. Taniguchi, K. Watanabe, A. H. MacDonald, L. F. Register, and E. Tutuc, “Strongly enhanced tunneling at total charge neutrality in double-bilayer graphene-WSe₂ heterostructures”, *Phys. Rev. Lett.* **120**, 177702 (2018).
- ²Z. Wang, D. A. Rhodes, K. Watanabe, T. Taniguchi, J. C. Hone, J. Shan, and K. F. Mak, “Evidence of high-temperature exciton condensation in two-dimensional atomic double layers”, *Nature (London)* **574**, 76–80 (2019).
- ³L. Ma, P. X. Nguyen, Z. Wang, Y. Zeng, K. Watanabe, T. Taniguchi, A. H. MacDonald, K. F. Mak, and J. Shan, “Strongly correlated excitonic insulator in atomic double layers”, *Nature (London)* **598**, 585–589 (2021).
- ⁴A. Gamucci, D. Spirito, M. Carrega, B. Karmakar, A. Lombardo, M. Bruna, L. Pfeiffer, K. West, A. Ferrari, M. Polini, et al., “Anomalous low-temperature Coulomb drag in graphene-GaAs heterostructures”, *Nat. Commun.* **5** (2014).
- ⁵J. Gu, L. Ma, S. Liu, K. Watanabe, T. Taniguchi, J. C. Hone, J. Shan, and K. F. Mak, “Dipolar excitonic insulator in a moiré lattice”, *Nat. Phys.* **18**, 395–400 (2022).
- ⁶P. X. Nguyen, L. Ma, R. Chaturvedi, K. Watanabe, T. Taniguchi, J. Shan, and K. F. Mak, “Perfect Coulomb drag in a dipolar excitonic insulator”, *ArXiv:cond-mat/2309.14940* (2023).
- ⁷S. Conti, A. Perali, A. R. Hamilton, F. M. Peeters, and D. Neilson, “Chester supersolid of spatially indirect excitons in double-layer semiconductor heterostructures”, *Phys. Rev. Lett.* **130**, 057001 (2023).
- ⁸V. G. Kogan and B. A. Tavger, “Possibility of pair correlation of electrons and holes in a sandwich consisting of n- and p-type semiconductor films”, in *Physics of p-n junctions and semiconductor devices*, Vol. 130 (Springer US, Boston, MA, 1971), pp. 39–45.
- ⁹Y. E. Lozovik and V. I. Yudson, “A new mechanism for superconductivity: pairing between spatially separated electrons and holes”, *Sov. Phys. JETP* **44**, (Zh. Eksp. Teor. Fiz. **71**, 738-753 (1976)), 389–397 (1976).
- ¹⁰J. I. A. Li, T. Taniguchi, K. Watanabe, J. Hone, and C. Dean, “Excitonic superfluid phase in double bilayer graphene”, *Nat. Phys.* **13**, 751 (2017).
- ¹¹G. E. Astrakharchik, J. Boronat, I. L. Kurbakov, and Y. E. Lozovik, “Quantum phase transition in a two-dimensional system of dipoles”, *Phys. Rev. Lett.* **98**, 060405 (2007).
- ¹²S. De Palo, F. Rapisarda, and G. Senatore, “Excitonic condensation in a symmetric electron-hole bilayer”, *Phys. Rev. Lett.* **88**, 206401 (2002).
- ¹³H. K. Onnes, “The resistance of pure mercury at helium temperatures”, *Commun. Phys. Lab. Univ. Leiden* **12**, 120 (1911).
- ¹⁴P. Kapitza, “Viscosity of liquid helium below the λ -point”, *Nature* **141**, 74 (1938).
- ¹⁵J. F. Allen and A. D. Misener, “Flow phenomena in liquid helium II”, *Nature* **142**, 643 (1938).

-
- ¹⁶S. N. Bose, "Plancks gesetz und lichtquantenhypothese", *Zeitschrift für Physik* **26**, 178–181 (1924).
- ¹⁷A. Einstein, "Quantentheorie des einatomigen idealen gases", *Ber. Berl. Akad.* **261**, 057001 (1924).
- ¹⁸L. Tisza, "Transport phenomena in helium II", *Nature* **141**, 913–913 (1938).
- ¹⁹L. Landau, "Theory of the superfluidity of helium II", *Phys. Rev.* **60**, 356–358 (1941).
- ²⁰F. London, "The λ -phenomenon of liquid helium and the Bose-Einstein degeneracy", *Nature* **141**, 643–644 (1938).
- ²¹J. Bardeen, L. N. Cooper, and J. R. Schrieffer, "Theory of superconductivity", *Phys. Rev.* **108**, 1175–1204 (1957).
- ²²H. Fröhlich, "Electrons in lattice fields", *Adv. in Phys.* **3**, 325–361 (1954).
- ²³J. M. Blatt, K. W. Böer, and W. Brandt, "Bose-Einstein condensation of excitons", *Phys. Rev.* **126**, 1691 (1962).
- ²⁴L. V. Keldysh and A. N. Kozlov, "Collective properties of excitons in semiconductors", *Sov. Phys. JETP* **27**, 521 (1968).
- ²⁵C. Comte and P. Nozières, "Exciton Bose condensation : The ground state of an electron-hole gas - I. Mean field description of a simplified model", *J. Phys. France* **43**, 1069 (1982).
- ²⁶P. Nozières and C. Comte, "Exciton Bose condensation: the ground state of an electron-hole gas - II. Spin states, screening and band structure effects", *J. Phys. France* **43**, 1083 (1982).
- ²⁷S. G. Tikhodeev, G. A. Kopelevich, and N. A. Gippius, "Exciton transport in Cu_2O : Phonon wind versus superfluidity", *Phys. Status Solidi B* **206**, 45 (1998).
- ²⁸J. I. Jang and J. P. Wolfe, "Auger recombination and biexcitons in Cu_2O : A case for dark excitonic matter", *Phys. Rev. B* **74**, 045211 (2006).
- ²⁹J. D. Cloizeaux, "Exciton instability and crystallographic anomalies in semiconductors", *J. Phys. Chem. Solids* **26**, 259–266 (1965).
- ³⁰D. Jérôme, T. M. Rice, and W. Kohn, "Excitonic insulator", *Phys. Rev.* **158**, 462–475 (1967).
- ³¹Y. E. Lozovik and V. I. Yudson, "Feasibility of superfluidity of paired spatially separated electrons and holes", *JETP Lett. (USSR)* **22**, 274–276 (1975).
- ³²A. F. Croxall, K. Das Gupta, C. A. Nicoll, M. Thangaraj, H. E. Beere, I. Farrer, D. A. Ritchie, and M. Pepper, "Anomalous Coulomb drag in electron-hole bilayers", *Phys. Rev. Lett.* **101**, 246801 (2008).
- ³³Y. E. Lozovik and A. A. Sokolik, "Electron-hole pair condensation in a graphene bilayer", *JETP Lett* **87**, 55 (2008).
- ³⁴P. Nozières and S. Schmitt-Rink, "Bose condensation in an attractive fermion gas: from weak to strong coupling superconductivity", *J. Low Temp. Phys.* **59**, 195 (1985).
- ³⁵M. H. Anderson, J. R. Ensher, M. R. Matthews, C. E. Wieman, and E. A. Cornell, "Observation of Bose-Einstein condensation in a dilute atomic vapor", *Science* **269**, 198 (1995).
- ³⁶C. Chin, R. Grimm, P. Julienne, and E. Tiesinga, "Feshbach resonances in ultracold gases", *Rev. Mod. Phys.* **82**, 1225–1286 (2010).

- ³⁷C. A. Regal, M. Greiner, and D. S. Jin, "Observation of resonance condensation of fermionic atom pairs", *Phys. Rev. Lett.* **92**, 040403 (2004).
- ³⁸W. Gunton, M. Semczuk, and K. W. Madison, "Realization of BEC-BCS-crossover physics in a compact oven-loaded magneto-optic-trap apparatus", *Phys. Rev. A* **88**, 023624 (2013).
- ³⁹M. W. Zwierlein, C. A. Stan, C. H. Schunck, S. M. F. Raupach, A. J. Kerman, and W. Ketterle, "Condensation of pairs of fermionic atoms near a Feshbach resonance", *Phys. Rev. Lett.* **92**, 120403 (2004).
- ⁴⁰J. R. Engelbrecht, M. Randeria, and C. A. R. Sáde Melo, "BCS to Bose crossover: broken-symmetry state", *Phys. Rev. B* **55**, 15153 (1997).
- ⁴¹M. W. Zwierlein, J. R. Abo-Shaer, A. Schirotzek, C. H. Schunck, and W. Ketterle, "Vortices and superfluidity in a strongly interacting Fermi gas", *Nature* **435**, 1047–1051 (2005).
- ⁴²Y. Zeng and A. H. MacDonald, "Electrically controlled two-dimensional electron-hole fluids", *Phys. Rev. B* **102**, 085154 (2020).
- ⁴³P. López Ríos, A. Perali, R. J. Needs, and D. Neilson, "Evidence from quantum Monte Carlo simulations of large-gap superfluidity and BCS-BEC crossover in double electron-hole layers", *Phys. Rev. Lett.* **120**, 177701 (2018).
- ⁴⁴F. Pascucci, S. Conti, A. Perali, J. Tempere, and D. Neilson, "Effects of intralayer correlations on electron-hole double-layer superfluidity", *Phys. Rev. B* **109**, 094512 (2024).
- ⁴⁵Y. E. Lozovik, S. L. Ogarkov, and A. A. Sokolik, "Condensation of electron-hole pairs in a two-layer graphene system: Correlation effects", *Phys. Rev. B* **86**, 045429 (2012).
- ⁴⁶A. Perali, D. Neilson, and A. R. Hamilton, "High-temperature superfluidity in double-bilayer graphene", *Phys. Rev. Lett.* **110**, 146803 (2013).
- ⁴⁷I. Sodemann, D. A. Pesin, and A. H. MacDonald, "Interaction-enhanced coherence between two-dimensional Dirac layers", *Phys. Rev. B* **85**, 195136 (2012).
- ⁴⁸D. Neilson, A. Perali, and A. R. Hamilton, "Excitonic superfluidity and screening in electron-hole bilayer systems", *Phys. Rev. B* **89**, 060502(R) (2014).
- ⁴⁹B. N. Narozhny and A. Levchenko, "Coulomb drag", *Rev. Mod. Phys.* **88**, 025003 (2016).
- ⁵⁰G. Vignale and A. H. MacDonald, "Drag in paired electron-hole layers", *Phys. Rev. Lett.* **76**, 2786 (1996).
- ⁵¹T. J. Gramila, J. P. Eisenstein, A. H. MacDonald, L. N. Pfeiffer, and K. W. West, "Mutual friction between parallel two-dimensional electron systems", *Phys. Rev. Lett.* **66**, 1216 (1991).
- ⁵²A. G. Rojo, "Electron-drag effects in coupled electron systems", *J. Phys. Condens. Mat.* **11**, R31 (1999).
- ⁵³L. Świerkowski, J. Szymański, and Z. W. Gortel, "Coupled electron-hole transport: Beyond the mean field approximation", *Phys. Rev. Lett.* **74**, 3245 (1995).
- ⁵⁴D. Nandi, A. D. K. Finck, J. P. Eisenstein, L. N. Pfeiffer, and K. W. West, "Exciton condensation and perfect Coulomb drag", *Nature* **488**, 481–484 (2012).
- ⁵⁵D. K. Efimkin and V. Galitski, "Anomalous Coulomb drag in electron-hole bilayers due to the formation of excitons", *Phys. Rev. Lett.* **116**, 046801 (2016).
- ⁵⁶J. P. Eisenstein, L. N Pfeiffer, and K. W. West, "Independently contacted two-dimensional electron systems in double quantum wells", *Appl. Phys. Lett.* **57**, 2324 (1990).

- ⁵⁷J. P. Eisenstein and A. H. MacDonald, "Bose–Einstein condensation of excitons in bilayer electron systems", *Nature* **432**, 691 (2004).
- ⁵⁸S. Latini, K. T. Winther, T. Olsen, and K. S. Thygesen, "Interlayer excitons and band alignment in MoS₂/hBN/WSe₂ van der Waals heterostructures", *Nano Letters* **17**, 938–945 (2017).
- ⁵⁹S. Ovesen, S. Brem, C. Linderälv, M. Kuisma, T. Korn, P. Erhart, M. Selig, and E. Malic, "Interlayer exciton dynamics in van der Waals heterostructures", *Commun. Phys.* **2**, 23 (2019).
- ⁶⁰J.-J. Su and A. H. MacDonald, "How to make a bilayer exciton condensate flow", *Nat. Phys.* **4**, 799–802 (2008).
- ⁶¹J. P. Eisenstein, G. S. Boebinger, L. N. Pfeiffer, K. W. West, and S. He, "New fractional quantum Hall state in double-layer two-dimensional electron systems", *Phys. Rev. Lett.* **68**, 1383 (1992).
- ⁶²E. Tutuc, M. Shayegan, and D. A. Huse, "Counterflow measurements in strongly correlated GaAs hole bilayers: Evidence for electron-hole pairing", *Phys. Rev. Lett.* **93**, 036802 (2004).
- ⁶³T. Huber, A. Zrenner, W. Wegscheider, and M. Bichler, "Electrostatic exciton traps", *Phys. Status Solidi. A* **166**, R5 (1998).
- ⁶⁴D. P. Trauernicht, A. Mysyrowicz, and J. P. Wolfe, "Strain confinement and thermodynamics of free excitons in a direct-gap semiconductor", *Phys. Rev. B* **28**, 3590 (1983).
- ⁶⁵K. Brunner, U. Bockelmann, G. Abstreiter, M. Walther, G. Böhm, G. Tränkle, and G. Weimann, "Photoluminescence from a single GaAs/AlGaAs quantum dot", *Phys. Rev. Lett.* **69**, 3216 (1992).
- ⁶⁶P. C. M. Christianen, F. Piazza, J. G. S. Lok, J. C. Maan, and W. Van der Vleuten, "Magnetic trap for excitons", *Phys. B: Cond. Matter* **249**, 624 (1998).
- ⁶⁷A. T. Hammack, M. Griswold, L. V. Butov, L. E. Smallwood, A. L. Ivanov, and A. C. Gossard, "Trapping of cold excitons in quantum well structures with laser light", *Phys. Rev. Lett.* **96**, 227402 (2006).
- ⁶⁸M. Alloing, A. Lemaître, E. Galopin, and F. Dubin, "Optically programmable excitonic traps", *Sci. Rep.* **3**, 1578 (2013).
- ⁶⁹L. V. Butov, A. C. Gossard, and D. S. Chemla, "Macroscopically ordered state in an exciton system", *Nature (London)* **418**, 751 (2002).
- ⁷⁰V. B. Timofeev and A. V. Gorbunov, "Collective state of the Bose gas of interacting dipolar excitons", *J. Appl. Phys.* **101**, 081708 (2007).
- ⁷¹A. A. High, J. R. Leonard, M. Remeika, L. V. Butov, M. Hanson, and A. C. Gossard, "Condensation of excitons in a trap", *Nano Lett.* **12**, 2605 (2012).
- ⁷²M. Combescot, O. Betbeder-Matibet, and R. Combescot, "Bose-Einstein condensation in semiconductors: The key role of dark excitons", *Phys. Rev. Lett.* **99**, 176403 (2007).
- ⁷³J.-D. Lin, P.-Y. Lo, G.-H. Peng, W.-H. Li, S.-Y. Huang, G.-Y. Chen, and S.-J. Cheng, "Essential role of momentum-forbidden dark excitons in the energy transfer responses of monolayer transition-metal dichalcogenides", *npj 2D Materials and Applications* **7**, 51 (2023).
- ⁷⁴R. Anankine, M. Beian, S. Dang, M. Alloing, E. Cambril, K. Merghem, C. G. Carbonell, A. Lemaître, and F. Dubin, "Quantized vortices and four-component superfluidity of semiconductor excitons", *Phys. Rev. Lett.* **118**, 127402 (2017).

- ⁷⁵X. Zhu, P. B. Littlewood, M. S. Hybertsen, and T. M. Rice, "Exciton condensate in semiconductor quantum well structures", *Phys. Rev. Lett.* **74**, 1633 (1995).
- ⁷⁶S. Saberi-Pouya, S. Conti, A. Perali, A. F. Croxall, A. R. Hamilton, F. M. Peeters, and D. Neilson, "Experimental conditions for the observation of electron-hole superfluidity in GaAs heterostructures", *Phys. Rev. B* **101**, 140501(R) (2020).
- ⁷⁷J. A. Seamons, C. P. Morath, J. L. Reno, and M. P. Lilly, "Coulomb drag in the exciton regime in electron-hole bilayers", *Phys. Rev. Lett.* **102**, 026804 (2009).
- ⁷⁸P. Pieri, D. Neilson, and G. C. Strinati, "Effects of density imbalance on the BCS-BEC crossover in semiconductor electron-hole bilayers", *Phys. Rev. B* **75**, 113301 (2007).
- ⁷⁹P. Fulde and R. A. Ferrell, "Superconductivity in a strong spin-exchange field", *Phys. Rev.* **135**, A550 (1964).
- ⁸⁰G. Sarma, "On the influence of a uniform exchange field acting on the spins of the conduction electrons in a superconductor", *J. Phys. Chem. Solids* **24**, 1029 (1963).
- ⁸¹C. Lagoin, K. Baldwin, L. Pfeiffer, and F. Dubin, "Superlattice quantum solid of dipolar excitons", *Phys. Rev. Lett.* **132**, 176001 (2024).
- ⁸²B. Frank, J. Lang, and W. Zwerger, "Universal phase diagram and scaling functions of imbalanced Fermi gases", *J. Exp. Theor. Phys.* **127**, 812–825 (2018).
- ⁸³K. S. Novoselov, A. K. Geim, S. V. Morozov, D. Jiang, Y. Zhang, S. V. Dubonos, I. V. Grigorieva, and A. A. Firsov, "Electric field effect in atomically thin carbon films", *Science* **306**, 666 (2004).
- ⁸⁴C. R. Dean, A. F. Young, I. Meric, C. Lee, L. Wang, S. Sorgenfrei, K. Watanabe, T. Taniguchi, P. Kim, K. L. Shepard, and J. Hone, "Boron nitride substrates for high-quality graphene electronics", *Nat. Nanotechnol.* **5**, 722 (2010).
- ⁸⁵L. Britnell, R. V. Gorbachev, R. Jalil, B. D. Belle, F. Schedin, A. Mishchenko, T. Georgiou, M. I. Katsnelson, L. Eaves, S. V. Morozov, N. M. R. Peres, J. Leist, A. K. Geim, K. S. Novoselov, and L. A. Ponomarenko, "Field-effect tunneling transistor based on vertical graphene heterostructures", *Science* **335**, 947–950 (2012).
- ⁸⁶R. V. Gorbachev, A. K. Geim, M. I. Katsnelson, K. S. Novoselov, T. Tudorovskiy, I. V. Grigorieva, A. H. MacDonald, S. V. Morozov, K. Watanabe, T. Taniguchi, and L. A. Ponomarenko, "Strong Coulomb drag and broken symmetry in double-layer graphene", *Nat. Phys.* **8**, 896 (2012).
- ⁸⁷K. K. Kim, A. Hsu, X. Jia, S. M. Kim, Y. Shi, M. Dresselhaus, T. Palacios, and J. Kong, "Synthesis and characterization of hexagonal boron nitride film as a dielectric layer for graphene devices", *ACS Nano* **6**, 8583 (2012).
- ⁸⁸M. Zarenia, A. Perali, D. Neilson, and F. Peeters, "Enhancement of electron-hole superfluidity in double few-layer graphene", *Sci. Rep.* **4**, 7319 (2014).
- ⁸⁹J. I. A. Li, T. Taniguchi, K. Watanabe, J. Hone, A. Levchenko, and C. R. Dean, "Negative Coulomb drag in double bilayer graphene", *Phys. Rev. Lett.* **117**, 046802 (2016).
- ⁹⁰K. Lee, J. Xue, D. C. Dillen, K. Watanabe, T. Taniguchi, and E. Tutuc, "Giant frictional drag in double bilayer graphene heterostructures", *Phys. Rev. Lett.* **117**, 046803 (2016).
- ⁹¹K. Lee, B. Fallahazad, J. Xue, D. C. Dillen, K. Kim, T. Taniguchi, K. Watanabe, and E. Tutuc, "Chemical potential and quantum Hall ferromagnetism in bilayer graphene", *Science* **345**, 58 (2014).
- ⁹²M. Zarenia, A. R. Hamilton, F. M. Peeters, and D. Neilson, "Multiband mechanism for the sign reversal of Coulomb drag observed in double bilayer graphene heterostructures", *Phys. Rev. Lett.* **121**, 036601 (2018).

- ⁹³S. Conti, A. Perali, F. M. Peeters, and D. Neilson, "Multicomponent screening and superfluidity in gapped electron-hole double bilayer graphene with realistic bands", *Phys. Rev. B* **99**, 144517 (2019).
- ⁹⁴A. K. Geim and I. V. Grigorieva, "Van der Waals heterostructures", *Nature (London)* **499**, 419 (2013).
- ⁹⁵T. C. Berkelbach, M. S. Hybertsen, and D. R. Reichman, "Theory of neutral and charged excitons in monolayer transition metal dichalcogenides", *Phys. Rev. B* **88**, 045318 (2013).
- ⁹⁶F. Wu, F. Qu, and A. H. MacDonald, "Exciton band structure of monolayer MoS₂", *Phys. Rev. B* **91**, 075310 (2015).
- ⁹⁷K. F. Mak and J. Shan, "Photonics and optoelectronics of 2D semiconductor transition metal dichalcogenides", *Nat. Photonics* **10**, 216 (2016).
- ⁹⁸Y. Gong, J. Lin, X. Wang, G. Shi, S. Lei, Z. Lin, X. Zou, G. Ye, R. Vajtai, B. I. Yakobson, H. Terrones, M. Terrones, B. K. Tay, J. Lou, S. T. Pantelides, Z. Liu, W. Zhou, and P. M. Ajayan, "Vertical and in-plane heterostructures from WS₂/MoS₂ monolayers", *Nat. Mater.* **13**, 1135 (2014).
- ⁹⁹E. V. Calman, C. J. Dorow, M. M. Fogler, L. V. Butov, S. Hu, A. Mishchenko, and A. K. Geim, "Control of excitons in multi-layer van der Waals heterostructures", *Appl. Phys. Lett.* **108**, 101901 (2016).
- ¹⁰⁰I. C. Gerber and X. Marie, "Dependence of band structure and exciton properties of encapsulated WSe₂ monolayers on the hBN-layer thickness", *Phys. Rev. B* **98**, 245126 (2018).
- ¹⁰¹M. M. Fogler, L. V. Butov, and K. S. Novoselov, "High-temperature superfluidity with indirect excitons in van der Waals heterostructures", *Nat. Commun.* **5**, 4555 (2014).
- ¹⁰²O. L. Berman, G. Gumbs, and R. Y. Kezerashvili, "Bose-Einstein condensation and superfluidity of dipolar excitons in a phosphorene double layer", *Phys. Rev. B* **96**, 014505 (2017).
- ¹⁰³D. Neilson, "Excitonic superfluidity in electron-hole bilayer systems", in *Encyclopedia of condensed matter physics (second edition)*, Vol. 130, edited by T. Chakraborty, Second Edition (Academic Press, Oxford, 2024), pp. 38–50.
- ¹⁰⁴R. Maezono, P. López Ríos, T. Ogawa, and R. J. Needs, "Excitons and biexcitons in symmetric electron-hole bilayers", *Phys. Rev. Lett.* **110**, 216407 (2013).
- ¹⁰⁵J. Szymański, L. Świerkowski, and D. Neilson, "Correlations in coupled layers of electrons and holes", *Phys. Rev. B* **50**, 11002 (1994).
- ¹⁰⁶J. Böning, A. Filinov, and M. Bonitz, "Crystallization of an exciton superfluid", *Phys. Rev. B* **84**, 075130 (2011).
- ¹⁰⁷J. Mazierska and C. Wilker, "Accuracy issues in surface resistance measurements of high temperature superconductors using dielectric resonators", *IEEE Transactions on Applied Superconductivity* **11**, 3217–3225 (2001).
- ¹⁰⁸B. D. Josephson, "Possible new effects in superconductive tunnelling", *Phys. Lett.* **1**, 251 (1962).
- ¹⁰⁹F. Ancilotto, L. Salasnich, and F. Toigo, "DC Josephson effect with Fermi gases in the Bose-Einstein regime", *Phys. Rev. A* **79**, 033627 (2009).
- ¹¹⁰A. Spuntarelli, P. Pieri, and G. C. Strinati, "Josephson effect throughout the BCS-BEC crossover", *Phys. Rev. Lett.* **99**, 040401 (2007).

- ¹¹¹M. Tinkham, *Introduction to superconductivity*, Vol. 130, Dover Books on Physics Series (Dover Publications, 2004), p. 057001.
- ¹¹²A. A. Golubov, M. Y. Kupriyanov, and E. Il'ichev, "The current-phase relation in Josephson junctions", *Rev. Mod. Phys.* **76**, 411–469 (2004).
- ¹¹³D. E. Miller, J. K. Chin, C. A. Stan, Y. Liu, W. Setiawan, C. Sanner, and W. Ketterle, "Critical velocity for superfluid flow across the BEC-BCS crossover", *Phys. Rev. Lett.* **99**, 070402 (2007).
- ¹¹⁴W. Weimer, K. Morgener, V. P. Singh, J. Siegl, K. Hueck, N. Luick, L. Mathey, and H. Moritz, "Critical velocity in the BEC-BCS crossover", *Phys. Rev. Lett.* **114**, 095301 (2015).
- ¹¹⁵W. J. Kwon, G. D. Pace, R. Panza, M. Inguscio, W. Zwerger, M. Zaccanti, F. Scazza, and G. Roati, "Strongly correlated superfluid order parameters from dc Josephson supercurrents", *Science* **369**, 84–88 (2020).
- ¹¹⁶F. Pascucci and L. Salasnich, "Josephson effect with superfluid fermions in the two-dimensional BCS-BEC crossover", *Phys. Rev. A* **102**, 013325 (2020).
- ¹¹⁷V. Piselli, S. Simonucci, and G. C. Strinati, "Josephson effect at finite temperature along the BCS-BEC crossover", *Phys. Rev. B* **102**, 144517 (2020).
- ¹¹⁸R. Combescot, M. Y. Kagan, and S. Stringari, "Collective mode of homogeneous superfluid Fermi gases in the BEC-BCS crossover", *Phys. Rev. A* **74**, 042717 (2006).
- ¹¹⁹M. Marini, F. Pistolesi, and G. C. Strinati, "Evolution from BCS superconductivity to Bose condensation: Analytic results for the crossover in three dimensions", *Eur. Phys. J. B* **1**, 151–159 (1998).
- ¹²⁰H. Weinstock, *Applications of superconductivity*, Vol. 130, NATO science series: Applied sciences (Springer Netherlands, 2000), p. 057001.
- ¹²¹C. Ryu, P. W. Blackburn, A. A. Blinova, and M. G. Boshier, "Experimental realization of Josephson junctions for an atom SQUID", *Phys. Rev. Lett.* **111**, 205301 (2013).
- ¹²²Q. Guo, C. Ma, X. Zhang, Y. Xu, M. Fan, P. Yu, T. Hu, Y. Chang, and X. Yang, "SQUID-based magnetic resonance imaging at ultra-low field using the backprojection method", *Concepts in Magnetic Resonance Part B, Magnetic Resonance Engineering* **2020**, 8882329 (2020).
- ¹²³B. Zenker, H. Fehske, and H. Beck, "Excitonic Josephson effect in double-layer graphene junctions", *Phys. Rev. B* **92**, 081111 (2015).
- ¹²⁴D. Pekker and C. Varma, "Amplitude/Higgs modes in condensed matter physics", *Annual Review of Condensed Matter Physics* **6**, 269–297 (2015).
- ¹²⁵G. C. Strinati, P. Pieri, G. Röpke, P. Schuck, and M. Urban, "The BCS–BEC crossover: From ultra-cold Fermi gases to nuclear systems", *Phys. Rep.* **738**, 1–76 (2018).
- ¹²⁶M. Y. Kagan and A. V. Turlapov, "BCS–BEC crossover, collective excitations, and hydrodynamics of superfluid quantum liquids and gases", *Physics-Uspekhi* **62**, 215 (2019).
- ¹²⁷A. Sedrakian and J. W. Clark, "Superfluidity in nuclear systems and neutron stars", *Eur. Phys. J. A* **55**, 167 (2019).
- ¹²⁸R. Shimano and N. Tsuji, "Higgs mode in superconductors", *Annual Review of Condensed Matter Physics* **11**, 103–124 (2020).
- ¹²⁹R. Matsunaga, Y. I. Hamada, K. Makise, Y. Uzawa, H. Terai, Z. Wang, and R. Shimano, "Higgs amplitude mode in the BCS superconductors $\text{Nb}_{1-x}\text{Ti}_x\text{N}$ induced by terahertz pulse excitation", *Phys. Rev. Lett.* **111**, 057002 (2013).

-
- ¹³⁰S. Hoinka, P. Dyke, M. G. Lingham, J. J. Kinnunen, G. M. Bruun, and C. J. Vale, “Goldstone mode and pair-breaking excitations in atomic Fermi superfluids”, *Nat. Phys.* **13**, 943–946 (2017).
- ¹³¹G. Giuliani and G. Vignale, *Quantum theory of the electron liquid*, Vol. 130, Masters Series in Physics and Astronomy (Cambridge University Press, 2005), p. 057001.
- ¹³²P. Nozières, “Le problème à N corps: propriétés générales des gaz de fermions”, in , Vol. 130 (Dunod (impr. Jouve), 1963), p. 057001.
- ¹³³S. N. Klimin, H. Kurkjian, and J. Tempere, “Anderson-Bogoliubov collective excitations in superfluid Fermi gases at nonzero temperatures”, *J. Low Temp. Phys.* **196**, 102–110 (2019).
- ¹³⁴A. L. Fetter, “Electrodynamics of a layered electron gas. II. Periodic array”, *Annals of Physics* **88**, 1 (1974).
- ¹³⁵P. W. Anderson, “Random-phase approximation in the theory of superconductivity”, *Phys. Rev.* **112**, 1900–1916 (1958).
- ¹³⁶Y. Ohashi and A. Griffin, “Superfluidity and collective modes in a uniform gas of Fermi atoms with a Feshbach resonance”, *Phys. Rev. A* **67**, 063612 (2003).
- ¹³⁷R. B. Diener, R. Sensarma, and M. Randeria, “Quantum fluctuations in the superfluid state of the BCS-BEC crossover”, *Phys. Rev. A* **77**, 023626 (2008).
- ¹³⁸Y. Ohashi and S. Takada, “On the plasma oscillation in superconductivity”, *English, J. Phys. Soc. Jpn* **67**, 551–559 (1998).
- ¹³⁹T. Repplinger, S. Klimin, M. Gélédan, J. Tempere, and H. Kurkjian, “Plasmons in three-dimensional superconductors”, *Phys. Rev. B* **107**, 014504 (2023).
- ¹⁴⁰S. N. Klimin, J. Tempere, T. Repplinger, and H. Kurkjian, “Collective excitations of a charged Fermi superfluid in the BCS-BEC crossover”, *New J. Phys.* **25**, 063011 (2023).
- ¹⁴¹P. B. Patel, Z. Yan, B. Mukherjee, R. J. Fletcher, J. Struck, and M. W. Zwierlein, “Universal sound diffusion in a strongly interacting Fermi gas”, *Science* **370**, 1222–1226 (2020).
- ¹⁴²S. De Palo, P. E. Trevisanutto, G. Senatore, and G. Vignale, “Collective excitations and quantum incompressibility in electron-hole bilayers”, *Phys. Rev. B* **104**, 115165 (2021).
- ¹⁴³X. Gao, J. Tao, G. Vignale, and I. V. Tokatly, “Continuum mechanics for quantum many-body systems: linear response regime”, *Phys. Rev. B* **81**, 195106 (2010).
- ¹⁴⁴G. Kalman, V. Valtchinov, and K. I. Golden, “Collective modes in strongly coupled electronic bilayer liquids”, *Phys. Rev. Lett.* **82**, 3124–3127 (1999).
- ¹⁴⁵S. T. Chui, N. Wang, and C. Y. Wan, “Quantum exciton solid in bilayer two-dimensional electron-hole systems”, *Phys. Rev. B* **102**, 125420 (2020).
- ¹⁴⁶F. Pascucci, S. Conti, D. Neilson, J. Tempere, and A. Perali, “Josephson effect as a signature of electron-hole superfluidity in bilayers of van der Waals heterostructures”, *Phys. Rev. B* **106**, L220503 (2022).
- ¹⁴⁷S. Conti, A. Perali, D. Neilson, and F. M. Peeters, “Tuning the BEC-BCS crossover in electron-hole double bilayer graphene superfluidity using multiband effects.”, *Belgian Physical Society Magazine* **03**, 6 (2017).
- ¹⁴⁸R. P. Feynman and A. R. Hibbs, *Quantum mechanics and path integrals*, Vol. 130, International series in pure and applied physics (McGraw-Hill, New York, NY, 1965), p. 057001.
- ¹⁴⁹H. Kleinert, *Path integrals in quantum mechanics, statistics, polymer physics, and financial markets; 3rd ed.* Vol. 130 (World Scientific, River Edge, NJ, 2004), p. 057001.

- ¹⁵⁰L. Schulman, *Techniques and applications of path integration*, Vol. 130 (Wiley, 1996), p. 057001.
- ¹⁵¹G. Roepstorff, *Path integral approach to quantum physics: an introduction*, Vol. 130, Theoretical and Mathematical Physics (Springer Berlin Heidelberg, 2012), p. 057001.
- ¹⁵²J. Zinn-Justin, *Path integrals in quantum mechanics*, Vol. 130, Oxford graduate texts in mathematics (Oxford University Press, 2005), p. 057001.
- ¹⁵³S. Conti, A. Perali, F. M. Peeters, and D. Neilson, "Effect of mismatched electron-hole effective masses on superfluidity in double layer solid-state systems", *Condens. Matter* **6**, 057001 (2021).
- ¹⁵⁴W. Heisenberg, "Über quantentheoretische Umdeutung kinematischer und mechanischer Beziehungen.", *Zeitschrift für Physik* **33**, 879–893 (1925).
- ¹⁵⁵E. Schrödinger, "An undulatory theory of the mechanics of atoms and molecules", *Phys. Rev.* **28**, 1049–1070 (1926).
- ¹⁵⁶P. A. M. Dirac, "The Lagrangian in quantum mechanics", *Phys. Z. Sowjetunion* **3**, 64–72 (1933).
- ¹⁵⁷R. L. Stratonovich, "On a method of calculating quantum distribution functions", *Soviet Physics Doklady* **2**, 416 (1957).
- ¹⁵⁸A. Altland and B. D. Simons, *Condensed matter field theory*, Vol. 130 (Cambridge University Press, 2010), p. 057001.
- ¹⁵⁹J. Tempere and J. P. Devreese, "Path–integral description of Cooper pairing", in *Superconductors*, Vol. 130 (IntechOpen, Rijeka, 2012) Chap. 16, p. 057001.
- ¹⁶⁰E. Vermeyen, C. A. R. Sá de Melo, and J. Tempere, "Exchange interactions and itinerant ferromagnetism in ultracold Fermi gases", *Phys. Rev. A* **98**, 023635 (2018).
- ¹⁶¹Y. Nambu, "Quasi-particles and gauge invariance in the theory of superconductivity", *Phys. Rev.* **117**, 648–663 (1960).
- ¹⁶²A. L. Subasi, P. Pieri, G. Senatore, and B. Tanatar, "Stability of Sarma phases in density imbalanced electron-hole bilayer systems", *Phys. Rev. B* **81**, 075436 (2010).
- ¹⁶³A. M. Clogston, "Upper limit for the critical field in hard superconductors", *Phys. Rev. Lett.* **9**, 266–267 (1962).
- ¹⁶⁴M. W. Zwierlein, C. H. Schunck, A. Schirotzek, and W. Ketterle, "Direct observation of the superfluid phase transition in ultracold fermi gases", *Nature* **442**, 54–58 (2006).
- ¹⁶⁵S. Conti, A. Perali, F. M. Peeters, and D. Neilson, "Multicomponent electron-hole superfluidity and the BCS-BEC crossover in double bilayer graphene", *Phys. Rev. Lett.* **119**, 257002 (2017).
- ¹⁶⁶J. P. A. Devreese, J. Tempere, and C. A. R. Sá de Melo, "Effects of spin-orbit coupling on the Berezinskii-Kosterlitz-Thouless transition and the vortex–antivortex structure in two–dimensional Fermi gases", *Phys. Rev. Lett.* **113**, 165304 (2014).
- ¹⁶⁷L.-P. Lumbeck, J. Tempere, and S. Klimin, "Dispersion and damping of phononic excitations in Fermi superfluid gases in 2D", *Condensed Matter* **5**, 13 (2020).
- ¹⁶⁸F. J. Dyson, "The S matrix in quantum electrodynamics", *Phys. Rev.* **75**, 1736–1755 (1949).
- ¹⁶⁹D. Neilson, and L. Liu, "Excitations of the strongly correlated electron liquid in coupled layers", *Phys. Rev. Lett.* **71**, 4035–4038 (1993).
- ¹⁷⁰L. V. Keldysh and Y. V. Kopayev, "Possible instability of semimetallic state toward Coulomb interaction", *Sov. Phys. Solid State USSR* **6**, 2219 (1965).

- ¹⁷¹W. Nolting, *Theoretical physics 7: quantum mechanics - methods and applications*, Vol. 71 (Springer International Publishing, 2017), pp. 4035–4038.
- ¹⁷²J. Negele and H. Orland, *Quantum many particle systems*, Vol. 71 (Basic Books, 1995), pp. 4035–4038.
- ¹⁷³N. Nagaosa, *Quantum field theory in condensed matter physics*, Vol. 71, Texts and monographs in physics (Springer, 1999), pp. 4035–4038.
- ¹⁷⁴P. Rai-Choudhury, “Handbook of microlithography, micromachining, and microfabrication, volume 2: micromachining and microfabrication”, in , Vol. 71 (1997), pp. 4035–4038.
- ¹⁷⁵H. Taghinejad, A. A. Eftekhar, and A. A. Dibi, “Lateral and vertical heterostructures in two-dimensional transition-metal dichalcogenides”, *Opt. Mater. Express* **9**, 1590–1607 (2019).
- ¹⁷⁶M. Mahjouri-Samani, M.-W. Lin, K. Wang, A. R. Lupini, J. Lee, L. Basile, A. Boulesbaa, C. M. Rouleau, A. A. Puretzky, I. N. Ivanov, K. Xiao, M. Yoon, and D. B. Geohegan, “Patterned arrays of lateral heterojunctions within monolayer two-dimensional semiconductors”, *Nat. Commun.* **6**, 7749 (2015).
- ¹⁷⁷R. Frisenda, A. J. Molina-Mendoza, T. Mueller, A. Castellanos-Gomez, and H. S. J. van der Zant, “Atomically thin p–n junctions based on two-dimensional materials”, *Chem. Soc. Rev.* **47**, 3339–3358 (2018).
- ¹⁷⁸C. Gong, H. Zhang, W. Wang, L. Colombo, R. M. Wallace, and K. Cho, “Band alignment of two-dimensional transition metal dichalcogenides: Application in tunnel field effect transistors”, *App. Phys. Lett.* **107**, 139904 (2015).
- ¹⁷⁹P. W. Anderson and J. M. Rowell, “Probable observation of the Josephson superconducting tunneling effect”, *Phys. Rev. Lett.* **10**, 230–232 (1963).
- ¹⁸⁰S. Shapiro, “Josephson currents in superconducting tunneling: the effect of microwaves and other observations”, *Phys. Rev. Lett.* **11**, 80–82 (1963).
- ¹⁸¹P. Rivera, J. R. Schaibley, A. M. Jones, J. S. Ross, S. Wu, G. Aivazian, P. Klement, K. Seyler, G. Clark, N. J. Ghimire, J. Yan, D. G. Mandrus, W. Yao, and X. Xu, “Observation of long-lived interlayer excitons in monolayer MoSe₂-WSe₂ heterostructures”, *Nat. Commun.* **6**, 6242 (2015).
- ¹⁸²S. Giorgini, L. P. Pitaevskii, and S. Stringari, “Theory of ultracold atomic Fermi gases”, *Rev. Mod. Phys.* **80**, 1215–1274 (2008).
- ¹⁸³N. N. Bogoliubov, “On the theory of superfluidity”, *J. Phys.* **11**, 23 (1947).
- ¹⁸⁴L. Salasnich and F. Toigo, “Composite bosons in the two-dimensional BCS–BEC crossover from Gaussian fluctuations”, *Phys. Rev. A* **91**, 011604 (2015).
- ¹⁸⁵F. Palestini and G. C. Strinati, “Temperature dependence of the pair coherence and healing lengths for a fermionic superfluid throughout the BCS-BEC crossover”, *Phys. Rev. B* **89**, 224508 (2014).
- ¹⁸⁶F. Meier and W. Zwerger, “Josephson tunneling between weakly interacting Bose-Einstein condensates”, *Phys. Rev. A* **64**, 033610 (2001).
- ¹⁸⁷M. Zaccanti and W. Zwerger, “Critical Josephson current in BCS-BEC–crossover superfluids”, *Phys. Rev. A* **100**, 063601 (2019).
- ¹⁸⁸S. Giorgini, L. P. Pitaevskii, and S. Stringari, “Condensate fraction and critical temperature of a trapped interacting Bose gas”, *Phys. Rev. A* **54**, 4633 (1996).

- ¹⁸⁹L. Salasnich, N. Manini, and A. Parola, “Condensate fraction of a Fermi gas in the BCS-BEC crossover”, *Phys. Rev. A* **72**, 023621 (2005).
- ¹⁹⁰C. N. Yang, “Concept of off-diagonal long-range order and the quantum phases of liquid He and of superconductors”, *Rev. Mod. Phys.* **34**, 694 (1962).
- ¹⁹¹A. Guidini and A. Perali, “Band-edge BCS–BEC crossover in a two-band superconductor: Physical properties and detection parameters”, *Supercond. Sci. Tech.* **27**, 124002 (2014).
- ¹⁹²X. Liu, J. I. A. Li, K. Watanabe, T. Taniguchi, J. Hone, B. I. Halperin, P. Kim, and C. R. Dean, “Crossover between strongly coupled and weakly coupled exciton superfluids”, *Science* **375**, 205–209 (2022).
- ¹⁹³M. W. Klein, “Dipole correlations in a random dilute ferroelectric”, *Phys. Rev.* **141**, 489–498 (1966).
- ¹⁹⁴A. L. Fetter and J. D. Walecka, *Quantum theory of many-particle systems*, Vol. 71 (McGraw-Hill, Boston, 1971), pp. 4035–4038.
- ¹⁹⁵B. Debnath, Y. Barlas, D. Wickramaratne, M. R. Neupane, and R. K. Lake, “Exciton condensate in bilayer transition metal dichalcogenides: Strong coupling regime”, *Phys. Rev. B* **96**, 174504 (2017).
- ¹⁹⁶F. Nilsson and F. Aryasetiawan, “Effects of dynamical screening on the BCS-BEC crossover in double bilayer graphene: density functional theory for exciton bilayers”, *Phys. Rev. Materials* **5**, L050801 (2021).
- ¹⁹⁷Y. J. Chen, E. S. Koteles, B. S. Elman, and C. A. Armiento, “Effect of electric fields on excitons in a coupled double-quantum-well structure”, *Phys. Rev. B* **36**, 4562 (1987).
- ¹⁹⁸K. Das Gupta, A. F. Croxall, J. Waldie, C. A. Nicoll, H. E. Beere, I. Farrer, D. A. Ritchie, and M. Pepper, “Experimental progress towards probing the ground state of an electron-hole bilayer by low-temperature transport”, *Adv. Condens. Mat. Phys.* **2011**, 727958 (2011).
- ¹⁹⁹A. Perali, F. Palestini, P. Pieri, G. C. Strinati, J. T. Stewart, J. P. Gaebler, T. E. Drake, and D. S. Jin, “Evolution of the normal state of a strongly interacting fermi gas from a pseudogap phase to a molecular Bose gas”, *Phys. Rev. Lett.* **106**, 060402 (2011).
- ²⁰⁰F. Pistolesi and G. C. Strinati, “Evolution from BCS superconductivity to Bose condensation: role of the parameter $k_F \xi$ ”, *Phys. Rev. B* **49**, 6356 (1994).
- ²⁰¹N. Andrenacci, P. Pieri, and G. C. Strinati, “Size shrinking of composite bosons for increasing density in the BCS to Bose-Einstein crossover”, *Eur. Phys. J. B* **13**, 637 (2000).
- ²⁰²Y. E. Lozovik and A. A. Sokolik, “Multi-band pairing of ultrarelativistic electrons and holes in graphene bilayer”, *Phys. Lett. A* **374**, 326 (2009).
- ²⁰³A. Mazloom and S. H. Abedinpour, “Interplay of interlayer pairing and many-body screening in a bilayer of dipolar fermions”, *Phys. Rev. B* **98**, 014513 (2018).
- ²⁰⁴H. Kurkjian, S. N. Klimin, J. Tempere, and Y. Castin, “Pair-breaking collective branch in BCS superconductors and superfluid Fermi gases”, *Phys. Rev. Lett.* **122**, 093403 (2019).
- ²⁰⁵L. N. Cooper, “Microscopic quantum interference effects in the theory of superconductivity”, in *Nobel lectures*, Vol. 71, Physics 1971-1980 (World Scientific Publishing Co., 1992), p. 73.
- ²⁰⁶R. Kubo, “Statistical-mechanical theory of irreversible processes. I. general theory and simple applications to magnetic and conduction problems”, *J. Phys. Soc. Jpn* **12**, 570–586 (1957).

-
- ²⁰⁷H. Kurkjian, J. Tempere, and S. N. Klimin, “Linear response of a superfluid Fermi gas inside its pair-breaking continuum”, *Sci. Rep.* **10**, 11591 (2020).
- ²⁰⁸S. Van Loon and C. A. R. Sá de Melo, “Effects of quantum fluctuations on the low-energy collective modes of two-dimensional superfluid Fermi gases from the BCS to the Bose limit”, *Phys. Rev. Lett.* **131**, 113001 (2023).
- ²⁰⁹J. M. Kosterlitz and D. J. Thouless, “Ordering, metastability and phase transitions in two-dimensional systems”, *J. Phys. C: Solid State* **6**, 1181–1203 (1973).
- ²¹⁰A. Perali, P. Pieri, G. C. Strinati, and C. Castellani, “Pseudogap and spectral function from superconducting fluctuations to the bosonic limit”, *Phys. Rev. B* **66**, 024510 (2002).
- ²¹¹T. Kirzhner and G. Koren, “Pairing and the phase diagram of the normal coherence length $\xi_N(T, x)$ above T_c of $\text{La}_{(2-x)}\text{Sr}_x\text{CuO}_4$ thin films probed by the Josephson effect”, *Sci. Rep.* **4**, 6244 (2014).
- ²¹²F. Palestini, A. Perali, P. Pieri, and G. C. Strinati, “Dispersions, weights, and widths of the single-particle spectral function in the normal phase of a Fermi gas”, *Phys. Rev. B* **85**, 024517 (2012).
- ²¹³A. Damascelli, Z. Hussain, and Z.-X. Shen, “Angle-resolved photoemission studies of the cuprate superconductors”, *Rev. Mod. Phys.* **75**, 473–541 (2003).
- ²¹⁴S. Rist, A. A. Varlamov, A. H. MacDonald, R. Fazio, and M. Polini, “Photoemission spectra of massless Dirac fermions on the verge of exciton condensation”, *Phys. Rev. B* **87**, 075418 (2013).
- ²¹⁵D. Neilson, L. Świerkowski, J. Szymański, and L. Liu, “Collective modes in the two-dimensional electron liquid near the Wigner phase transition”, *J. Low Temp. Phys.* **89**, 251–256 (1992).

Curriculum Vitae

Name: Filippo Pascucci

Address: Van Schoonbekestraat 91, 2018, Antwerpen, Belgium

Phone number: +39 3342315104

E-mail: filippo.pascucci@unicam.it

Skype: filippopascucci

Date of birth: 23 July 1994

Nationality: Italian

Gender: Male



Education and training

- **Joint PhD in Theoretical and Experimental Physics** 2020 - present
University of Camerino, Camerino(MC), Italy.
University of Antwerpen, CMT group, Antwerp, Belgium.
- **2nd level degree in Theretical Physics** 2017–2020
University of Padova, Padova (PD), Italy.
Thesis: Ginzburg-Landau Theory and Josephson Effect in BCS-BEC crossover.
- **1st level degree in Physics** 2013–2017
University of Camerino, Camerino(MC), Italy.
Thesis: Superconductivity in stripes of superlattice.

Publications

- F. Pascucci, and L. Salasnich, *Josephson effect with superfluid fermions in the two-dimensional BCS-BEC crossover.*, Phys. Rev. A 102, 013325 (2020).
- F. Pascucci, A. Perali, and L. Salasnich, *Reliability of the Ginzburg–Landau Theory in the BCS-BEC Crossover by Including Gaussian Fluctuations for 3D Attractive Fermions.*, Condens. Matter 2021, 6(4), 49 (2021).
- F. Pascucci, S. Conti, D. Neilson, J. Tempere, and A. Perali, *Josephson effect as a signature of electron-hole superfluidity in bilayers of van der Waals heterostructures.* Phys. Rev. B 106, L220503 (2022).
- F. Pascucci, S. Conti, A. Perali, J. Tempere and D. Neilson, *Effects of intralayer correlations on electron-hole double-layer superfluidity.*, Phys. Rev. B 109, 094512 (2024).

Conferences and Workshops

- SuperFluctuations 2022, Padova, Italy (Poster presentation)

-
- Quantum Microwaves, Heat transfer and Many-Body Physics in Superconducting Devices, Workshop 2022, Trieste Italy
 - Strongly Couple Coulomb System 2022, Gorlitz, Germany (Poster presentation)
 - Superstripes 2023, Ischia, Italy (Invited Talk)
 - CMD30-FisMat2023 "Two-Dimensional excitonic insulators", Milano, Italy (Contributed Talk)
 - CMD30-FisMat2023 "Quantum gases as analogous of condensed matter system", Milano, Italy (Contributed Talk)
 - MultiSuper2023, San Benedetto del Tronto, Italy (Poster presentation)
 - FLEET International Conference 2023, San Benedetto del Tronto, Italy (Invited Talk)
 - Solvay Workshop 2023, Brussels, Belgium

Teaching Activities

- 08/2023 - "Elements of Physics" for degrees in Pharmacy (University of Camerino).

Personal Skills

•LANGUAGES

NATIVE Italian

FOREIGN English (B2)

•COMPUTER SKILLS

OPERATING SYSTEMS

Linux, Windows

TEXT AND TYPESETTING EDITORS

Excel, Powerpoint, Word, LaTeX

PROGRAMMING LANGUAGES

Fortran, Python

MATHEMATICAL SOFTWARE

Mathematica, Gnuplot